UNIVERSITY OF AMSTERDAM

UvA-DARE (Digital Academic Repository)

Search for squarks and gluinos in events with isolated leptons, jets and missing transverse momentum at √s = 8 TeV with the ATLAS detector

Aad, G.; et al., [Unknown]; Aben, R.; Angelozzi, I.; Beemster, L.J.; Bentvelsen, S.; Berge, D.; Bobbink, G.J.; Bos, K.; Boterenbrood, H.; Butti, P.; Castelli, A.; Colijn, A.P.; de Jong, P.; de Nooij, L.; Deigaard, I.; Deluca, C.; Dhaliwal, S.; Ferrari, P.; Gadatsch, S.; Geerts, D.A.A.; Hartjes, F.; Hessey, N.P.; Hod, N.; Igonkina, O.; Kluit, P.; Koffeman, E.; Lee, H.; Linde, F.; Mahlstedt, J.; Mechnich, J.; Oussoren, K.P.; Pani, P.; Sabato, G.; Salek, D.; Slawinska, M.; Valencic, N.; van den Wollenberg, W.; van der Deijl, P.C.; van der Geer, R.; van der Graaf, H.; van der Leeuw, R.; van Vulpen, I.; Verkerke, W.; Vermeulen, J.C.; Vreeswijk, M.; Weits, H.

DOI
10.1007/JHEP04(2015)116

Publication date
2015

Document Version
Final published version

Published in
The Journal of High Energy Physics

Link to publication

Citation for published version (APA):
Aad, G., et al., U., Aben, R., Angelozzi, I., Beemster, L. J., Bentvelsen, S., Berge, D., Bobbink, G. J., Bos, K., Boterenbrood, H., Butti, P., Castelli, A., Colijn, A. P., de Jong, P., de Nooij, L., Deigaard, I., Deluca, C., Dhaliwal, S., Ferrari, P., ... Weits, H. (2015). Search for squarks and gluinos in events with isolated leptons, jets and missing transverse momentum at √s = 8 TeV with the ATLAS detector. *The Journal of High Energy Physics*, *2015*(04), Article 116. https://doi.org/10.1007/JHEP04(2015)116

General rights
It is not permitted to download or to forward/distribute the text or part of it without the consent of the author(s) and/or copyright holder(s), other than for strictly personal, individual use, unless the work is under an open content license (like Creative Commons).

UvA-DARE is a service provided by the library of the University of Amsterdam (https://dare.uva.nl)

Disclaimer/Complaints regulations
If you believe that digital publication of certain material infringes any of your rights or (privacy) interests, please let the Library know, stating your reasons. In case of a legitimate complaint, the Library will make the material inaccessible and/or remove it from the website. Please Ask the Library: https://uba.uva.nl/en/contact, or a letter to: Library of the University of Amsterdam, Secretariat, Singel 425, 1012 WP Amsterdam, The Netherlands. You will be contacted as soon as possible.

Download date:05 Aug 2025

Published for SISSA by Springer

Received: *January 16, 2015*
Accepted: *March 26, 2015*
Published: *April 21, 2015*

Search for squarks and gluinos in events with isolated leptons, jets and missing transverse momentum at $\sqrt{s} = 8$ TeV with the ATLAS detector

The ATLAS collaboration

E-mail: atlas.publications@cern.ch

Abstract: The results of a search for supersymmetry in final states containing at least one isolated lepton (electron or muon), jets and large missing transverse momentum with the ATLAS detector at the Large Hadron Collider are reported. The search is based on proton-proton collision data at a centre-of-mass energy $\sqrt{s} = 8$ TeV collected in 2012, corresponding to an integrated luminosity of 20 fb^{-1}. No significant excess above the Standard Model expectation is observed. Limits are set on supersymmetric particle masses for various supersymmetric models. Depending on the model, the search excludes gluino masses up to 1.32 TeV and squark masses up to 840 GeV. Limits are also set on the parameters of a minimal universal extra dimension model, excluding a compactification radius of $1/R_c = 950$ GeV for a cut-off scale times radius (ΛR_c) of approximately 30.

Keywords: Hadron-Hadron Scattering

ArXiv ePrint: 1501.03555

Open Access, Copyright CERN,
for the benefit of the ATLAS Collaboration.
Article funded by SCOAP^3.

doi:10.1007/JHEP04(2015)116

JHEP04(2015)116

Contents

1 Introduction **2**

2 The ATLAS detector **3**

3 SUSY signal modelling and simulated event samples **3**
- 3.1 Signal event samples 3
  - 3.1.1 Simplified models 4
  - 3.1.2 Phenomenological models 5
  - 3.1.3 Event generation 7
- 3.2 Standard Model event samples 7
- 3.3 Detector simulation 7

4 Trigger and data collection **8**

5 Object reconstruction **9**
- 5.1 Object preselection 9
- 5.2 Signal object selection 10

6 Event selection **11**
- 6.1 Signal regions 12

7 Background estimation **18**
- 7.1 Backgrounds from $t\bar{t}$ and W/Z+jets 19
- 7.2 Fake-lepton background 23
- 7.3 Other backgrounds 27

8 Systematic uncertainties **27**
- 8.1 Experimental uncertainties 27
- 8.2 Theoretical uncertainties on the background estimation 28
- 8.3 Dominant uncertainties on the background estimation 29
- 8.4 Theoretical uncertainties on the signal expectation 30

9 Background fit **30**

10 Results and interpretation **34**
- 10.1 Background fit results and limits on the visible cross section 34
- 10.2 Exclusion limits on specific models 36
  - 10.2.1 Limits on phenomenological models 39
  - 10.2.2 Limits on simplified models 42

11 Conclusion **44**

JHEP04(2015)116

1 Introduction

Supersymmetry (SUSY) [1–9] postulates the existence of particles (sparticles) which differ by half a unit of spin from their Standard Model (SM) partners. The squarks ($\tilde{q}_{\mathrm{L}}$ and $\tilde{q}_{\mathrm{R}}$) and sleptons ($\tilde{\ell}_{\mathrm{L}}$ and $\tilde{\ell}_{\mathrm{R}}$) are the scalar partners of the left-handed and right-handed quarks and leptons, the gluinos ($\tilde{g}$) are the fermionic partners of the gluons, and the charginos ($\tilde{\chi}_i^{\pm}$ with $i = 1, 2$) and neutralinos ($\tilde{\chi}_i^0$ with $i = 1, 2, 3, 4$) are the mass eigenstates (ordered from the lightest to the heaviest) formed from the linear superpositions of the SUSY partners of the Higgs and electroweak gauge bosons. An attractive feature of SUSY is that it can solve the SM hierarchy problem [10–15] if the gluino, higgsino and top squark masses are not much higher than the TeV scale.

If strongly interacting sparticles exist at the TeV scale, they should be accessible at the Large Hadron Collider (LHC). In the minimal supersymmetric extension of the SM such particles decay into jets, possibly leptons, and the lightest sparticle (LSP). If the LSP is stable owing to R-parity conservation [15–19] and only weakly interacting, it escapes detection, leading to missing transverse momentum ($\boldsymbol{p}_{\mathrm{T}}^{\mathrm{miss}}$ and its magnitude $E_{\mathrm{T}}^{\mathrm{miss}}$) in the final state. In this scenario, the LSP can be a dark-matter candidate. Significant $E_{\mathrm{T}}^{\mathrm{miss}}$ can also arise in R-parity-violating scenarios in which the LSP decays to final states containing neutrinos or in scenarios where neutrinos are present in the cascade decay chains of the produced sparticles.

This paper presents a search with the ATLAS detector [20, 21] for SUSY in final states containing jets, at least one isolated lepton (electron or muon) and large $E_{\mathrm{T}}^{\mathrm{miss}}$. Different search channels are used in order to cover a broad parameter space: the events are selected by different requirements on the transverse momentum (p_{T}) of the leptons, either using low-p_{T} leptons (referred to as the "soft" lepton selection), or high-p_{T} leptons (referred to as the "hard" lepton selection). Each of these categories is further subdivided into a single-lepton and a dilepton search channel. The soft-lepton and hard-lepton channels are complementary, being more sensitive to supersymmetric spectra with small or large mass splittings, respectively, while the different lepton multiplicities cover different production and decay modes. To enhance the sensitivity to gluino or squark production, high and low jet multiplicity signal regions are defined.

Previous searches in these final states have been conducted by the ATLAS [22, 23] and CMS [24] collaborations using their full 2011 dataset at a centre-of-mass energy of 7 TeV. In this paper, the analysis is performed on the full 2012 ATLAS dataset at a centre-of-mass energy of 8 TeV, corresponding to an integrated luminosity of up to 20.3 fb^{-1}. All signal regions defined in this search are optimised for this dataset.

The paper is organised as follows. After a brief description of the ATLAS detector in section 2, the simulation of the background and signal processes used in the analysis is detailed in section 3. Section 4 discusses the trigger strategy and the dataset used,

JHEP04(2015)116

while the object reconstruction and the event selection are addressed in sections 5 and 6. The background estimation and the systematic uncertainties are discussed in sections 7 and 8. The fitting procedure used is described in section 9 and the results are presented in section 10. Finally, section 11 presents the conclusions.

2 The ATLAS detector

ATLAS is a multi-purpose detector which provides a nearly full solid angle coverage around the interaction point.[1] It consists of a tracking system (inner detector or ID) surrounded by a thin superconducting solenoid providing a 2 T magnetic field, electromagnetic and hadronic calorimeters and a muon spectrometer (MS). The ID consists of pixel and silicon microstrip detectors covering the pseudorapidity region $|\eta| < 2.5$, surrounded by the transition radiation tracker (TRT) which provides electron identification in the region $|\eta| < 2.0$. The calorimeters cover $|\eta| < 4.9$, the forward region ($3.2 < |\eta| < 4.9$) being instrumented with a liquid-argon (LAr) calorimeter for both the electromagnetic and hadronic measurements. In the central region, a high-granularity lead/LAr electromagnetic calorimeter covers $|\eta| < 3.2$, while the hadronic calorimeter uses two different detector technologies, with scintillator tiles ($|\eta| < 1.7$) or LAr ($1.5 < |\eta| < 3.2$) as active medium. The MS is based on three large superconducting toroids arranged with an eight-fold azimuthal coil symmetry around the calorimeters, and a system of three layers of precision tracking chambers providing coverage over $|\eta| < 2.7$, while dedicated fast chambers allow triggering over $|\eta| < 2.4$. The ATLAS trigger system [25] consists of three levels; the first level (L1) is a hardware-based system, while the second and third levels are software-based systems and are collectively referred to as the High Level Trigger (HLT).

3 SUSY signal modelling and simulated event samples

3.1 Signal event samples

The signal models considered cover simplified [26, 27] and phenomenological SUSY models, as well as a minimal Universal Extra Dimension (mUED) scenario [28, 29]. Some of these models were also probed by other ATLAS searches based on the 8 TeV pp dataset, using different final-state selections [30–34]. The simplified models studied here include the pair production of gluinos or first- and second-generation squarks with different hypotheses for their decay chains, as well as gluino-mediated top squark pair production. In these models, the LSP is always the lightest neutralino. The phenomenological models include scenarios for minimal super-gravity-mediated SUSY breaking (mSUGRA/CMSSM) [35–40], bilinear R-parity violation (bRPV) [41], natural gauge mediation (nGM) [42] and a non-universal Higgs-boson mass with gaugino mediation (NUHMG) [43].

[1] The nominal pp interaction point at the centre of the detector is defined as the origin of a right-handed coordinate system. The positive x-axis is defined by the direction from the interaction point to the centre of the LHC ring, with the positive y-axis pointing upwards, while the beam direction defines the z-axis. The azimuthal angle ϕ is measured around the beam axis and the polar angle θ is the angle from the z-axis. The pseudorapidity is defined as $\eta = -\ln\tan(\theta/2)$.

JHEP04(2015)116

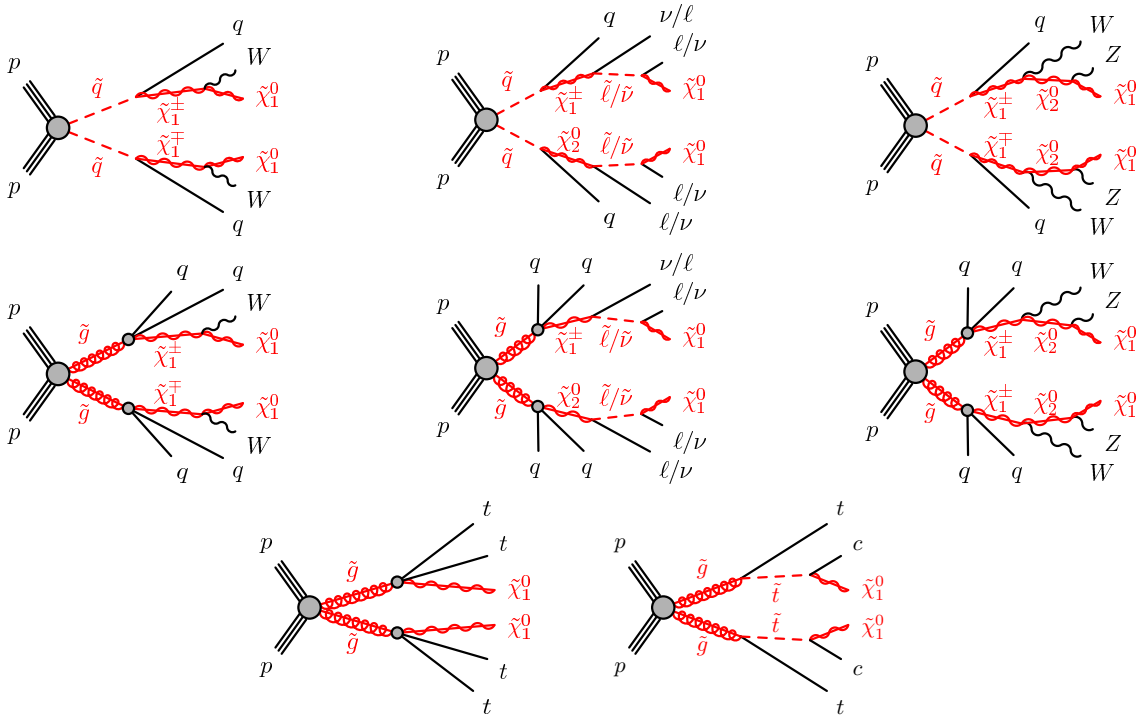

Figure 1. Examples of the decay topologies of the $\tilde{q}_{\mathrm{L}}$ (top) or $\tilde{g}$ (middle) pair production, in the simplified model with "one step" (left) and "two steps" with (centre) or without (right) sleptons. The bottom diagrams show examples of the topologies considered for gluino-mediated production of top squarks.

3.1.1 Simplified models

The topologies of the simplified models considered in this paper are illustrated in figure 1.

In these simplified models, all the sparticles which do not directly enter the production and decay chain are effectively decoupled.

The first category of simplified models focuses on the pair production of left-handed squarks or of gluinos, the latter assuming degenerate first- and second-generation squarks. This category of models is subdivided into three different decay chains: "one-step" models, "two-step" models with sleptons, and "two-step" models without sleptons.

In the "one-step" models, the pair-produced strongly interacting sparticles decay via the lighter chargino into a W boson and the lightest neutralino. The free parameters in these models are chosen to be the mass of the squark/gluino and either the mass of the chargino, with a fixed $\tilde{\chi}_1^0$ mass set to 60 GeV, or the mass of the $\tilde{\chi}_1^0$, with the chargino mass set to $m_{\tilde{\chi}_1^\pm} = (m_{\tilde{g}/\tilde{q}} + m_{\tilde{\chi}_1^0})/2$.

In the "two-step" models with sleptons, the strongly interacting sparticles decay with equal probability via either the lightest chargino or the next-to-lightest neutralino. These subsequently decay via left-handed sleptons (or sneutrinos) which decay into a lepton (or neutrino) and the lightest neutralino. In these models, the free parameters are chosen to be the initial sparticle mass and the $\tilde{\chi}_1^0$ mass. The masses of the intermediate

JHEP04(2015)116

charginos/neutralinos are set to be equal, $m_{\tilde{\chi}_1^\pm,\tilde{\chi}_2^0} = (m_{\tilde{g}/\tilde{q}} + m_{\tilde{\chi}_1^0})/2$, while the slepton and sneutrino masses (all three lepton flavours are mass degenerate in this model) are set to $m_{\tilde{\ell}_\mathrm{L},\tilde{\nu}} = (m_{\tilde{\chi}_1^\pm/\tilde{\chi}_2^0} + m_{\tilde{\chi}_1^0})/2$.

Finally, in the "two-step" models without sleptons, the initial sparticle decays via the lighter chargino, which itself decays into a W boson and the next-to-lightest neutralino. The latter finally decays into a Z boson and the $\tilde{\chi}_1^0$. The lighter chargino mass is fixed at $m_{\tilde{\chi}_1^\pm} = (m_{\tilde{g}/\tilde{q}} + m_{\tilde{\chi}_1^0})/2$ and the next-to-lightest neutralino mass is set to be $m_{\tilde{\chi}_2^0} = (m_{\tilde{\chi}_1^\pm} + m_{\tilde{\chi}_1^0})/2$. This signature could be realised in the Minimal Supersymmetric Standard Model (MSSM) in a region of parameter space where additional decay modes, not contained in the simplified model, may lead to a significant reduction in the cross section times branching fraction of the WZ signature.

The second category of simplified models considers the gluino-mediated production of top squarks.[2] In these models, the lightest squark is the lightest top squark mass eigenstate $\tilde{t}_1$ formed from the mixing of $\tilde{t}_L$ and $\tilde{t}_R$, and the squarks of all other flavours are effectively decoupled. Two models are considered in this specific search for gluino-mediated top squark production. In the first model, $\tilde{t}_1$ is effectively decoupled and its mass is set to 2.5 TeV, a mass for which there is no current sensitivity to direct production. Each gluino decays with 100% branching fraction to a top quark and a virtual top squark, the latter exclusively decaying to a top quark and the $\tilde{\chi}_1^0$, leading to a final state with a pair of top quarks and a neutralino, $\tilde{g} \to t\bar{t}\tilde{\chi}_1^0$. The mass of the gluino is a free parameter and is varied up to 1.4 TeV, a value representative of the expected reach of the analysis. This final state is therefore characterised by the presence of four top quarks (decaying to four b-jets and four W bosons) and two $\tilde{\chi}_1^0$. In the second model, the gluino is heavier than the $\tilde{t}_1$, and the mass gap between the $\tilde{t}_1$ and the $\tilde{\chi}_1^0$ is smaller than the W boson mass and fixed to 20 GeV. Gluinos decay to a top quark and a top squark, $\tilde{g} \to \bar{t}\tilde{t}_1$, and the $\tilde{t}_1$ is set to exclusively decay to a charm quark and the $\tilde{\chi}_1^0$, $\tilde{t}_1 \to c\tilde{\chi}_1^0$. Using gluino-mediated production to probe this decay is particularly interesting as it is complementary to the direct pair production of $\tilde{t}_1$, which is more difficult to extract from the background for this specific decay mode of $\tilde{t}_1$ (see ref. [44]). This final state is therefore characterised by the presence of two top quarks (decaying to two b-jets and two W bosons), two c-quarks and two $\tilde{\chi}_1^0$.

3.1.2 Phenomenological models

Phenomenological models are also considered in this paper. The mSUGRA/CMSSM model is specified by five parameters: the universal scalar mass m_0, the universal gaugino mass $m_{1/2}$, the universal trilinear scalar coupling A_0, the ratio $\tan\beta$ of the vacuum expectation values of the two Higgs fields, and the sign of the higgsino mass parameter μ. In the mSUGRA/CMSSM model studied here, the values $\tan\beta = 30$, $A_0 = -2m_0$ and $\mu > 0$ were chosen, such that the lightest scalar Higgs boson mass is approximately 125 GeV in most of the (m_0,$m_{1/2}$) parameter space studied.

A bRPV scenario is also studied; it uses the same parameters as the mSUGRA/CMSSM model, but with non-zero bilinear R-parity-violating couplings, which are determined by a

[2] In these models, the $\tilde{t}$ mixing angle is taken to be 56°, but the value of this mixing angle has no impact on the results of the analyses presented in this paper.

JHEP04(2015)116

fit to atmospheric and solar neutrino data [45] under the tree-level dominance scenario [46]. In this scenario, the $\tilde{\chi}_1^0$ LSP decays promptly to $W\mu$, $W\tau$, $Z\nu$ or $h\nu$ (where the $W/Z/h$ boson can either be on shell or off shell) with branching fractions which are weakly dependent on m_0 and $m_{1/2}$ but which are typically of the order of 20–40%, 20–40%, 20–30% and 0–20%, respectively.

The nGM scenario differs from the general gauge mediation models [47, 48] in that all sparticles that are not relevant to the tuning of the Higgs sector are decoupled. The relevant sparticles are thus the higgsinos, one or two light top squarks, a light gluino and a very light gravitino ($\tilde{G}$) LSP. This configuration results in minimal fine tuning while obeying all current collider constraints. The sparticles that play no role in fine tuning can subsequently be reintroduced while retaining the naturalness of the model. In the model considered here, and described in detail in ref. [34], the stau ($\tilde{\tau}$) is assumed to be the next-to-lightest SUSY particle (NLSP), and the gluino is assumed to be the only light coloured sparticle. Therefore, the only relevant production process in this model is gluino pair production followed by two possible decay chains: $\tilde{g} \to g\tilde{\chi}_{1,2}^0 \to g\tilde{\tau}\tau \to g\tau\tau\tilde{G}$ and $\tilde{g} \to qq'\tilde{\chi}_1^{\pm} \to qq'\nu_\tau\tilde{\tau} \to qq'\nu_\tau\tau\tilde{G}$, where q and q' are almost exclusively top or bottom quarks. The exact proportion of the two processes depends on the mass of the decoupled squarks, with the first process only happening for low gluino masses. The higgsino mass parameter μ is set to 400 GeV, which fixes the mass of the chargino and the neutralinos, such that strong production is the dominant process at the LHC. A range of signals with varying gluino and stau masses are studied. The lightest Higgs-boson mass is specifically set to 125 GeV.

NUHMG is an R-parity-conserving model with the tau-sneutrino as the NLSP. There are six parameters which can be varied to obtain different phenomenologies: $\tan\beta$, $m_{1/2}$, A_0 and the sign of μ, defined above, as well as the squared mass terms of the two Higgs doublets: $m_{H_1}^2$ and $m_{H_2}^2$. These parameters are set as follows: $\tan\beta = 10$, $\mu > 0$, $m_{H_2}^2 = 0$; $m_{1/2}$ and $m_{H_1}^2$ are chosen such that the NLSP is a tau-sneutrino with properties satisfying Big Bang Nucleosynthesis constraints (see ref. [43]); A_0 is chosen to maximise the mass of the lightest Higgs boson (in NUHMG models, the Higgs boson mass obtained is usually lower than the measured value: varying A_0 allows the models considered here to minimise this difference to the level of a few GeV). In this model, there is a significant production of gluinos and squarks throughout the parameter space studied. The gluino decays mainly to a first- or second-generation quark/squark pair $q\tilde{q}$ ($\approx 50\%$), but also to $t\tilde{t}$ ($\approx 30\%$) or $b\tilde{b}$ ($\approx 20\%$), while the squark cascade decay typically involves charginos, neutralinos and/or sleptons.

This analysis also considers the mUED model, which is the minimal extension of the SM with one additional universal spatial dimension. The properties of the model depend on only three parameters: the compactification radius R_c, the cut-off scale Λ and the Higgs boson mass m_h. In this model, the mass spectrum is naturally degenerate and the decay chain of the Kaluza-Klein (KK) quark to the lightest KK particle, the KK photon, gives a signature very similar to the supersymmetric decay chain of a squark to the lightest neutralino. Signal events for this model are generated with a Higgs-boson mass of 125 GeV.

JHEP04(2015)116

3.1.3 Event generation

SUSY-HIT and SDECAY 1.3b [49, 50], interfaced to SOFTSUSY 3.1.6 [51], are used to calculate the sparticle mass spectra and decay tables, and to ensure consistent electroweak symmetry breaking in the mSUGRA/CMSSM models. All the simplified models except the gluino-mediated top squark production are generated with up to one extra parton in the matrix element using MADGRAPH 5 1.3.33 [52] interfaced to PYTHIA 6.426 [53]; MLM matching [54] is applied with a scale parameter that is set to a quarter of the mass of the lightest sparticle in the hard-scattering matrix element. HERWIG++ 2.5.2 [55] is used to generate the mUED, mSUGRA and nGM samples, as well as the samples for the simplified model with gluino-mediated top squark production. Finally, the NUHMG and bRPV samples are generated with PYTHIA 6.426. The ATLAS underlying-event tune AUET2 is used [56] for MADGRAPH 5 and PYTHIA 6 samples while the CTEQ6L1-UE-EE-3 tune [57] is used for HERWIG++ samples. The parton distribution functions (PDFs) from CTEQ6L1 [58] are used for all signal samples.

For all except the mUED sample, the signal cross sections are calculated at next-to-leading order (NLO) in the strong coupling constant, adding the resummation of soft gluon emission at next-to-leading-logarithmic accuracy (NLO+NLL) [59–63]. The nominal cross section is taken from an envelope of cross-section predictions using different PDF sets and factorisation and renormalisation scales, as described in ref. [64]. For the mUED model, the cross section is taken at leading order from HERWIG++.

3.2 Standard Model event samples

The simulated event samples for the SM backgrounds are summarised in table 1, along with the PDFs and tunes used. Further samples are also used to compute systematic uncertainties, as explained in section 8. The Drell-Yan samples used in the hard-lepton analyses have a filter which selects events at generation level by requiring the leptons to satisfy ${p_{\mathrm{T}}}^{\ell_1(\ell_2)} > 9(5)$ GeV and $|\eta_{\ell_{1,2}}| < 2.8$. This filter prevents its use in the soft-lepton analyses which use ALPGEN samples with a lepton p_{T} cut at 5 GeV. The ALPGEN [85] samples are generated with the MLM matching scheme and with $0 \leq N_{\mathrm{parton}} \leq 5$; for these samples HERWIG 6.520 [86] is used for simulating the parton shower and fragmentation processes in combination with JIMMY [87] for underlying-event simulation. PYTHIA 6.426 is used for the MADGRAPH 5, ACERMC [75] and all POWHEG [69–71] samples except for the diboson POWHEG samples, which use PYTHIA 8.163 [88]. The POWHEG diboson samples have dilepton filters which increase the number of Monte Carlo events available for the dilepton analyses. SHERPA uses its own parton shower and fragmentation, and the SHERPA W+jets and Z/γ^*+jets samples are generated with massive b/c-quarks to improve the treatment of the associated production of W/Z bosons with heavy flavour.

3.3 Detector simulation

The detector simulation is performed either with a full ATLAS detector simulation [89] based on GEANT4 [90] or a fast simulation based on the parameterisation of the performance of the ATLAS electromagnetic and hadronic calorimeters [91] and on GEANT4

JHEP04(2015)116

Physics process	Generator	Cross-section normalisation	PDF set	Tune
$W(\to \ell\nu)$ + jets	SHERPA 1.4.1 [65]	NNLO [66, 67]	NLO CT10 [68]	SHERPA default
$Z/\gamma^*(\to \ell\ell)$ + jets ($m_{\ell\ell} > 40$ GeV)	SHERPA 1.4.1	NNLO [66, 67]	NLO CT10	SHERPA default
$t\bar{t}$	POWHEG-BOX r2129 [69–71]	NNLO+NNLL [72, 73]	NLO CT10	PERUGIA2011C [74]
Single-top (t-channel)	ACERMC 3.8 [75]	NNLO+NNLL [76]	CTEQ6L1 [58]	PERUGIA2011C
Single-top (s-channel and Wt)	POWHEG-BOX r1556	NNLO+NNLL [77, 78]	NLO CT10	PERUGIA2011C
$t + Z$	MADGRAPH 5 1.3.28 [52]	LO	CTEQ6L1	AUET2 [56]
$t\bar{t} + W(W)/Z$	MADGRAPH 5 1.3.28	NLO [79, 80]	CTEQ6L1	AUET2
Single-lepton analyses:				
WW, WZ and ZZ	SHERPA 1.4.1	NLO [81, 82]	NLO CT10	SHERPA default
$W\gamma$ and $Z\gamma$	SHERPA 1.4.1	LO	NLO CT10	SHERPA default
Dilepton analyses:				
WW, WZ and ZZ	POWHEG-BOX r1508 [83]	NLO [81, 82]	NLO CT10	AUET2
Hard-lepton analyses:				
Drell-Yan ($8 < m_{\ell\ell} < 40$ GeV)	SHERPA 1.4.1	NNLO [84]	NLO CT10	SHERPA default
Soft-lepton analyses:				
$Z/\gamma^*(\to \ell\ell)$ + jets ($10 < m_{\ell\ell} < 60$ GeV)	ALPGEN 2.14 [85]	NNLO [84]	CTEQ6L1	AUET2

Table 1. Simulated background event samples used in this paper (where $\ell = e, \mu, \tau$): the corresponding generators, cross-section normalisation, PDF set and underlying event tune are shown. More details (e.g. concerning the parton showers) can be found in the text.

elsewhere. All simulated samples are generated with a range of minimum-bias interactions (simulated using PYTHIA 8 with the MSTW2008LO PDF set [92] and the A2 tune [93]) overlaid on the hard-scattering event to account for the multiple pp interactions in the same bunch crossing (pile-up). The overlay also treats the impact of pile-up on bunch crossings other than the bunch crossing in which the event occurred. Event-level weights are applied to the simulated samples to account for differences between data and simulation for the lepton trigger, identification and reconstruction efficiencies, and for the efficiency and misidentification rate of the algorithm used to identify jets containing b-hadrons (b-tagging).

4 Trigger and data collection

The data used in this paper were collected in 2012, during which the instantaneous luminosity of the LHC reached 7.7×10^{33} cm^{-2}s^{-1}. The average number of expected interactions per bunch crossing ranged from approximately 6 to 40, with a mean of 21. After applying data-quality requirements related to the beam and detector conditions, the total integrated

JHEP04(2015)116

luminosity is 20.1 fb^{-1} in the soft-lepton channel and 20.3 fb^{-1} in the hard-lepton channel; the integrated luminosities differ as these channels use different trigger requirements. The uncertainty on the integrated luminosity is $\pm 2.8\%$. It is derived, following the same methodology as that detailed in ref. [94], from a preliminary calibration of the luminosity scale derived from beam-separation scans performed in November 2012.

In the hard single-electron channel the L1 decision is based on electron requirements only, while electron and $E_{\text{T}}^{\text{miss}}$ requirements are used at the HLT. The trigger thresholds on HLT objects are 24 GeV for the electron and 35 GeV for $E_{\text{T}}^{\text{miss}}$. The $E_{\text{T}}^{\text{miss}}$ trigger is fully efficient for $E_{\text{T}}^{\text{miss}} > 80$ GeV. The electron trigger selects events containing one or more electron candidates, based on the presence of an energy cluster in the electromagnetic calorimeter, with a shower shape consistent with that of an electron, and has no explicit electron isolation requirement except a loose one at L1. For electrons with $p_{\text{T}} > 25$ GeV, the trigger efficiency increases from 70% to close to 100% as the electron p_{T} increases from 24 to 30 GeV.

In the hard single-muon channel the L1 decision is based on muon and jet requirements only, while the HLT also includes requirements on $E_{\text{T}}^{\text{miss}}$. The trigger thresholds on HLT objects are at 24 GeV for the muon, 65 GeV for the jet and 40 GeV for $E_{\text{T}}^{\text{miss}}$. The muon trigger selects events containing one or more muon candidates based on the hit patterns in the MS and ID, and has no muon isolation requirement. The combined trigger reaches its maximal efficiency of approximately 70% (90%) for a muon in the barrel (end-cap) for muons satisfying $p_{\text{T}} > 25$ GeV, $E_{\text{T}}^{\text{miss}} > 100$ GeV and fully calibrated jets with $p_{\text{T}} > 80$ GeV.

In the hard two-lepton channel, a combination of single-lepton and dilepton triggers is used with different p_{T} requirements on the electron(s) and muon(s). The maximal trigger efficiency is reached when requiring the leading lepton to have $p_{\text{T}} > 14$ GeV in ee and $\mu\mu$ events or $p_{\text{T}}^{e}(p_{\text{T}}^{\mu}) > 10(18)$ GeV in $e\mu$ events. If both leptons are in the barrel (end-cap), these plateau efficiencies are approximately 96%, 88% and 80% (91%, 92% and 82%) for ee, $e\mu$ and $\mu\mu$ events, respectively.

Since the thresholds in the single-lepton and dilepton triggers are too high to be suitable for the soft-lepton event selections, this channel relies on a $E_{\text{T}}^{\text{miss}} > 80$ GeV trigger which is fully efficient for events with a jet with $p_{\text{T}} > 80$ GeV and $E_{\text{T}}^{\text{miss}} > 150$ GeV.

5 Object reconstruction

In this section, the final-state object reconstruction and selection requirements are described. The preselection described below identifies candidate objects. Some objects are also required to pass a tighter selection before they are used in the event selection. The event selection criteria and the various signal regions are described in detail in section 6.

5.1 Object preselection

The primary vertex of the event [95] is required to be consistent with the beam-spot envelope. When more than one such vertex is found, the vertex with the largest summed $|p_{\text{T}}|^2$ of the associated tracks is chosen.

Jets are reconstructed from three-dimensional calorimeter energy clusters using the anti-k_{t} algorithm [96, 97] with a radius parameter $R = 0.4$. Jets arising from detector noise,

JHEP04(2015)116

cosmic rays or other non-collision sources are rejected, as described in ref. [98]. To take into account the differences in calorimeter response between electrons/photons and hadrons, each cluster is classified, prior to the jet reconstruction, as coming from an electromagnetic or hadronic shower on the basis of its shape [21]. The jet energy is then corrected at cluster level by weighting electromagnetic and hadronic energy deposits with correction factors derived from Monte Carlo simulation. A correction is applied to subtract the expected contamination from pile-up: it is calculated as the product of the jet area in the (η, ϕ) space and the average energy density of the event [99]. A further calibration, relating the response of the calorimeter to true jet energy [98, 100], is then applied, with a residual correction to account for differences between the data in situ measurements and the Monte Carlo simulation. Once calibrated, the "preselected" jets are required to have $p_{\mathrm{T}} > 20\,\mathrm{GeV}$ and $|\eta| < 2.5$.

Electrons are reconstructed from clusters in the electromagnetic calorimeter matched to tracks in the ID [101]. The "preselected" electrons are required to pass a variant of the "medium" selection of ref. [101], which was modified in 2012 to reduce the impact of pile-up. These electrons must have $|\eta| < 2.47$ and $p_{\mathrm{T}} > 7$ (10) GeV in the soft(hard)-lepton channel. As each electron can also be reconstructed as a jet, electrons with $\Delta R(e, \mathrm{jet}) < 0.2$ are kept, where $\Delta R = \sqrt{(\Delta\eta)^2 + (\Delta\phi)^2}$, and the jet is discarded in order to resolve the ambiguity; for $0.2 < \Delta R(e, \mathrm{jet}) < 0.4$, the electron is discarded and the jet is kept; for $\Delta R(e, \mathrm{jet}) > 0.4$ both the electron and the jet are kept. The electrons are also required to be well separated from the preselected muons described below, with $\Delta R(e, \mu) > 0.01$. If two preselected electrons are found to have an angular separation $\Delta R(e, e) < 0.05$, only the higher-p_{T} electron is kept. Finally, any event containing a preselected electron in the transition region between the barrel and end-cap electromagnetic calorimeters, $1.37 < |\eta| < 1.52$, is rejected.

Muons are identified either as a combined track in the MS and ID systems, or as an ID track matched to a MS segment [102]. Requirements on the quality of the ID track are identical to those in ref. [103]. "Preselected" muons in the soft(hard)-lepton channel are required to have $p_{\mathrm{T}} > 6$ (10) GeV, $|\eta| < 2.40$ and $\Delta R(\mu, \mathrm{jet}) > 0.4$ with respect to the closest preselected jet.

The missing transverse momentum is computed from the transverse momenta of identified electrons, photons, jets and muons, and from all calorimeter clusters within $|\eta| < 4.5$ not associated with such objects [104].

5.2 Signal object selection

For the final selection of events used to define the various signal regions, some objects are required to pass more stringent requirements, which are described below.

"Signal" jets have a higher threshold than preselected jets, with $p_{\mathrm{T}} > 25\,\mathrm{GeV}$. Signal jets with $|\eta| < 2.4$ are further required to be associated with the hard-scattering process by demanding that at least 25% of the scalar sum of the p_{T} of all tracks associated with the jet comes from tracks associated with the primary vertex in the event. This jet vertex fraction requirement is applied in order to remove jets which come from pile-up [105]; it is not applied to jets with p_{T} greater than 50 GeV nor to the b-tagged jets (see below), since the probability of a pile-up jet satisfying either of these requirements is negligible.

JHEP04(2015)116

Signal jets containing b-hadrons are identified using the neural-network-based algorithm MV1 described in ref. [106], which uses information about track impact parameters and reconstructed secondary vertices. The presence of b-jets is vetoed in the hard dilepton signal regions and in some of the soft-lepton signal regions in order to reduce the $t\bar{t}$ background. In the single-lepton channels, there is no requirement on b-jets in the event selection, but they are used in the background estimation, as explained in section 7. The tightness of the selection criteria used in the b-tagging is optimised for each channel. In all signal regions except for the soft dimuon signal region, the chosen criteria give an inclusive b-tagging efficiency of 60% in a simulated sample of $t\bar{t}$ events; in the soft dimuon signal region they are chosen to give an inclusive efficiency of 80%. For a b-jet efficiency of 60% (80%), the algorithm provides a rejection factor of approximately 585 (25) for light-quark and gluon jets, and of approximately 8 (3) for charm jets [107].

The "signal" electrons are required to be isolated, and the isolation requirement depends on the electron transverse momentum. For $p_{\mathrm{T}} < 25\,\mathrm{GeV}$ ($p_{\mathrm{T}} \geq 25$ GeV), the scalar sum of the p_{T} of tracks within a cone of size $\Delta R = 0.3$ (0.2) around the electron, excluding the electron itself, is required to be less than 16% (10%) of the electron p_{T}. For $p_{\mathrm{T}} < 25\,\mathrm{GeV}$, the distance $|z_0 \sin\theta|$ must be ≤ 0.4 mm, where z_0 is the longitudinal impact parameter with respect to the primary vertex. For $p_{\mathrm{T}} \geq 25$ GeV, $|z_0|$ is required to be ≤ 2 mm. Finally, for electrons with $p_{\mathrm{T}} < 25\,\mathrm{GeV}$, the significance of the distance of closest approach of the electron to the primary vertex in the transverse plane must be $|d_0/\sigma_{d_0}| < 5$, while for electrons with $p_{\mathrm{T}} \geq 25\,\mathrm{GeV}$, the distance of closest approach itself must be $|d_0| \leq 1$ mm.

Isolation is also required in the "signal" muon definition. For $p_{\mathrm{T}} < 25\,\mathrm{GeV}$, the scalar sum of the p_{T} of tracks within a cone of size $\Delta R = 0.3$ around the muon candidate, excluding the muon itself, is required to be less than 12% of the muon p_{T}, while for $p_{\mathrm{T}} \geq 25$ GeV, the same sum within a cone of size $\Delta R = 0.2$ is required to be less than 1.8 GeV. Muons with $p_{\mathrm{T}} < 25\,\mathrm{GeV}$ are required to have $|z_0 \sin\theta|$ less than 1 mm and $|d_0/\sigma_{d_0}|$ less than 3.

With the lepton selection described above, the combined isolation and identification efficiency measured in simulated $t\bar{t}$ events for electrons (muons) is 56% (72%) at $p_{\mathrm{T}} = 20\,\mathrm{GeV}$ and 84% (82%) at $p_{\mathrm{T}} = 100\,\mathrm{GeV}$.

6 Event selection

Events selected by the triggers are required to have a primary vertex with at least five associated tracks with $p_{\mathrm{T}} > 400$ MeV. An event is rejected if it contains any preselected jet which fails to satisfy the quality criteria which are designed to suppress non-collision backgrounds and detector noise [108, 109], or any preselected muon with $|z_0| > 1.0$ mm and $|d_0| > 0.2$ mm in order to remove cosmic-ray muons. These selection criteria remove $\mathcal{O}(2\%)$ of data events.

This analysis is based on a number of signal regions (SR), each designed to maximise the sensitivity to different SUSY topologies in terms of the chosen discriminating variables. As described in detail in section 7, a number of control regions (CR) are constructed to constrain the dominant backgrounds. These control regions are designed to have a high purity, a small statistical uncertainty in terms of the background process of interest and to

JHEP04(2015)116

contain only a small fraction of the potential SUSY signal. Because of these requirements, the CRs are not necessarily close to the SRs in terms of the main discriminating variables. As described in section 9, validation regions (VR), closer to the SRs than the CRs, are used to verify the compatibility between data and MC. Figures 2–4 illustrate these concepts, respectively for the soft-lepton, hard single-lepton and hard dilepton analyses.

6.1 Signal regions

The selection criteria used to define the various signal regions in this paper are summarised in table 2 for the soft-lepton signal regions, in table 3 for the hard single-lepton signal regions and in table 4 for the hard dilepton signal regions.

The soft and hard single-lepton signal regions are designed with lower jet multiplicities to cover squark pair production and with higher jet multiplicities to cover gluino pair production. The soft single-lepton channel focuses on models with a compressed mass spectrum, with the 3-jet inclusive selection being defined to make the analysis sensitive to squark pair production in the case where there is a large mass gap between the squark and the LSP. The soft dimuon channel is optimised for mUED searches. The hard dilepton channel targets gluino and first- and second-generation squark production, as well as mUED searches; it is not designed to search for signal events in which a real Z boson is present. The correspondence between the analysis channels and the various models probed is summarised in table 5.

The following variables, derived from the kinematic properties of the objects, are used in the event selection.

The minimum angular separation between the signal lepton ℓ and all preselected jets,

$$\Delta R_{\mathrm{min}}(\mathrm{jet}, \ell) = \min\left(\Delta R(\mathrm{jet}_1, \ell), \Delta R(\mathrm{jet}_2, \ell), \ldots, \Delta R(\mathrm{jet}_n, \ell)\right), \tag{6.1}$$

is used to reduce the background coming from misidentified or non-prompt leptons in the soft-lepton signal region with three jets and in the soft dimuon signal region. In the latter case, the subleading signal muon is used to compute ΔR_{min}. As the expected signal jet multiplicity grows, the ΔR_{min} requirement starts to impair the signal acceptance; this requirement is hence not applied in the soft-lepton 5-jet and 3-jet inclusive signal regions (see table 2).

The dilepton mass $m_{\ell\ell}$ for leptons of the same flavour and opposite charge is required to be outside the Z boson mass window in the soft and hard dileptonic channels in order to reject background events in which a real Z boson decays to leptons.

The transverse mass (m_{T}) of the lepton (ℓ) and $\boldsymbol{p}_{\mathrm{T}}^{\mathrm{miss}}$ is defined as

$$m_{\mathrm{T}} = \sqrt{2 p_{\mathrm{T}}^{\ell} E_{\mathrm{T}}^{\mathrm{miss}} (1 - \cos[\Delta\phi(\vec{\ell}, \boldsymbol{p}_{\mathrm{T}}^{\mathrm{miss}})])}, \tag{6.2}$$

and is used in all signal regions to reject events containing a $W \to \ell\nu$ decay, except in the hard dilepton signal regions where this background is expected to be small. In the soft dimuon channel, the transverse mass is defined using the subleading muon.

JHEP04(2015)116

	Single-bin (binned) soft single-lepton			Soft dimuon
	3-jet	**5-jet**	**3-jet inclusive**	**2-jet**
N_ℓ	1 electron or muon			2 muons
p_{T}^{ℓ}[GeV]	[7,25] for electron, [6,25] for muon			[6,25]
Lepton veto	No additional electron or muon with $p_{\mathrm{T}}>$ 7 GeV or 6 GeV, respectively			
$m_{\mu\mu}$ [GeV]	–	–	–	[15,60]
N_{jet}	[3,4]	≥ 5	≥ 3	≥ 2
$p_{\mathrm{T}}{}^{\mathrm{jet}}$[GeV]	$>$ 180, 25, 25	$>$ 180, 25, 25, 25, 25	$>$ 130, 100, 25	$>$ 80, 25
$N_{b-\mathrm{tag}}$	–	–	0	0
$E_{\mathrm{T}}^{\mathrm{miss}}$ [GeV]	$>$400	$>$300	$>$ 180	
m_{T} [GeV]	$>$ 100		$>$120	$>$ 40
$E_{\mathrm{T}}^{\mathrm{miss}}/m_{\mathrm{eff}}^{\mathrm{incl}}$	$>$ 0.3 (0.1)		$>$ 0.1	$>$ 0.3
$\Delta R_{\mathrm{min}}(\mathrm{jet},\ell)$	$>$ 1.0	–	–	$>$ 1.0 (2nd muon)
Binned variable	($E_{\mathrm{T}}^{\mathrm{miss}}/m_{\mathrm{eff}}^{\mathrm{incl}}$ in 4 bins)			–
Bin width	(0.1, 4th is inclusive)			–

Table 2. Overview of the selection criteria for the soft single-lepton and dimuon signal regions. For each jet multiplicity in the single-lepton channel, two sets of requirements are defined, corresponding to single-bin and binned signal regions (see the text at the end of section 6.1). The requirements of the binned signal region are shown in parentheses when they differ from those of the single-bin signal region. The variables $\Delta R_{\mathrm{min}}(\mathrm{jet},\ell)$, m_{T} and $m_{\mathrm{eff}}^{\mathrm{incl}}$ are defined in equations (6.1)), (6.2) and (6.3), respectively.

The inclusive effective mass ($m_{\mathrm{eff}}^{\mathrm{inc}}$) is the scalar sum of the p_{T} of the lepton(s), the jets and $E_{\mathrm{T}}^{\mathrm{miss}}$:

$$m_{\mathrm{eff}}^{\mathrm{inc}} = \sum_{i=1}^{N_\ell} p_{\mathrm{T},i}^{\ell} + \sum_{j=1}^{N_{\mathrm{jet}}} p_{\mathrm{T},j} + E_{\mathrm{T}}^{\mathrm{miss}} \tag{6.3}$$

where the index i identifies all the signal leptons and the index j all the signal jets in the event. The inclusive effective mass is correlated with the overall mass scale of the hard scattering and provides good discrimination against SM backgrounds, without being too sensitive to the details of the SUSY decay cascade. It is used in the hard single-lepton channel.

The ratio $E_{\mathrm{T}}^{\mathrm{miss}}/m_{\mathrm{eff}}^{\mathrm{inc}}$ is used in the soft-lepton signal regions; it reflects the change in the $E_{\mathrm{T}}^{\mathrm{miss}}$ resolution as a function of the calorimeter activity in the event. In the hard single-lepton channel, a similar ratio is computed, $E_{\mathrm{T}}^{\mathrm{miss}}/m_{\mathrm{eff}}^{\mathrm{excl}}$, where the exclusive effective mass, $m_{\mathrm{eff}}^{\mathrm{excl}}$, is defined in a similar way to $m_{\mathrm{eff}}^{\mathrm{inc}}$, with the exception that only the three leading signal jets are considered. This variable is used to remove events with large $E_{\mathrm{T}}^{\mathrm{miss}}$ coming from a poorly reconstructed jet.

Razor variables [110] are used in the hard dilepton signal region. They are a set of kinematic variables that exploit the symmetry in the visible portion of sparticle decays when sparticles are produced in pairs. The final-state jets and leptons are grouped into two "mega-jets", where all visible objects from one side of the di-sparticle decay are collected

JHEP04(2015)116

	Single-bin (binned) hard single-lepton		
	3-jet	**5-jet**	**6-jet**
N_ℓ	1 electron or muon		
p_{T}^{ℓ}[GeV]	> 25		
Lepton veto	${p_{\mathrm{T}}}^{2^{\mathrm{nd}}\mathrm{lepton}} < 10$ GeV		
N_{jet}	≥ 3	≥ 5	≥ 6
${p_{\mathrm{T}}}^{\mathrm{jet}}$[GeV]	$> 80, 80, 30$	$> 80, 50, 40, 40, 40$	$> 80, 50, 40, 40, 40, 40$
Jet veto	(${p_{\mathrm{T}}}^{5^{\mathrm{th}}\mathrm{jet}} < 40$ GeV)	(${p_{\mathrm{T}}}^{6^{\mathrm{th}}\mathrm{jet}} < 40$ GeV)	–
$E_{\mathrm{T}}^{\mathrm{miss}}$ [GeV]	>500 (300)	>300	>350 (250)
m_{T} [GeV]	> 150	> 200 (150)	> 150
$E_{\mathrm{T}}^{\mathrm{miss}}/m_{\mathrm{eff}}^{\mathrm{excl}}$	> 0.3	–	–
$m_{\mathrm{eff}}^{\mathrm{incl}}$ [GeV]	> 1400 (800)		> 600
Binned variable	($m_{\mathrm{eff}}^{\mathrm{incl}}$ in 4 bins)		($E_{\mathrm{T}}^{\mathrm{miss}}$ in 3 bins)
Bin width	(200 GeV, 4th is inclusive)		(100 GeV, 3rd is inclusive)

Table 3. Overview of the selection criteria for the hard single-lepton signal regions. For each jet multiplicity, two sets of requirements are defined, corresponding to single-bin and binned signal regions (see the text at the end of section 6.1). The requirements of the binned signal region are shown in parentheses when they differ from those of the single-bin signal region. The variables m_{T} and $m_{\mathrm{eff}}^{\mathrm{incl}}$ are defined in equations (6.2) and (6.3), respectively, while $m_{\mathrm{eff}}^{\mathrm{excl}}$ is defined in the text.

	Single-bin (binned) hard dilepton			
	Low-multiplicity ($\leq$ 2-jet)		**3-jet**	
	$ee/\mu\mu$	$e\mu$	$ee/\mu\mu$	$e\mu$
N_ℓ	2, 2 of opposite sign or ≥ 2			
p_{T}^{ℓ}[GeV]	>14,10			
$N_{\ell\ell}$ with 81< $m_{\ell\ell}$ <101 GeV	0	–	0	–
N_{jet}	≤ 2		≥ 3	
${p_{\mathrm{T}}}^{\mathrm{jet}}$[GeV]	$> 50,50$		$> 50, 50, 50$	
$N_{b-\mathrm{tag}}$	0			
R	>0.5		>0.35	
$M_R^{'}$ [GeV]	> 600 (> 400 in 8 bins)		> 800 (> 800 in 5 bins)	
$M_R^{'}$ bin width [GeV]	(100, the last is inclusive)			

Table 4. Overview of the selection criteria for the hard dilepton signal regions. The requirements on the number and charge of the leptons depend on the model probed (see the text). For each jet multiplicity, two sets of requirements are defined, corresponding to single-bin and binned signal regions (see the text at the end of section 6.1). The requirements of the binned signal region are shown in parentheses when they differ from those of the single-bin signal region. The variables $M_R^{'}$ and R are defined in equations (6.4) and (6.6), respectively.

JHEP04(2015)116

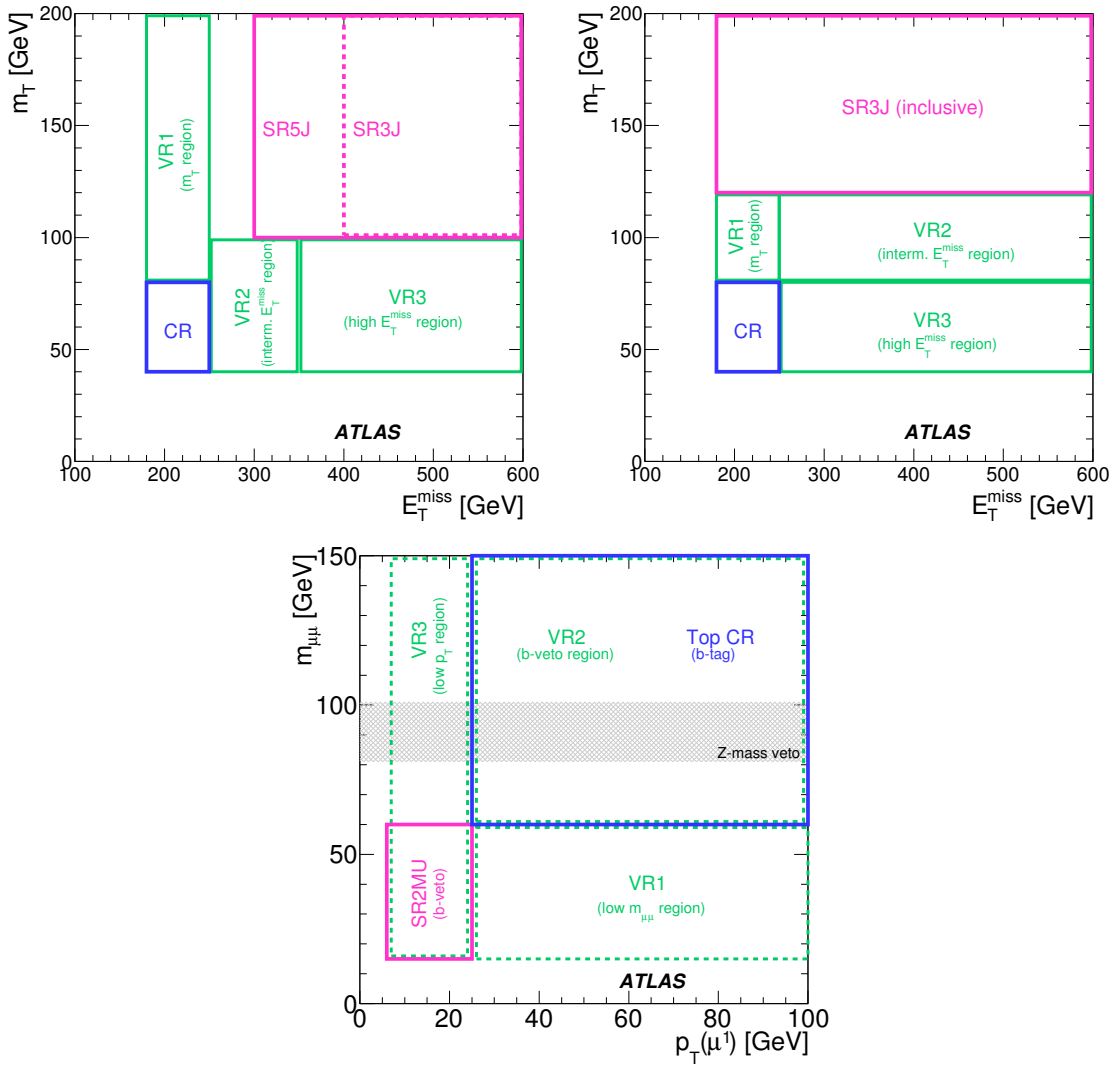

Figure 2. Graphical illustration of the soft lepton signal regions (SR) used in this paper. The soft single-lepton signal regions are shown in the plane of transverse mass m_{T} (see equation (6.2)) versus missing transverse momentum $E_{\mathrm{T}}^{\mathrm{miss}}$: the 3- and 5-jet regions are depicted in the upper left plot while the 3-jet inclusive region is shown in the upper right plot; the soft dimuon signal region is shown in the bottom plot in the plane of the dimuon mass, $m_{\mu\mu}$, versus the p_{T} of the leading muon, $p_{\mathrm{T}}(\mu^1)$. The control regions (CR) and validation regions (VR) described in sections 7 and 9, respectively, are also shown.

together to create a single four-vector, representing the decay products of a single sparticle. The mega-jet construction involves iterating over all possible combinations of the four-vectors of the visible reconstructed objects, with the favoured combination being that which minimises the sum of the squared masses of the mega-jet four-vectors. Using this mega-jet configuration, with some simplifying assumptions (e.g. symmetric sparticle production), the rest frame of the sparticles (the so-called "R-frame" described in ref. [110]) can be

JHEP04(2015)116

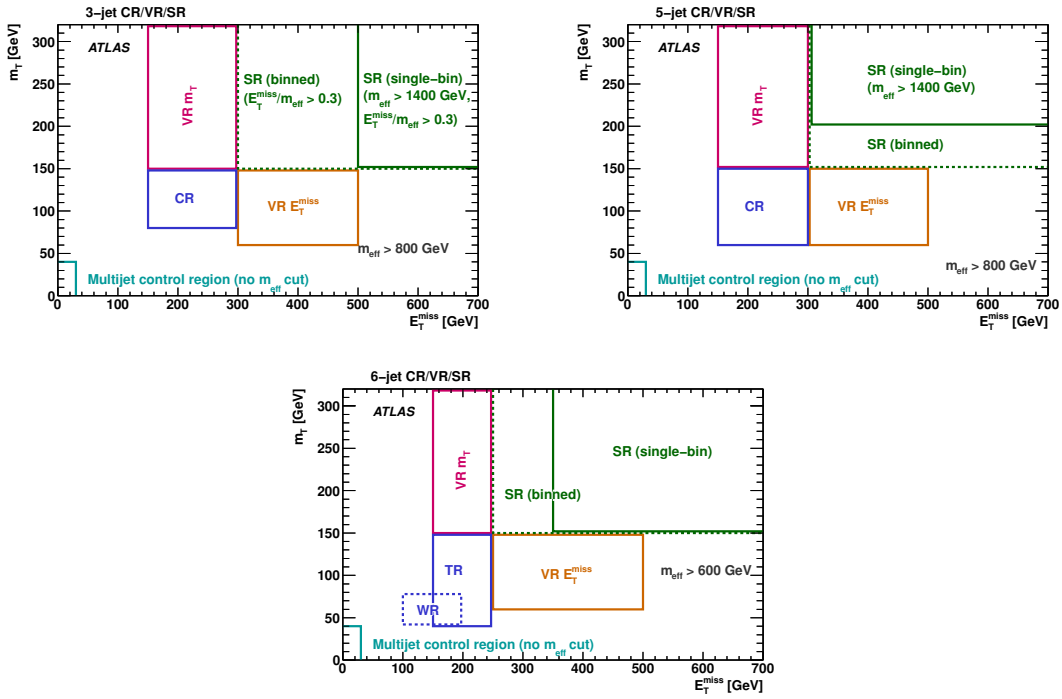

Figure 3. Graphical illustration of the hard single-lepton 3-jet (top left), 5-jet (top right) and 6-jet (bottom) signal regions (SR) used in this paper, shown in the plane of transverse mass m_{T} (see equation (6.2)) versus missing transverse momentum $E_{\mathrm{T}}^{\mathrm{miss}}$. The control regions (CR) and validation regions (VR) described in sections 7 and 9, respectively, are also shown.

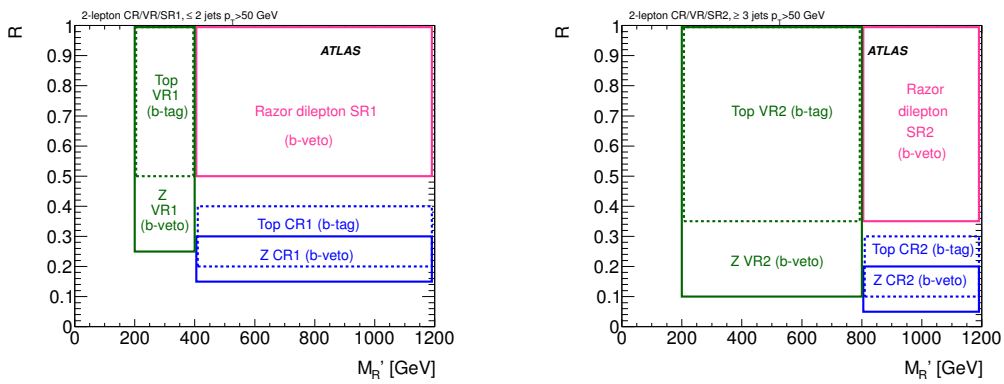

Figure 4. Graphical illustration of the hard dilepton signal regions (SR) used in this paper. The low-multiplicity (left) and 3-jet (right) hard dilepton signal regions are shown in the plane of R-frame mass M_R' versus razor variable R (see equations (6.2) and (6.6)). The control regions (CR) and validation regions (VR) described in sections 7 and 9, respectively, are also shown.

JHEP04(2015)116

Model	Soft		Hard	
	single-lepton	dimuon	single-lepton	dilepton
mSUGRA/CMSSM			✓	
bRPV mSUGRA/CMSSM			✓	
nGM			✓	
NUHMG			✓	
mUED		✓		✓
$\tilde{g}\tilde{g}$ production, $\tilde{g} \to tc\tilde{\chi}_1^0$			✓	
$\tilde{g}\tilde{g}$ production, $\tilde{g} \to t\bar{t}\tilde{\chi}_1^0$			✓	
$\tilde{g}\tilde{g}$ production, $\tilde{g} \to qqW\tilde{\chi}_1^0$	✓		✓	
$\tilde{q}\tilde{q}$ production, $\tilde{q} \to qW\tilde{\chi}_1^0$	✓		✓	
$\tilde{g}\tilde{g}$ production, $\tilde{g} \to qq(\ell\ell/\ell\nu/\nu\nu)\tilde{\chi}_1^0$			✓	✓
$\tilde{q}\tilde{q}$ production, $\tilde{q} \to q(\ell\ell/\ell\nu/\nu\nu)\tilde{\chi}_1^0$				✓
$\tilde{g}\tilde{g}$ production, $\tilde{g} \to qqWZ\tilde{\chi}_1^0$			✓	

Table 5. Analysis channels used to probe each of the models described in section 3.1.

reconstructed, and a characteristic mass M'_R can be defined in this frame:

$$M'_R = \sqrt{(j_{1,E} + j_{2,E})^2 - (j_{1,\mathrm{L}} + j_{2,\mathrm{L}})^2}, \tag{6.4}$$

where $j_{i,\mathrm{L}}$ denotes the longitudinal momentum, and $j_{i,E}$ the energy in the R-frame, of the mega-jet i. The transverse information of the event is contained in another variable, M_T^R. In the di-sparticle decay there are two mega-jets, each with associated $E_\mathrm{T}^\mathrm{miss}$ from the escaping LSPs. Assigning half of the missing transverse momentum per event to each of the LSPs, M_T^R is defined as

$$M_\mathrm{T}^R = \sqrt{\frac{|\boldsymbol{p}_\mathrm{T}^\mathrm{miss}|(|\vec{j}_{1,\mathrm{T}}| + |\vec{j}_{2,\mathrm{T}}|) - \boldsymbol{p}_\mathrm{T}^\mathrm{miss} \cdot (\vec{j}_{1,\mathrm{T}} + \vec{j}_{2,\mathrm{T}})}{2}}, \tag{6.5}$$

where $j_{i,\mathrm{T}}$ denotes the transverse momentum of the mega-jet i.

Finally, the razor variable is defined as:

$$R = \frac{M_\mathrm{T}^R}{M'_R}. \tag{6.6}$$

For SM processes, R tends to have a low value, while it is approximately uniformly distributed between zero and one for SUSY-like signal events. Thus R can be used as a discriminant between signal and background. A selection using R is made to reduce background processes before a search for new physics phenomena is performed using the distribution of the variable M'_R.

In order to have signal regions which are orthogonal to each other in lepton multiplicity, a veto is placed on the presence of a second lepton in the hard and soft single-lepton channels. Following this veto, all signal regions are orthogonal except the inclusive and

JHEP04(2015)116

exclusive soft single-lepton signal regions and the soft dilepton and hard dilepton signal regions. A veto on the third lepton in the soft dimuon channel is placed to reduce the fake lepton contribution (see section 7). For the hard dilepton channel, the requirements on the number of leptons and on their charge depends on the model probed: in the case of models where only two leptons are expected in the final state, events containing any additional lepton are vetoed. Furthermore, for models with squark pair production followed by one-step decays, only events with opposite-sign dilepton pairs are selected.

In all the search channels except the soft dimuon channel, two sets of requirements are optimised for each jet multiplicity: one single-bin signal region optimised for discovery reach, which is also used to place limits on the visible cross section, and one signal region which is binned in an appropriate variable in order to exploit the expected shape of the distribution of signal events when placing model-dependent limits. The binned variables are: $E_{\mathrm{T}}^{\mathrm{miss}}/m_{\mathrm{eff}}^{\mathrm{incl}}$ in the soft single-lepton regions (four bins of width 0.1), $m_{\mathrm{eff}}^{\mathrm{incl}}$ in the hard single-lepton 3-jet and 5-jet signal regions (four bins of 200 GeV), $E_{\mathrm{T}}^{\mathrm{miss}}$ in the hard single-lepton 6-jet signal region (three bins of 100 GeV) and M_R' in the hard dilepton signal regions (eight bins of 100 GeV in the low-multiplicity signal region and five bins of 100 GeV in the 3-jet signal region). In all regions, the last bin is inclusive. The binned signal regions can differ from the single-binned signal regions in that some requirements may be relaxed. The binned hard single-lepton signal regions are made orthogonal in jet multiplicity to one another by placing a jet veto, as can be seen in table 3, in order to allow their statistical combination and have finer-grained requirements than in a single combined signal region.

7 Background estimation

The dominant background in all the analyses presented here is top quark pair production. The W+jets and Z+jets backgrounds are also important in the single-lepton and hard dilepton channels, respectively. These backgrounds are estimated using control regions optimised to be enriched in SM events from the background process of interest,while containing only a small contribution from the signal of interest, as described below. The normalisation of the simulation for these background processes is obtained simultaneously in all control regions for each signal region using the fit described in section 9. The simulation is thus used only to extrapolate the results to the signal region, and is therefore not affected by potentially large theoretical uncertainties on the total expected rates in specific regions of phase space. The control regions are chosen to be kinematically close to the signal regions in order to minimise the theoretical uncertainties related to the extrapolation, while containing enough events to avoid compromising the background estimate with a large statistical uncertainty.

Events with "fake" or non-prompt leptons can also mimic the signal if they have sufficiently large $E_{\mathrm{T}}^{\mathrm{miss}}$. A jet can be misidentified as a lepton (fake lepton), or a real lepton can arise as a decay product of b- or c-hadrons in jets but can still be sufficiently isolated (non-prompt lepton). Such lepton-like objects are collectively referred to as fake leptons in this paper.

JHEP04(2015)116

7.1 Backgrounds from $t\bar{t}$ and W/Z+jets

The control regions used in the soft single-lepton and soft dimuon channels are illustrated in figure 2 and summarised precisely in table 6. The soft single-lepton control regions are built using events with lower $E_{\mathrm{T}}^{\mathrm{miss}}$ and m_{T} values than in the signal regions by requiring 180 $< E_{\mathrm{T}}^{\mathrm{miss}} <$ 250 GeV and 40 $< m_{\mathrm{T}} <$ 80 GeV, and by removing the requirement on $E_{\mathrm{T}}^{\mathrm{miss}}/m_{\mathrm{eff}}^{\mathrm{incl}}$. The W+jets and $t\bar{t}$ background components in these control regions are separated by a requirement on the number of b-tagged signal jets. Events in the $t\bar{t}$ control region are defined by requiring that at least one signal jet is b-tagged; otherwise, they are associated with the W+jets control region.

In the soft dimuon analysis, the $t\bar{t}$ control region is defined by requiring the leading muon to have $p_{\mathrm{T}} > 25$ GeV instead of $p_{\mathrm{T}} < 25$ GeV. The veto on b-tagged jets is reversed to require at least one b-tagged signal jet among the three leading jets and the requirement on $E_{\mathrm{T}}^{\mathrm{miss}}/m_{\mathrm{eff}}^{\mathrm{incl}}$ is removed. The dimuon mass is required to be higher than in the signal region, $m_{\mu\mu} > 60$ GeV, and at least 10 GeV away from the Z boson mass.

The hard single-lepton control regions are defined by lowering the requirements on $E_{\mathrm{T}}^{\mathrm{miss}}$ and m_{T} and by removing the $E_{\mathrm{T}}^{\mathrm{miss}}/m_{\mathrm{eff}}^{\mathrm{excl}}$ requirement in the 3-jet region. Table 7 lists the control region requirements which differ from the signal region selections for the hard single-lepton channel. These various control regions are illustrated in figure 3. The different regions are kept orthogonal by vetoing on the presence of a fifth (sixth) jet in the 3 (5)-jet control region. To increase the number of events, the p_{T} requirements on subleading jets are also lowered with respect to the signal regions. Finally, the W+jets and $t\bar{t}$ components of these control regions are separated by a requirement on the number of signal jets which are b-tagged, considering the first three leading jets. In order to enhance the W+jets contribution over the $t\bar{t}$ contribution in the 6-jet W+jets control region, the m_{T} and $E_{\mathrm{T}}^{\mathrm{miss}}$ requirements are lowered in this region with respect to the 6-jet $t\bar{t}$ control region.

As summarised in table 8 and illustrated in figure 4, the control regions for the hard dilepton channel are defined at lower values of the R variable for events in which there are exactly two leptons of opposite sign in order to enhance the background processes. The Z+jets and $t\bar{t}$ components of these control regions are separated by a requirement on the number of signal jets which are b-tagged. The control regions are binned in the discriminating variable $M_R^{'}$ in order to use the same shape information as in the signal regions.

The $t\bar{t}$ control regions in all channels include a small fraction of at most 11% of Wt events; this background is not normalised by the fit in the control region, but evaluated directly from simulation, as are other lower-rate background processes involving top quarks (see section 7.3).

Figures 5–7 show the m_{T} and $m_{\mu\mu}$ distributions, prior to the upper m_{T} and lower $m_{\mu\mu}$ cuts, in the soft single-lepton and soft dimuon control regions, respectively. Figures 8 and 9 show the $E_{\mathrm{T}}^{\mathrm{miss}}$ distribution, prior to the upper $E_{\mathrm{T}}^{\mathrm{miss}}$ cut, in the hard single-lepton control regions. Figure 10 shows the R distribution in the hard dilepton control regions. All these distributions are shown after the fitting procedure is applied to adjust the MC normalisation, as described in section 9. For illustration, examples of expected signal distributions are also shown in these figures. The fraction of events in the control regions

JHEP04(2015)116

	Soft single-lepton			Soft dimuon
	3-jet	**5-jet**	**3-jet inclusive**	**2-jet**
	W+**jets** / $t\bar{t}$			$t\bar{t}$
p_{T}^{ℓ}[GeV]	[7,25] (electron) , [6,25] (muon)			>25,6
$m_{\mu\mu}$ [GeV]	–			> 60, $\lvert m_{\mu\mu} - m_Z \rvert > 10$
$N_{b-\mathrm{tag}}$	0 / ≥ 1			≥ 1
$E_{\mathrm{T}}^{\mathrm{miss}}$ [GeV]	[180,250]			> 180
m_{T} [GeV]	[40,80]			> 40
$\Delta R_{\mathrm{min}}(\mathrm{jet}, \ell)$	> 1.0	–	–	> 1.0

Table 6. Overview of the selection criteria for the CR used in the soft single-lepton and soft dimuon channels: only the criteria which differ from the corresponding signal region selections in at least one CR are shown (see figure 2 for an illustration of the above CRs).

	Hard single-lepton		
	3-jet	**5-jet**	**6-jet**
	W+**jets** / $t\bar{t}$		
$p_{\mathrm{T}}{}^{\mathrm{jet}}$[GeV]	> 80, 80, 30	> 80, 50, 30, 30, 30	> 80, 50, 30, 30, 30, 30
Jet veto	$p_{\mathrm{T}}{}^{5^{\mathrm{th}}\mathrm{jet}} < 30$ GeV	$p_{\mathrm{T}}{}^{6^{\mathrm{th}}\mathrm{jet}} < 30$ GeV	–
$N_{b-\mathrm{tag}}$	0 / ≥ 1		
$E_{\mathrm{T}}^{\mathrm{miss}}$ [GeV]	[150,300]		[100,200] / [150,250]
m_{T} [GeV]	[80,150]	[60,150]	[40,80] / [40,150]
$E_{\mathrm{T}}^{\mathrm{miss}}/m_{\mathrm{eff}}^{\mathrm{excl}}$	–	–	–

Table 7. Overview of the selection criteria for the W+jets and $t\bar{t}$ CR used in the hard single-lepton channel: only the criteria which differ from the corresponding signal region selections in at least one CR are shown (see figure 3 for an illustration of the above CRs).

coming from the background of interest, hereafter called purity, is given in the caption of these figures. As the normalisation factors are obtained in a simultaneous fit to all control regions for a given signal region, the cross-contamination of the control regions with different processes is taken into account and lower purity in some regions does not degrade significantly the accuracy of the background estimation. The agreement between the data and the SM background estimate is reasonable within the statistical and systematic uncertainties. The systematic uncertainties shown do not include an uncertainty on the cross sections of the backgrounds that are normalised using the fitting procedure, but do include the relevant theoretical uncertainties on the extrapolation of the background normalisation obtained from each CR to the relevant SR (see section 8). The results of the fit, in particular the signal region predictions, are further discussed in section 10.

JHEP04(2015)116

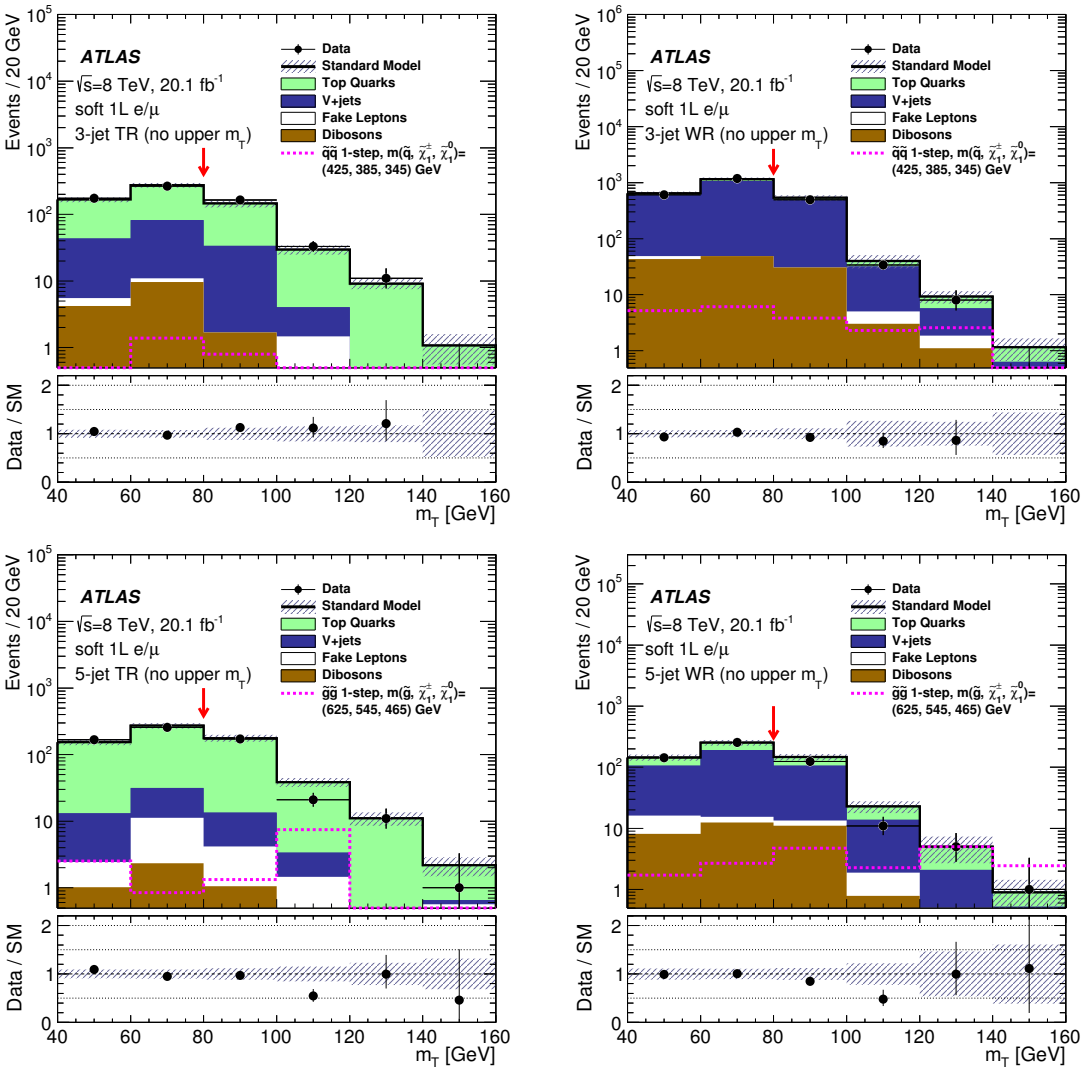

Figure 5. Distribution of the transverse mass m_{T} in the 3-jet (top) and 5-jet (bottom) $t\bar{t}$ (left) and W+jets (right) control regions used in the soft single-lepton channel. The upper m_{T} cut, indicated by the arrow, is not applied in these distributions. The purity in the background of interest is 56% (87%) for the 3-jet $t\bar{t}$ (W) control region and 82% (66%) for the 5-jet $t\bar{t}$ (W) control region. The "Data/SM" plots show the ratio of data to the summed Standard Model expectation, which is derived from the fit described in section 9. The uncertainty band on the Standard Model expectation shown here combines the statistical uncertainty on the simulated event samples with the relevant systematic uncertainties (see text). The last bin includes the overflow. The "Top Quarks" label includes all top-quark-related backgrounds, while "V+jets" includes W+jets, Z+jets and other Drell-Yan backgrounds such as $Z \to \tau^+\tau^-$ and γ^*/Z outside the Z pole region. For illustration, the expected signal distribution is shown for first- and second-generation squark pair production with $m_{\tilde{q}} = 425$ GeV, $m_{\tilde{\chi}_1^\pm} = 385$ GeV and $m_{\tilde{\chi}_1^0} = 345$ GeV (top), and for gluino pair production with $m_{\tilde{g}} = 625$ GeV, $m_{\tilde{\chi}_1^\pm} = 545$ GeV and $m_{\tilde{\chi}_1^0} = 465$ GeV (bottom).

JHEP04(2015)116

	Hard dilepton					
	Low-multiplicity			3-jet		
	$ee/\mu\mu$		$e\mu$	$ee/\mu\mu$		$e\mu$
	Z CR	$t\bar{t}$ CR	$t\bar{t}$ CR	Z CR	$t\bar{t}$ CR	$t\bar{t}$ CR
N_ℓ	2 of opposite sign					
$N_{b-\mathrm{tag}}$	0	1		0	1	
R	[0.15,0.3]	[0.2,0.4]		[0.05,0.2]	[0.1,0.3]	
$M_R^{'}$ [GeV]	[400,1200]			[800,1600]		
$M_R^{'}$ bin width [GeV]	100			200		

Table 8. Overview of the selection criteria for the Z+jets and $t\bar{t}$ CR used in the hard dilepton channel: only the criteria which differ from the corresponding signal region selections in at least one CR are shown (see figure 4 for an illustration of the above CRs).

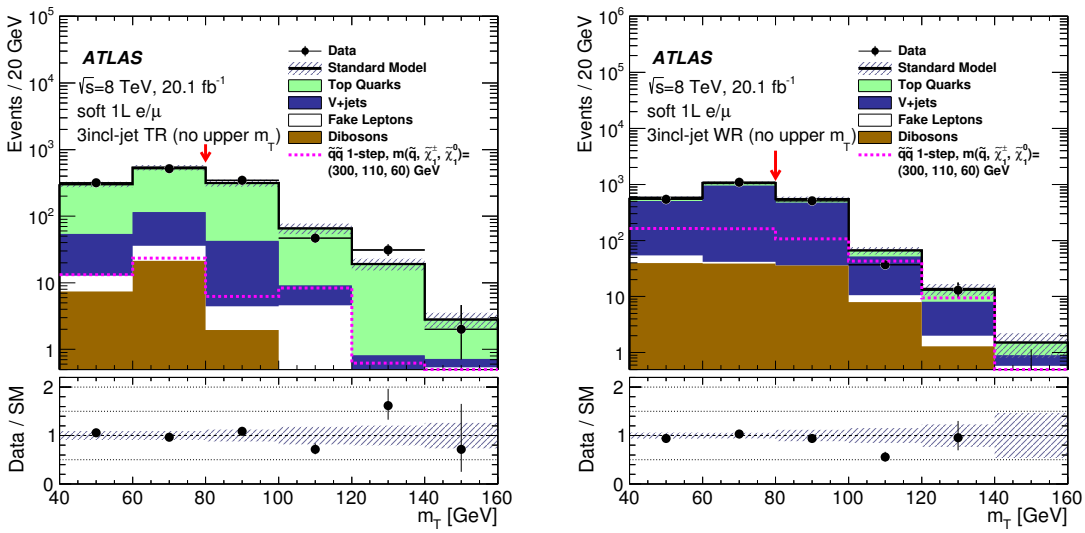

Figure 6. Distribution of the transverse mass m_{T} in the 3-jet inclusive $t\bar{t}$ (left) and W+jets (right) control regions used in the soft single-lepton channel. The upper m_{T} cut, indicated by the arrow, is not applied in these distributions. The purity in the background of interest is 70% (82%) for $t\bar{t}$ (W) control region. The "Data/SM" plots show the ratio of data to the summed Standard Model expectation, which is derived from the fit described in section 9. The uncertainty band on the Standard Model expectation shown here combines the statistical uncertainty on the simulated event samples with the relevant systematic uncertainties (see text). The last bin includes the overflow. The "Top Quarks" label includes all top-quark-related backgrounds, while "V+jets" includes W+jets, Z+jets and other Drell-Yan backgrounds such as $Z \to \tau^+\tau^-$ and γ^*/Z outside the Z pole region. For illustration, the expected signal distribution is shown for first- and second-generation squark pair production with $m_{\tilde{q}} = 300$ GeV, $m_{\tilde{\chi}_1^\pm} = 110$ GeV and $m_{\tilde{\chi}_1^0} = 60$ GeV.

JHEP04(2015)116

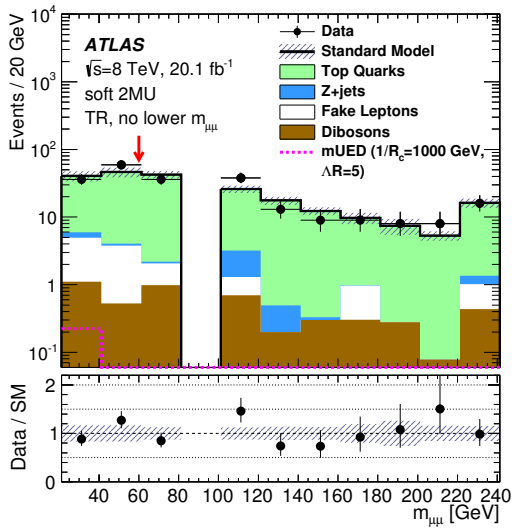

Figure 7. Distribution of the dimuon invariant mass $m_{\mu\mu}$ in the $t\bar{t}$ control region used in the soft dimuon channel. The lower $m_{\mu\mu}$ cut, indicated by the arrow, is not applied in this distribution. The purity in $t\bar{t}$ is 83% for this region. The "Data/SM" plots show the ratio of data to the summed Standard Model expectation, which is derived from the fit described in section 9. The uncertainty band on the Standard Model expectation shown here combines the statistical uncertainty on the simulated event samples with the relevant systematic uncertainties (see text). The last bin includes the overflow. The "Top Quarks" label includes all top-quark-related backgrounds, while "V+jets" includes W+jets, Z+jets and other Drell-Yan backgrounds such as $Z \to \tau^+\tau^-$ and γ^*/Z outside the Z pole region. For illustration, the expected signal distribution of the mUED model point with $R_c^{-1} = 1000$ GeV and $\Lambda R_c = 5$ is also shown.

7.2 Fake-lepton background

The multijet and $Z(\to \nu\nu)$+jets processes are important sources of fake-lepton background in the single-lepton analyses, while $W(\to \ell\nu)$+jets and $t\bar{t}$ production (where one of the leptons comes from a W boson decay and the other is from a b-hadron decay) are expected to dominate the fake-lepton background in the soft dimuon and hard dilepton analyses.

The fake-lepton background in the signal region as well as in the control regions, where it is more significant, is estimated entirely from the data by means of a matrix method described in ref. [111] and briefly summarised below; the procedure is applied separately for electrons and muons.

In this method, the process creating the fake lepton is enhanced in a control sample where preselected leptons are used instead of the signal leptons, and all signal or control region criteria are applied. If N_{pass} and N_{fail} are the number of events found passing or failing the signal lepton selection in this control sample, then the number of events with a fake lepton in a single-lepton signal or control region is given by:

$$N_{\text{pass}}^{\text{fake}} = \frac{N_{\text{fail}} - (1/\epsilon^{\text{real}} - 1)N_{\text{pass}}}{1/\epsilon^{\text{fake}} - 1/\epsilon^{\text{real}}} \tag{7.1}$$

where ϵ^{real} is the relative identification efficiency (from preselection to selection) for prompt leptons and ϵ^{fake} is the probability to misidentify jets or non-prompt leptons as prompt

JHEP04(2015)116

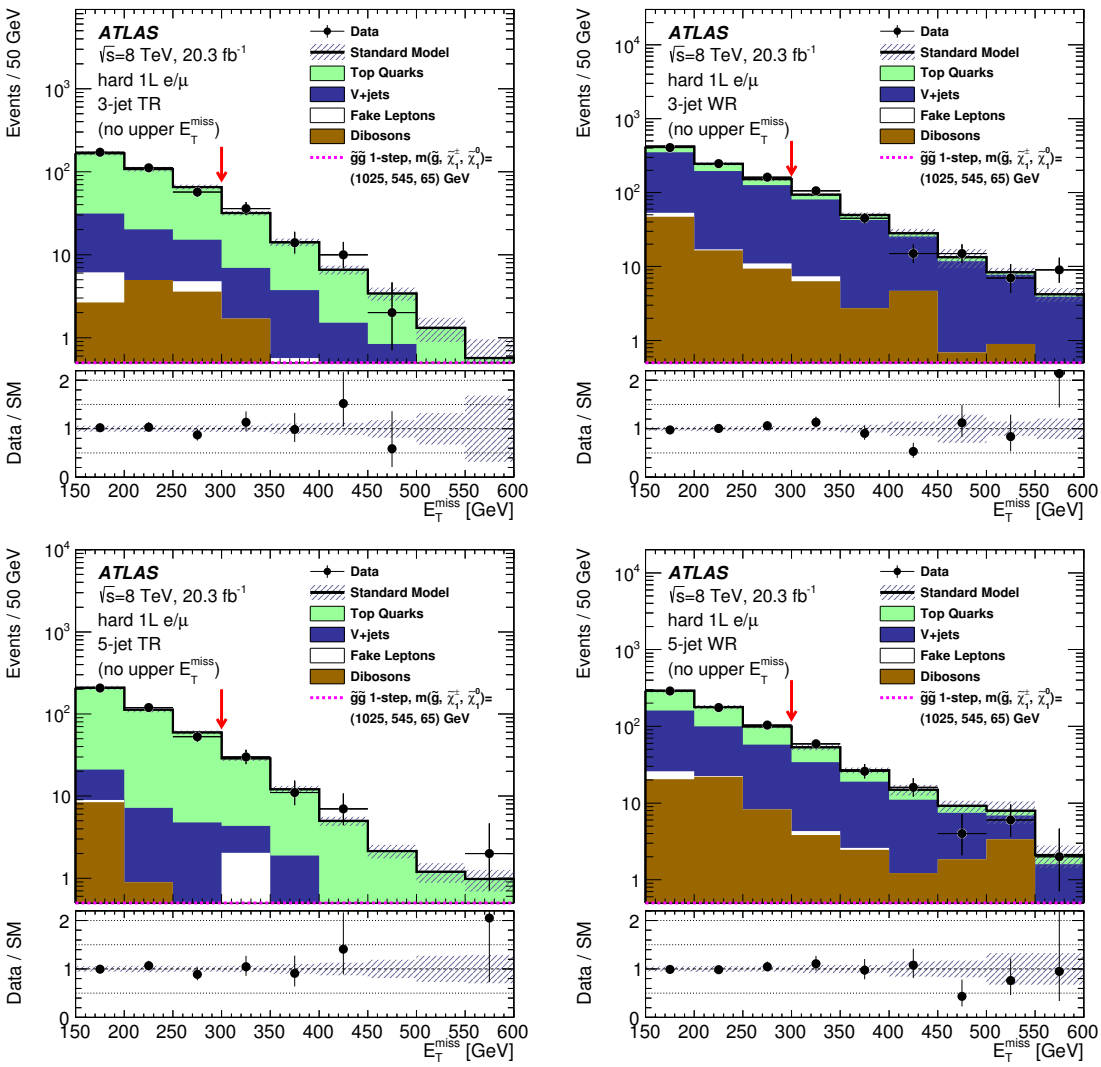

Figure 8. Distribution of the missing transverse momentum $E_{\mathrm{T}}^{\mathrm{miss}}$ in the 3-jet (top) and 5-jet (bottom) $t\bar{t}$ (left) and W+jets (right) control regions used in the hard single-lepton channel. The upper $E_{\mathrm{T}}^{\mathrm{miss}}$ cut, indicated by the arrow, is not applied in these distributions. The purity in the background of interest is 66% (72%) for the 3-jet $t\bar{t}$ (W) control region and 81% (45%) for the 5-jet $t\bar{t}$ (W) control region; the 5-jet W control region is cross-contaminated by $t\bar{t}$ events at the level of 40%. The "Data/SM" plots show the ratio of data to the summed Standard Model expectation, which is derived from the fit described in section 9. The uncertainty band on the Standard Model expectation shown here combines the statistical uncertainty on the simulated event samples with the relevant systematic uncertainties (see text). The last bin includes the overflow. The "Top Quarks" label includes all top-quark-related backgrounds, while "V+jets" includes W+jets, Z+jets and other Drell-Yan backgrounds such as $Z \to \tau^+\tau^-$ and γ^*/Z outside the Z pole region. For illustration, the expected signal distributions are shown for gluino pair production with $m_{\tilde{g}} = 1025\,\mathrm{GeV}, m_{\tilde{\chi}_1^\pm} = 545\,\mathrm{GeV}$ and $m_{\tilde{\chi}_1^0} = 65\,\mathrm{GeV}$.

JHEP04(2015)116

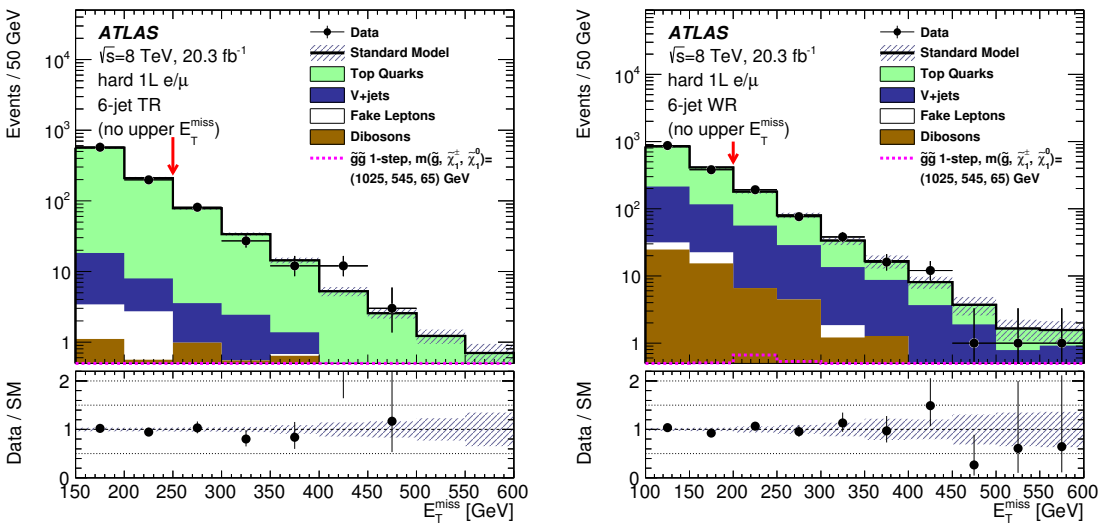

Figure 9. Distribution of the missing transverse momentum $E_{\mathrm{T}}^{\mathrm{miss}}$ in 6-jet $t\bar{t}$ (left) and W+jets (right) control regions used in the hard single-lepton channel. The upper $E_{\mathrm{T}}^{\mathrm{miss}}$ cut, indicated by the arrow, is not applied in these distributions. The purity in the background of interest is 90% (21%) for the $t\bar{t}$ (W) control region; the W control region is cross-contaminated by $t\bar{t}$ events at the 70% level. The "Data/SM" plots show the ratio of data to the summed Standard Model expectation, which is derived from the fit described in section 9. The uncertainty band on the Standard Model expectation shown here combines the statistical uncertainty on the simulated event samples with the relevant systematic uncertainties (see text). The last bin includes the overflow. The "Top Quarks" label includes all top-quark-related backgrounds, while "V+jets" includes W+jets, Z+jets and other Drell-Yan backgrounds such as $Z \to \tau^+\tau^-$ and γ^*/Z outside the Z pole region. For illustration, the expected signal distributions are shown for gluino pair production with $m_{\tilde{g}} = 1025\,\mathrm{GeV}, m_{\tilde{\chi}_1^\pm} = 545\,\mathrm{GeV}$ and $m_{\tilde{\chi}_1^0} = 65\,\mathrm{GeV}$.

leptons. For dileptonic signal or control regions, the estimation of this background is based on the same principle, this time using a four-by-four matrix to take into account the different fake combinations for the leading and subleading lepton: one prompt and one fake lepton, two fake leptons, or two prompt leptons.

The relative identification efficiency ϵ^{real} is obtained from data in bins of p_{T} and η using a tag-and-probe method in $Z \to \ell\ell$ events. The value of ϵ^{fake} is estimated in control regions enriched in multijet events. The multijet control region is composed of events with at least one preselected lepton and at least one signal jet with $p_{\mathrm{T}} > 60\,\mathrm{GeV}$, $m_{\mathrm{T}} < 40\,\mathrm{GeV}$ and $E_{\mathrm{T}}^{\mathrm{miss}} < 30\,\mathrm{GeV}$. Since the control region is defined at low $E_{\mathrm{T}}^{\mathrm{miss}}$ values, the triggers described in section 4 cannot be used. Instead, a combination of prescaled single-lepton triggers and unprescaled dilepton triggers is used. The prompt lepton contribution is subtracted from this multijet control region using MC simulation and ϵ^{fake} is given by the fraction of preselected leptons passing the signal lepton selection in this region. The events are split into two samples depending on whether they have at least one b-tagged jet or none, in order to allow ϵ^{fake} to vary as a function of the fake-lepton source. The value of ϵ^{fake} is also extracted in bins of p_{T} and η. The same relative efficiencies are used across all analysis channels.

JHEP04(2015)116

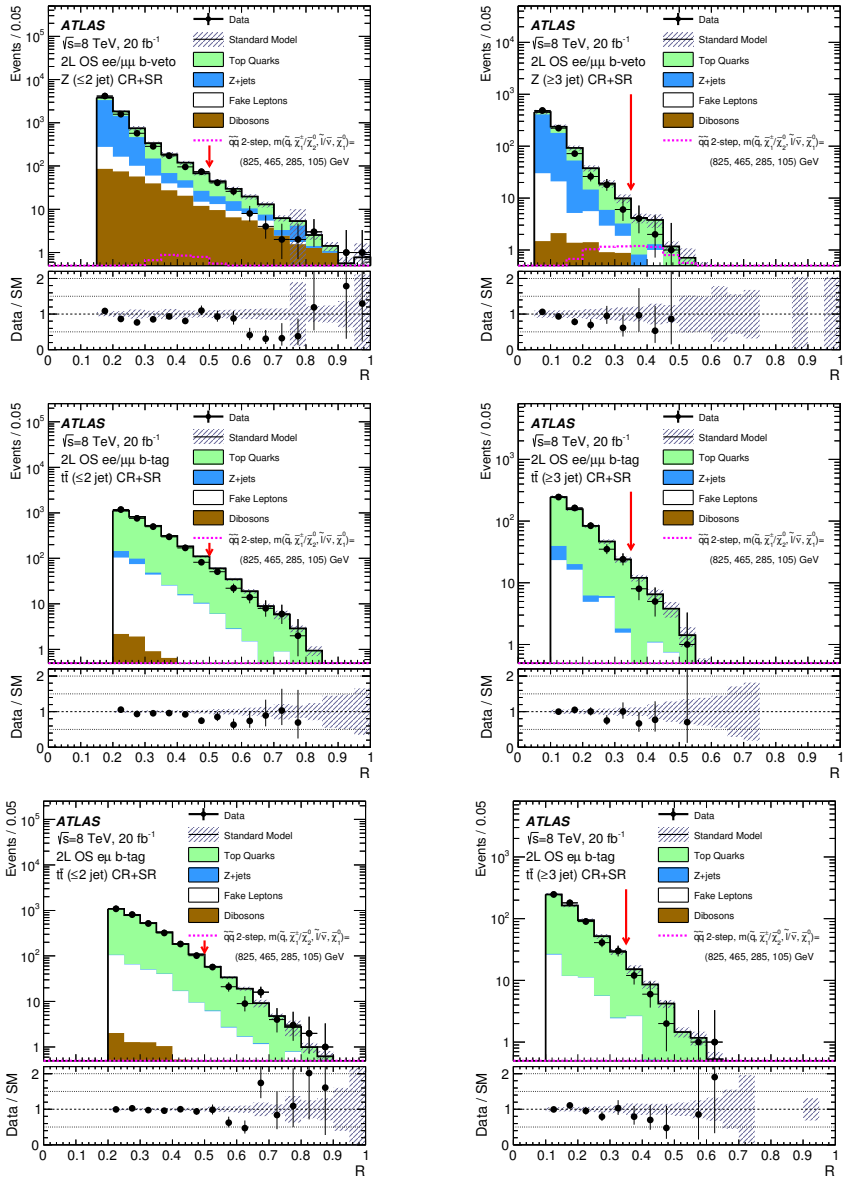

Figure 10. Distribution of the razor variable R in the low-multiplicity (left) and 3-jet (right) Z (top) control region and in the $t\bar{t}$ control region with same-flavour (middle) or opposite-flavour (bottom) leptons used in the hard dilepton channel. The upper cut on R (illustrated by the arrow) separating signal from control regions is not applied in these distributions. The purity in the background of interest is 85% and 75% for the $t\bar{t}$ and Z control regions, respectively. The "Data/SM" plots show the ratio of data to the summed Standard Model expectation, which is derived from the fit described in section 9. The uncertainty band on the Standard Model expectation shown here combines the statistical uncertainty on the simulated event samples with the relevant systematic uncertainties (see text). The "Top Quarks" label includes all top-quark-related backgrounds, while "V+jets" includes W+jets, Z+jets and other Drell-Yan backgrounds such as $Z \to \tau^+\tau^-$ and γ^*/Z outside the Z pole region. For illustration, the expected signal distributions are shown for squark pair production with $m_{\tilde{q}} = 825\,\text{GeV}, m_{\tilde{\chi}_1^\pm/\tilde{\chi}_2^0} = 465\,\text{GeV}, m_{\tilde{\ell}/\tilde{\nu}} = 285\,\text{GeV}$ and $m_{\tilde{\chi}_1^0} = 105\,\text{GeV}$.

JHEP04(2015)116

7.3 Other backgrounds

All other backgrounds are estimated from simulation, using the most accurate theoretical cross sections available. These include single-top (t-channel, s-channel, Wt), $t + Z$, di-bosons (WW, WZ, ZZ, $W\gamma$, $Z\gamma$), $t\bar{t} + W$, $t\bar{t} + Z$ and $t\bar{t} + WW$ production. In the soft dimuon channel, the Drell-Yan and Z+jets backgrounds are also estimated from simulation as there is no dedicated control region to evaluate their contribution.

8 Systematic uncertainties

Systematic uncertainties have an impact on the extrapolation factors used to derive the dominant background yields in the signal regions; they also impact the fake-lepton estimation and the yields of the backgrounds estimated from simulation only, which in turn affect the normalisation of the dominant backgrounds in the control regions. Finally, systematic uncertainties also affect the expected signal yields.

8.1 Experimental uncertainties

The following detector-related systematic uncertainties are taken into account.

Uncertainties on the lepton identification, momentum/energy scale and resolution are estimated from samples of $Z \to \ell^+\ell^-$, $J/\psi \to \ell^+\ell^-$ and $W \to \ell\nu$ decays [101, 102]. The jet energy scale (JES) uncertainty depends on p_{T} and η as well as on the event topology and flavour composition of the jet. It has been obtained from simulation and a combination of test beam and in-situ measurements from pp collisions, as described in refs. [98, 100]. The jet energy resolution (JER) uncertainty has also been estimated using in-situ measurements [112]. The JES and JER uncertainties arising from the high luminosity and pile-up in 2012 data are also taken into account. These jet and lepton uncertainties are propagated to the $E_{\mathrm{T}}^{\mathrm{miss}}$ calculation, which also includes an uncertainty coming from the energy deposits which are not associated with a well-identified physics object [104].

The jet vertex fraction requirement in the identification of signal jets has an associated uncertainty which is assessed by varying the threshold from its nominal value of 0.25 down to 0.21 and up to 0.28 (see ref. [113]).

Uncertainties associated with the b-tagging efficiency are derived from data-driven measurements in $t\bar{t}$ events [107, 114], while uncertainties associated with the probability of mistakenly b-tagging a jet which does not contain a b-hadron are determined using dijet samples [115].

Uncertainties (1–5%) are also assigned to the various trigger efficiencies, based on studies comparing their efficiencies as measured in data to those predicted by simulation.

Finally, uncertainties are also assigned to the fake-lepton background estimation, including a statistical uncertainty on the number of events in the control samples and an uncertainty on the relative identification efficiency obtained by comparing its value as measured in $t\bar{t}$ events to the value obtained in $Z \to \ell\ell$ events. In addition, a 20% uncertainty is assigned to the subtraction of the W/Z+jet backgrounds from the control samples used to estimate the relative misidentification efficiency. In the soft dimuon case, the misidentification efficiency is assigned an additional 30% uncertainty which covers the difference

JHEP04(2015)116

obtained when varying the origin of the misidentified prompt leptons (light jets or heavy-flavour jets).

8.2 Theoretical uncertainties on the background estimation

The following theory-related uncertainties are taken into account. For backgrounds with free normalization, the uncertainties affect only the change in the prediction in the VR or SR relative to the yield predicted in the CR.

The uncertainty due to the factorisation and renormalisation scales is computed by varying these scales up and down by a factor of two with respect to the nominal setting. PDF uncertainties are computed following the PDF4LHC recommendations [116].

For the W/Z+jets and $t\bar{t}$ $+W$ samples, an uncertainty derived by comparing samples generated with different numbers of partons is applied to cover the impact of the finite number of partons generated in the nominal samples. For the $t\bar{t}$, single-top and diboson backgrounds, a parton shower modelling uncertainty is evaluated by comparing Pythia to Herwig+Jimmy.

The uncertainty related to the choice of Monte Carlo generator for the $t\bar{t}$ background is derived by comparing powheg+Jimmy to Alpgen+Jimmy samples. For the $t\bar{t}$ and single-top backgrounds, uncertainties on the emission of initial- and final-state radiation (ISR/FSR) are also accounted for by the use of AcerMC+Pythia samples generated with different tunes.

The small contribution to the single-top background from $t + Z$ is assigned a total cross-section uncertainty of 50%, while the other single-top production channels are assigned uncertainties of 3.9% (s-channel [77]), $[+3.9, -2.2]$% (t-channel [76]), and 6.8% (Wt-channel [78]). Samples using diagram subtraction and diagram removal schemes are compared to incorporate interference effects between single-top and $t\bar{t}$ production at NLO. For the Wt channel, a Monte Carlo generator uncertainty is derived from the comparison between powheg and MC@NLO samples. For $t\bar{t}$ $+W$ a total cross-section uncertainty of 22%, derived from ref. [79], is applied.

The WW, WZ and ZZ backgrounds are estimated purely from MC simulation and assigned a 5%, 5% and 7% cross-section uncertainty, respectively, as estimated from missing higher order corrections, and from uncertainties on the PDF and on the value of the strong coupling constant. In addition to this, a generator uncertainty is applied, derived from comparing the nominal powheg diboson samples used in the dileptonic signal regions to samples generated with aMC@NLO [117], in both cases hadronised with Pythia.

For the diboson, single-top and $t\bar{t}$+W backgrounds, the theoretical uncertainties, with the exception of those on the cross section and PDF, are combined and applied as an uncertainty envelope. In the case of the small $t\bar{t}$+Z and $t\bar{t}$+WW backgrounds a total cross-section uncertainty of 50% is applied.

Finally, a statistical uncertainty corresponding to the finite size of the MC samples used is also taken into account.

JHEP04(2015)116

Source	Relative systematic uncertainty (%)			
	Binned soft single-lepton			**Soft dimuon**
	3-jet	**5-jet**	**3-jet inclusive**	**2-jet**
Total systematic uncertainty	20	24	17	43
Lepton identification	–	–	5	–
JER	6	–	–	–
JES (flavour composition)	–	–	–	5
Fake leptons	10	6	5	40
$t\bar{t}$ MC generator	11	9	7	8
$t\bar{t}$ parton shower	–	19	–	–
$t\bar{t}$ scales, ISR and FSR	–	–	9	5
$t\bar{t}$ normalisation	–	7	–	–
MC statistics	8	–	6	7
	Binned hard single-lepton			
	3-jet	**5-jet**	**6-jet**	
Total systematic uncertainty	9	22	24	
$t\bar{t}$ MC generator	–	9	23	
$t\bar{t}$ parton shower	–	17	–	
$t\bar{t}$ scales, ISR and FSR	–	7	–	
$t\bar{t}$ normalisation	5	6	–	
MC statistics	–	5	5	
	Binned hard dilepton			
	Low-multiplicity ($\leq$ 2-jet)		**3-jet**	
	$ee/\mu\mu$	$e\mu$	$ee/\mu\mu$	$e\mu$
Total systematic uncertainty	11	11	23	18
b-tagging	7	6	11	11
JES (in-situ measurement)	–	–	–	5
Fake leptons	5	–	–	–
MC statistics	6	–	–	–

Table 9. The main sources of systematic uncertainty on the SM background estimates for the various signal regions are shown and their value given as relative uncertainties (in %) on the signal region event yields. The values are only shown if the relative uncertainty is at least 5%.

8.3 Dominant uncertainties on the background estimation

The backgrounds in the signal region are estimated using a fit procedure that is described in section 9. The dominant uncertainties, after this procedure is applied, are reported in table 9.

The theoretical uncertainties related to the $t\bar{t}$ background are dominant for all the soft and hard single-lepton signal regions. The fake-lepton background uncertainty is the main uncertainty for the soft dimuon signal region. This uncertainty is also important in

JHEP04(2015)116

the other soft-lepton signal regions, reaching 5–10% of the total event yield. For the hard dilepton signal regions, the dominant uncertainties are those related to b-tagging.

8.4 Theoretical uncertainties on the signal expectation

The mUED model cross sections are based on a calculation at LO in QCD, and the events are generated with a leading order MC event generator. No theoretical uncertainties on the acceptance are considered for this case.

Several theoretical uncertainties on the acceptance for the remaining signal models are taken into account. These uncertainties are estimated using MADGRAPH 5+PYTHIA 6 samples for which the following parameters are varied up and down in turn by a factor of two: the MADGRAPH scale used to determine the event-by-event renormalisation and factorisation scales, the MADGRAPH parameter used to determine the scale for QCD radiation, the PYTHIA parameter which controls the QCD scale value used for final-state radiation (the upward variation of this parameter is by a factor of 1.5) and the MADGRAPH parameter used for jet matching. This results in an uncertainty of $\mathcal{O}(5\%–25\%)$; it is larger for smaller mass differences in the decay cascade and for higher jet multiplicity regions. The uncertainty on the modelling of initial-state radiation plays an important role for small mass differences in the decay cascade in the simplified models.

For all models but mUED, the NLO+NLL cross-section uncertainty is taken from an envelope of cross-section predictions using different PDF sets and factorisation and renormalisation scales, as described in ref. [64]. These uncertainties grow from 15% at low ($\sim 500\,\text{GeV}$) squark and gluino masses up to 25% at $m_{\tilde{q}} = 900\,\text{GeV}$ (30% at $m_{\tilde{g}} = 1150\,\text{GeV}$).

9 Background fit

As discussed in section 7, the background in the signal region is estimated with a fit based on the profile likelihood method [118] using the HistFitter [119] framework. The inputs to the fit, for each of the signal regions, are as follows:

1. The number of events observed in each of the control regions, and the corresponding number of events expected from simulation.

2. The extrapolation factors (obtained from the simulation) which relate the number of predicted W/Z+jets or $t\bar{t}$ events in their associated control region to that predicted in the signal region.

3. The number of fake-lepton events in each region obtained with the data-driven method.

4. The number of events predicted by the simulation in each region for the other backgrounds.

The numbers of observed and predicted events in each of these regions are described using Poisson probability density functions. There are two free parameters considered per

JHEP04(2015)116

signal region: a normalisation scale for the W+jets (or Z+jets) background and another scale for the $t\bar{t}$ background. The other backgrounds are allowed to vary in the fit within their respective uncertainties. The systematic uncertainties (see section 8) and the MC statistical uncertainties on the expected values are included in the fit as nuisance parameters which are constrained by a Gaussian function with a width corresponding to the size of the uncertainty considered and a Poissonian function, respectively. Correlations between these parameters are also taken into account.

The product of the various probability density functions forms the likelihood, which the fit maximises by adjusting the input parameters and the nuisance parameters described above. The fit may introduce a negative correlation between the $t\bar{t}$ and W+jets (or Z+jets) normalisation scales. The relative uncertainty on the individual contributions may therefore increase, but the sum of the contributions is estimated more precisely: the total background relative uncertainty may then be smaller than the sum in quadrature of the individual components.

The background fit results are cross-checked in validation regions defined to be kinematically close to the signal regions but orthogonal to both the control and signal regions. The data in the validation regions are not used to constrain the fits; they are only used to compare the results of the fits to statistically independent observations. The criteria used to define the validation regions are summarised in tables 10–12. The validation regions are also illustrated in figures 2–4. As shown in table 10, the soft single-lepton channel uses three validation regions to probe the m_{T} and $E_{\mathrm{T}}^{\mathrm{miss}}$ extrapolations of each control region (3-jet, 5-jet or 3-jet inclusive W+jets and $t\bar{t}$ regions); there are therefore eighteen validation regions in the soft single-lepton channel. In the soft dimuon case, shown in the same table, three validation regions are defined to cross-check the lepton p_{T} and $m_{\mu\mu}$ extrapolations and the extrapolation from requiring one b-jet in the control region to none in the signal region. In the hard single-lepton channel, each signal region is associated with two validation regions in order to probe the $E_{\mathrm{T}}^{\mathrm{miss}}$ and the m_{T} extrapolations independently, as shown in table 11. Finally, as shown in table 12, in the hard dilepton channel, a total of twelve validation regions are defined to verify the extrapolation in the razor variable R between the various control and signal regions.

The comparison of observed versus predicted event counts in the validation regions as obtained from the background-only fit are summarised in figure 11. More details on the normalisation factors found after the fit are given in section 10.1. Good agreement is seen between the predicted and observed yields in all regions. The systematic uncertainties are correlated across multiple control regions in each channel, see section 8, and are thus correlated for the validation regions in each channel. One of the main sources of systematic uncertainty in the validation regions is the theoretical uncertainty on the $t\bar{t}$ estimation related to the MC generator choice. The conservative uncertainty obtained from the comparison of ALPGEN to POWHEG is correlated across channels and could explain the somewhat small absolute values obtained for the pulls shown in this figure. Furthermore, the 3-jet inclusive soft single-lepton validation regions are not independent of the other soft single-lepton validation regions; the maximum overlap of $\sim 40\%$ occurs between the high-$E_{\mathrm{T}}^{\mathrm{miss}}$ 3-jet inclusive and 3-jet validation regions.

JHEP04(2015)116

	Soft single-lepton			**Soft dimuon**		
	m_{T} region	Interm. $E_{\mathrm{T}}^{\mathrm{miss}}$ region	High $E_{\mathrm{T}}^{\mathrm{miss}}$ region	Low $m_{\mu\mu}$ region	b-veto region	Low p_{T} region
p_{T}^{ℓ}[GeV]	[10,25] (electron), [6,25] (muon)			>25	>25	[6,25]
$N_{b-\mathrm{tag}}$	–			–	0	≥ 1
$E_{\mathrm{T}}^{\mathrm{miss}}$ [GeV]	[180,250]	[250,350] ($>$ 250)	>350 ($>$ 250)	$>$ 180		
m_{T} [GeV]	>80 ([80,120])	[40,100] ([80,120])	[40,100]	$>$ 40		
$m_{\mu\mu}$ [GeV]	–			$<$ 60	$>$ 60	–

Table 10. Validation region definitions for the soft single-lepton and dilepton channels (see figure 2). Only the variables for which the selection differs from the respective control region (see table 6) in at least one validation region are shown. When the 3-jet inclusive selection differs in $E_{\mathrm{T}}^{\mathrm{miss}}$ or in m_{T} from the 3-jet or 5-jet validation regions, the values are shown in parentheses.

	Hard single-lepton					
	3-jet		**5-jet**		**6-jet**	
	$E_{\mathrm{T}}^{\mathrm{miss}}$ **region**	m_{T} **region**	$E_{\mathrm{T}}^{\mathrm{miss}}$ **region**	m_{T} **region**	$E_{\mathrm{T}}^{\mathrm{miss}}$ **region**	m_{T} **region**
${p_{\mathrm{T}}}^{\mathrm{jet}}$[GeV]	$>$ 80, 80, 30		$>$ 80, 50, 40, 40, 40		$>$ 80, 50, 40, 40, 40, 40	
Jet veto	${p_{\mathrm{T}}}^{5^{\mathrm{th}}\mathrm{jet}} < 40$ GeV		${p_{\mathrm{T}}}^{6^{\mathrm{th}}\mathrm{jet}} < 40$ GeV		–	
$N_{b-\mathrm{tag}}$	–					
$E_{\mathrm{T}}^{\mathrm{miss}}$ [GeV]	[300,500]	[150,300]	[300,500]	[150,300]	[250,500]	[150,250]
m_{T} [GeV]	[60,150]	[150,320]	[60,150]	[150,320]	[60,150]	[120,320]

Table 11. Validation region definitions for the hard single-lepton channel (see figure 3). Only the variables for which the selection differs from the respective control region (see table 7) in at least one validation region are shown.

	Hard dilepton					
	Low-multiplicity			**3-jet**		
	$ee/\mu\mu$		$e\mu$	$ee/\mu\mu$		$e\mu$
	Z region	$t\bar{t}$ region	$t\bar{t}$ region	Z region	$t\bar{t}$ region	$t\bar{t}$ region
N_{ℓ}	2 or ≥ 2					
$N_{b-\mathrm{tag}}$	0	1		0	1	
R	[0.25,1.0]	[0.5,1.0]		[0.1,1.0]	[0.35,1.0]	
$M_R^{'}$ [GeV]	[200,400]			[200,800]		
$M_R^{'}$ bin width [GeV]	50			100		

Table 12. Validation region definitions for the hard dilepton channel (see figure 4). Only the criteria which differ from the respective control region selections (see table 8) in at least one validation region are shown.

JHEP04(2015)116

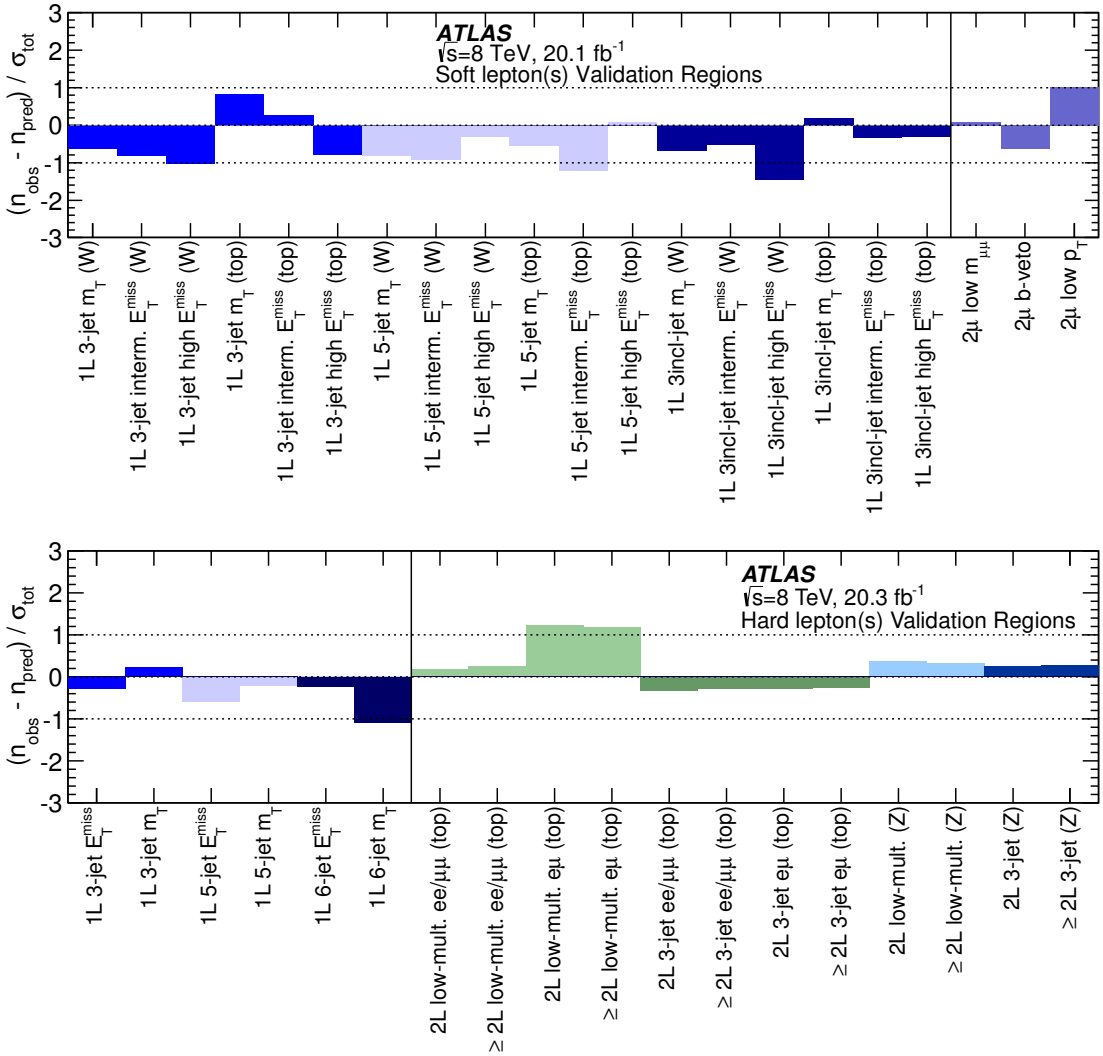

Figure 11. Summary of the fit results: for each validation region (see tables 10–12), the difference between the observed ($n_{\rm obs}$) and predicted ($n_{\rm pred}$) number of events, divided by the total (statistical and systematic) uncertainty on the prediction ($\sigma_{\rm tot}$), is shown. Soft-lepton (top) and hard-lepton (bottom) validation regions are shown. The hard single-lepton validation regions are a mixture of W+jets and top processes. All single-lepton and soft dimuon validation regions, except the 3-jet inclusive soft-lepton validation regions, are statistically independent. The hard dilepton validation regions with exactly two or at least two leptons largely overlap. The systematic uncertainties are partially correlated across multiple control regions defined for each of the four main channels (see section 8) and are thus correlated for the validation regions of each channel.

JHEP04(2015)116

10 Results and interpretation

10.1 Background fit results and limits on the visible cross section

The distributions of $E_{\mathrm{T}}^{\mathrm{miss}}/m_{\mathrm{eff}}$ in the soft single-lepton signal regions, of $E_{\mathrm{T}}^{\mathrm{miss}}$ in the soft dimuon signal region, of $m_{\mathrm{eff}}^{\mathrm{incl}}$ ($E_{\mathrm{T}}^{\mathrm{miss}}$) in the binned hard single-lepton 3-jet and 5-jet (6-jet) signal regions, and of M_R' in the hard dilepton inclusive signal regions are shown in figures 12–14. The results of the fit in these signal regions are shown in tables 13–15. The normalisation factors of the dominant backgrounds after the fit are found to be $\mathcal{O}(0.7\text{–}0.9)$ for $t\bar{t}$ (with the lowest value found in the soft dimuon channel), $\mathcal{O}(0.5\text{–}0.9)$ for W+jets (with the lowest values found in the high jet-multiplicity signal regions of the hard single-lepton channel) and $\mathcal{O}(0.9)$ for Z+jets. The ranges of values quoted for the W/Z+jets and $t\bar{t}$ background normalisation factors indicate that the event generators used (see table 1) predict significantly larger rates for these processes in certain control regions than is observed in data. This observation is compatible with the differential cross-section measurements published by ATLAS for these processes with looser selection requirements [120–124]. The inclusion of the systematic uncertainties as nuisance parameters in the fit has a negligible effect on the central value of the fitted normalisation factors.

The number of events observed in all the signal regions presented in this paper is consistent with the post-fit SM expectations. The signal regions are not all independent: some CRs are common to several SRs (e.g. binned and unbinned). The binned and unbinned signal regions overlap, and the 3-jet inclusive soft single-lepton signal region overlaps with the other soft single-lepton signal regions. The data and Monte Carlo distributions of the variables used in the extrapolation from control to signal regions are in agreement within uncertainties.

The observed and expected upper limits at 95% confidence level (CL) on the number of events from new phenomena beyond the SM (BSM) for each signal region (S_{obs}^{95} and S_{exp}^{95}) are derived using the CL_S prescription [125] and neglecting any possible signal contamination in the control regions; an uncertainty on S_{exp}^{95} is also computed from the $\pm 1\sigma$ uncertainty on the expectation. The observed upper limits, normalised by the integrated luminosity of the data sample, can be interpreted as upper limits on the visible BSM cross-section, ($\langle\epsilon\sigma\rangle_{\mathrm{obs}}^{95}$), where the visible cross section is defined as the product of acceptance, selection efficiency and production cross-section. The results obtained using asymptotic formulae [118] are given in table 16 for the single-bin signal regions.[3] For each signal region, the results are also shown split by lepton flavour to allow for comparison with new models which could favour a specific lepton flavour. In this table the value of CL_B, the confidence level observed for the background-only hypothesis, and the one-sided discovery p-value, $p(s=0)$, are also given; the latter represents, for each signal region, the probability that the event yield obtained in a single hypothetical background-only experiment (signal $s=0$) is greater than that observed in this dataset. CL_B and $p(s=0)$ are obtained using different test statistic definitions: the former has a conditional likelihood

[3]The method was cross-checked with pseudo experiments for various configurations and the results were found to be consistent.

JHEP04(2015)116

	Soft single-lepton					Soft dimuon
	3-jet incl.	3-jet		5-jet		
		Single-bin	Binned	Single-bin	Binned	
Observed events	34	7	8	11	19	6
Fitted background events	37.0 ± 6.3	7.5 ± 1.4	7.9 ± 1.6	15.9 ± 3.7	27.7 ± 6.7	6.0 ± 2.6
$t\bar{t}$	11.2 ± 4.7	2.0 ± 0.9	2.4 ± 1.1	8.5 ± 3.4	16.0 ± 6.4	1.8 ± 0.8
Other top quarks	1.4 ± 0.9	0.96 ± 0.31	1.0 ± 0.3	1.1 ± 0.4	1.6 ± 0.6	0.24 ± 0.14
V+jets	15.2 ± 2.8	2.9 ± 0.5	2.9 ± 0.5	2.6 ± 0.6	5.0 ± 1.2	0.28 ± 0.19
Diboson	5.1 ± 1.2	0.89 ± 0.36	0.91 ± 0.36	0.83 ± 0.50	1.3 ± 0.7	1.4 ± 0.5
Fake leptons	4.2 ± 1.9	$0.75^{+0.78}_{-0.75}$	$0.64^{+0.76}_{-0.64}$	2.9 ± 1.2	3.9 ± 1.7	$2.3^{+2.4}_{-2.3}$
Expected background events before the fit	43.1	8.4	8.8	18.3	32.3	6.8
$t\bar{t}$	14.9	2.4	2.9	10.2	19.0	2.6
Other top quarks	1.4	0.96	1.0	1.1	1.6	0.24
V+jets	17.6	3.4	3.4	3.4	6.5	0.28
Diboson	5.1	0.89	0.91	0.83	1.3	1.4
Fake leptons	4.2	0.75	0.64	2.9	3.9	2.3

Table 13. Background fit results (top) for the soft single-lepton and soft dimuon signal regions, for an integrated luminosity of 20.1 fb^{-1}. The V+jets events contain W+jets and Z+jets events. The background expectations before the fit (bottom) are given for comparison (see section 7 for a detailed description of how each background source is estimated). The uncertainties shown here combine the statistical uncertainty on the simulated event samples with the systematic uncertainties.

	Hard single-lepton					
	3-jet		5-jet		6-jet	
	Single-bin	Binned	Single-bin	Binned	Single-bin	Binned
Observed events	9	75	5	16	2	12
Fitted background events	8.5 ± 1.4	82.5 ± 7.2	7.3 ± 1.7	17.7 ± 4.0	4.9 ± 1.1	18.1 ± 4.3
$t\bar{t}$	2.2 ± 0.5	35.0 ± 6.2	4.8 ± 1.6	12.3 ± 4.1	3.7 ± 1.3	13.9 ± 4.7
Other top quarks	0.79 ± 0.35	7.6 ± 3.0	0.71 ± 0.18	2.1 ± 0.5	0.54 ± 0.18	1.7 ± 0.5
V+jets	2.5 ± 0.4	24.4 ± 3.6	0.80 ± 0.28	1.8 ± 0.6	0.5 ± 0.4	0.99 ± 0.80
Diboson	2.9 ± 1.0	14.3 ± 4.3	0.96 ± 0.69	1.5 ± 1.0	0.14 ± 0.07	0.70 ± 0.36
Fake leptons	$0.09^{+0.15}_{-0.09}$	$1.2^{+1.3}_{-1.2}$	$0.00^{+0.01}_{-0.00}$	$0.00^{+0.09}_{-0.00}$	0.00 ± 0.00	$0.82^{+0.87}_{-0.82}$
Expected background events before the fit	10.1	104.4	9.5	23.2	6.2	22.3
$t\bar{t}$	3.1	49.3	6.5	16.5	4.5	17.3
Other top quarks	0.79	7.6	0.7	2.1	0.54	1.7
V+jets	3.3	32.0	1.3	3.1	1.0	1.9
Diboson	2.9	14.3	0.96	1.5	0.14	0.70
Fake leptons	0.09	1.2	0.00	0.00	0.00	0.82

Table 14. Background fit results (top) for the hard single-lepton signal regions, for an integrated luminosity of 20.3 fb^{-1}. The V+jets events contain W+jets and Z+jets events. The background expectations before the fit (bottom) are given for comparison (see section 7 for a detailed description of how each background source is estimated). The uncertainties shown here combine the statistical uncertainty on the simulated event samples with the systematic uncertainties.

JHEP04(2015)116

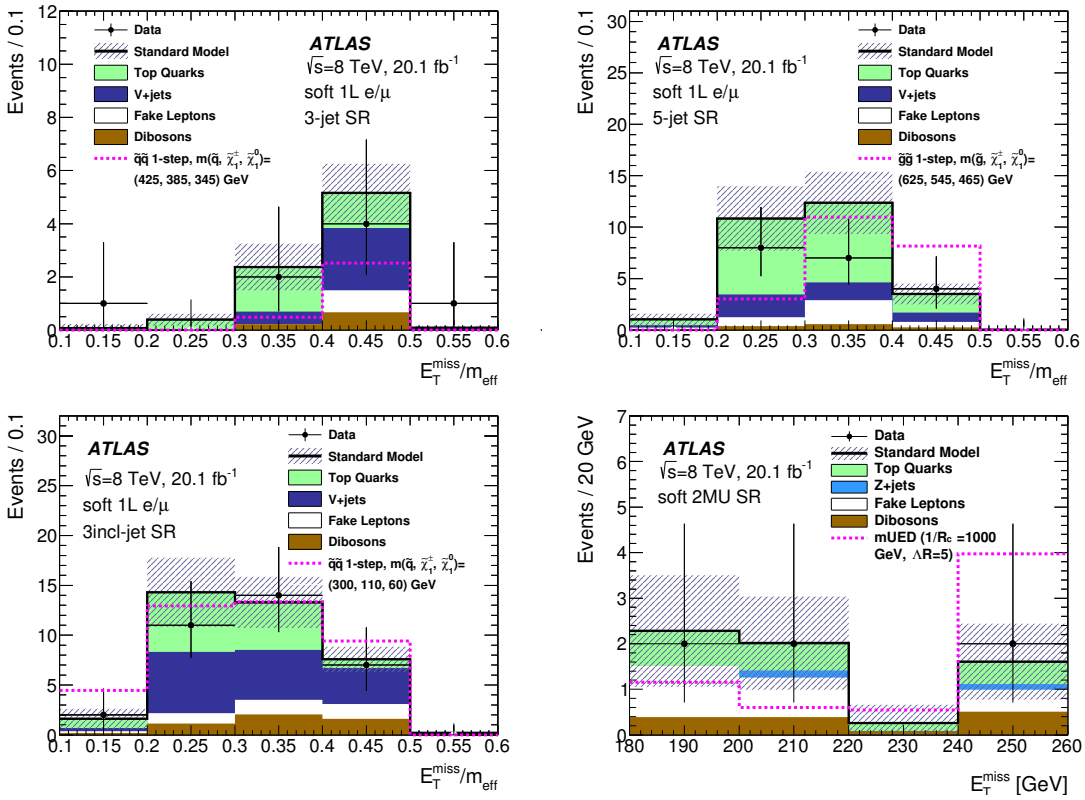

Figure 12. Distribution of the ratio of the missing transverse momentum to the effective mass $E_{\mathrm{T}}^{\mathrm{miss}}/m_{\mathrm{eff}}$ in soft single-lepton 3-jet (upper left), 5-jet (upper right) and 3-jet inclusive (bottom left) signal regions and distribution of the missing transverse momentum $E_{\mathrm{T}}^{\mathrm{miss}}$ in the soft dimuon signal region (bottom right). The Standard Model expectation is derived from the fit. The uncertainty band on the Standard Model expectation shown here combines the statistical uncertainty on the simulated event samples and the systematic uncertainties. The last bin includes the overflow. The "Top Quarks" include $t\bar{t}$, single top, t+Z, $t\bar{t}$+W and $t\bar{t}$+WW, while "V+jets" includes W+jets, Z+jets and Drell-Yan contributions. For illustration, the expected signal distributions are shown for three signal benchmark points: $(m_{\tilde{q}}, m_{\tilde{\chi}_1^{\pm}}, m_{\tilde{\chi}_1^0}) = (425, 385, 345)$ GeV, $(m_{\tilde{g}}, m_{\tilde{\chi}_1^{\pm}}, m_{\tilde{\chi}_1^0}) = (625, 545, 465)$ GeV and $(m_{\tilde{q}}, m_{\tilde{\chi}_1^{\pm}}, m_{\tilde{\chi}_1^0}) = (300, 110, 60)$ GeV in the single-lepton channel and for the mUED model point with $R_{\mathrm{c}}^{-1} = 1000$ GeV and $\Lambda R_{\mathrm{c}} = 5$ in the dimuon channel.

calculated with a signal strength μ set to 1, while the latter uses $\mu = 0$. For an observed number of events lower than expected, the discovery p-value is truncated at 0.5.

10.2 Exclusion limits on specific models

Given the absence of a significant excess above the SM background expectation, exclusion limits are also placed on the various specific models of physics beyond the SM described in section 3. In this case, the fit is modified in the following way:

1. there is an extra free parameter for a possible non-SM signal strength which is constrained to be non-negative;

JHEP04(2015)116

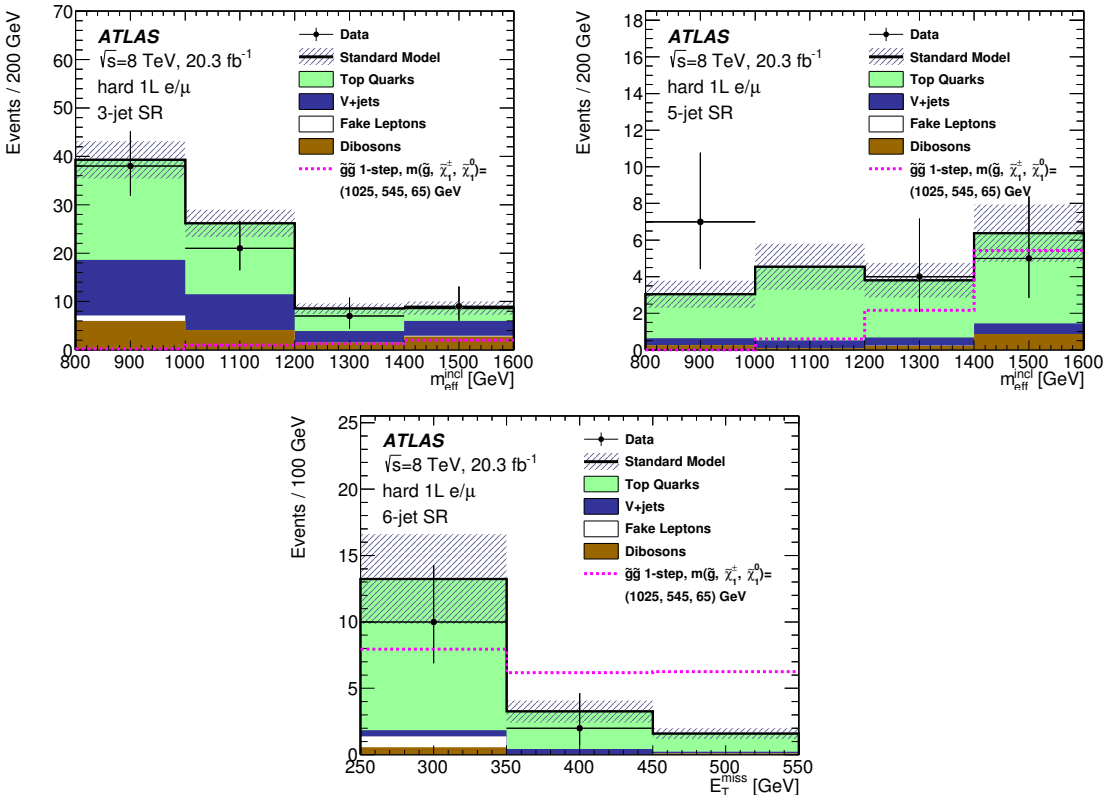

Figure 13. Distribution of the inclusive effective mass $m_{\mathrm{eff}}^{\mathrm{incl}}$ in the hard single-lepton 3-jet (upper left) and 5-jet (upper right) binned signal regions and distribution of the missing transverse momentum $E_{\mathrm{T}}^{\mathrm{miss}}$ in the hard single-lepton 6-jet binned signal region (bottom). The Standard Model expectation is derived from the fit. The uncertainty band on the Standard Model expectation shown here combines the statistical uncertainty on the simulated event samples and the systematic uncertainties. The last bin includes the overflow. The "Top Quarks" include $t\bar{t}$, single top, t+Z, $t\bar{t}$+W and $t\bar{t}$+WW, while "V+jets" includes W+jets, Z+jets and Drell-Yan contributions. For illustration, the expected signal distributions are shown for gluino pair production with $m_{\tilde{g}} = 1025\,\mathrm{GeV}, m_{\tilde{\chi}_1^{\pm}} = 545\,\mathrm{GeV}$ and $m_{\tilde{\chi}_1^0} = 65\,\mathrm{GeV}$.

2. the number of events observed in the signal region is now also considered as an input to the fit;

3. the expected contamination of the control regions by the signal is included in the fit.

For all regions except the soft dimuon channel, binned signal regions are used. The likelihood (see section 9) takes into account the model shape information in the signal regions as a further discriminant by including bin-by-bin expectations.

The systematic uncertainties on the signal expectations originating from detector effects and the theoretical uncertainties on the signal acceptance are included in the fit. The impact of the theoretical uncertainties on the signal cross section is shown on the limit plots obtained. Numbers quoted in the text are evaluated from the observed exclusion limit based on the nominal signal cross section minus its 1σ theoretical uncertainty.

JHEP04(2015)116

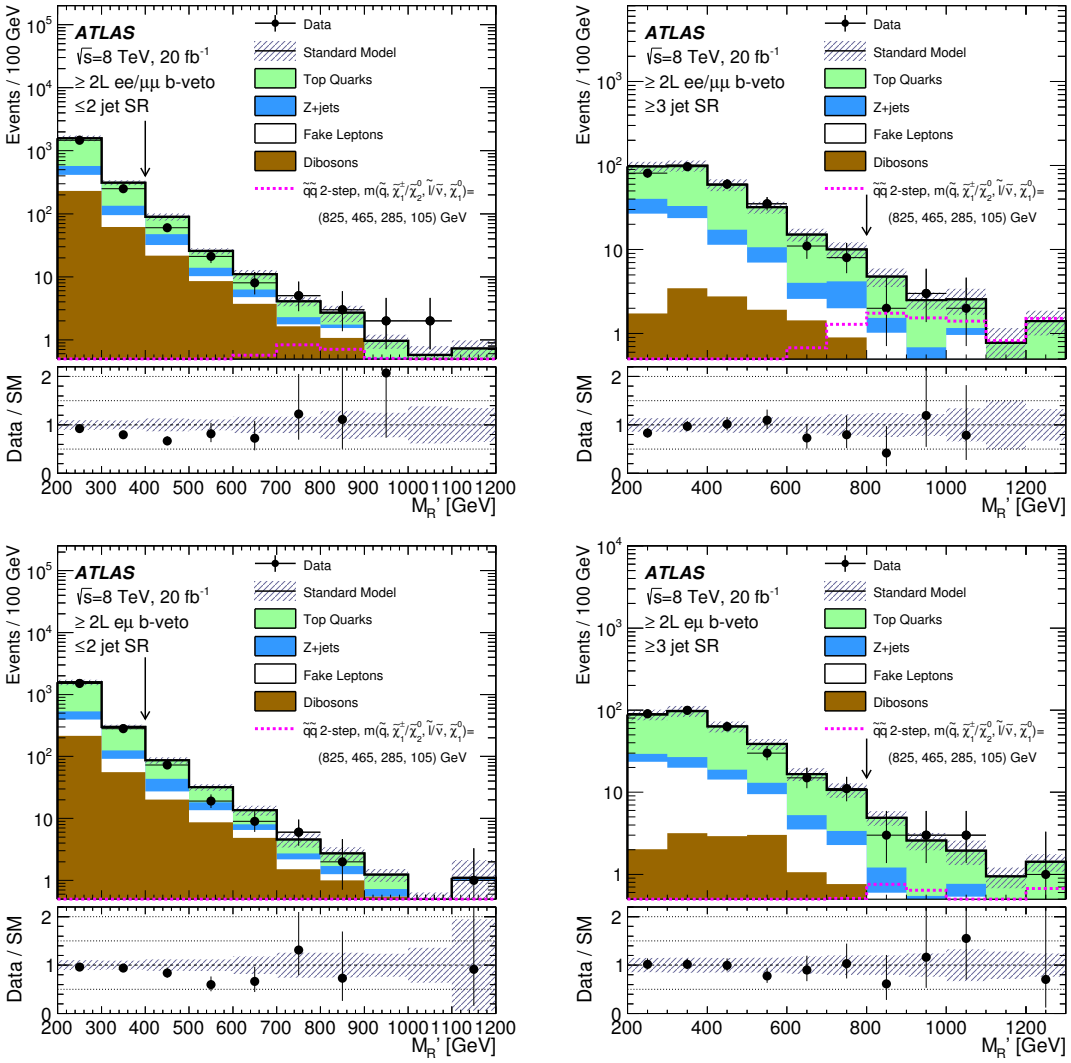

Figure 14. Distribution of the R-frame mass M'_R in the inclusive hard dilepton low-multiplicity (left) and 3-jet (right) signal regions for the same-flavour (top) and opposite-flavour (bottom) pairs. The arrow indicates the requirement defining the signal region. The Standard Model expectation is derived from the fit. The uncertainty band on the Standard Model expectation shown here combines the statistical uncertainty on the simulated event samples and the systematic uncertainties. The last bin includes the overflow. The "Top Quarks" include $t\bar{t}$, single top, t+Z, $t\bar{t}$+W and $t\bar{t}$+WW, while "V+jets" includes W+jets, Z+jets and Drell-Yan contributions. For illustration, the expected signal distributions are shown for squark pair production with $m_{\tilde{q}} = 825\,\text{GeV}, m_{\tilde{\chi}_1^\pm/\tilde{\chi}_2^0} = 465\,\text{GeV}, m_{\tilde{\ell}/\tilde{\nu}} = 285\,\text{GeV}$ and $m_{\tilde{\chi}_1^0} = 105\,\text{GeV}$.

JHEP04(2015)116

	Hard dilepton inclusive					
	Low-multiplicity				3-jet	
	$ee/\mu\mu$		$e\mu$		$ee/\mu\mu$	$e\mu$
	Single-bin	Binned	Single-bin	Binned		
Observed events	20	101	18	110	7	10
Fitted background events	20.0 ± 3.3	136 ± 15	24 ± 4	141 ± 16	11.8 ± 2.6	11.5 ± 2.0
$t\bar{t}$	6.7 ± 1.3	53 ± 9	7.7 ± 1.5	54 ± 9	5.9 ± 1.5	7.0 ± 1.6
Other top quarks	1.7 ± 0.7	10.8 ± 1.8	2.1 ± 0.7	11.1 ± 2.1	1.7 ± 0.3	1.4 ± 0.3
Diboson	7.4 ± 2.4	38 ± 5	8.5 ± 2.6	37 ± 5	1.3 ± 0.2	1.0 ± 0.3
Z+jets	2.6 ± 0.4	21 ± 4	2.8 ± 1.4	24 ± 4	1.3 ± 0.3	1.4 ± 0.4
Fake leptons	1.6 ± 1.4	13 ± 7	3.2 ± 2.1	15 ± 9	$1.5^{+2.0}_{-1.5}$	$0.6^{+0.9}_{-0.6}$
Expected background events before the fit	20.1	144	25	150	14.6	14.2
$t\bar{t}$	6.2	50	6.8	56	8.4	9.4
Other top quarks	1.5	10.1	2.1	10.3	1.8	1.4
Diboson	7.4	40	9.0	38	1.3	1.1
Z+jets	3.3	30	4.1	31	1.6	1.6
Fake leptons	1.6	13	3.2	15	1.5	0.6

Table 15. Background fit results (top) for the inclusive hard dilepton signal regions, for an integrated luminosity of 20.3 fb^{-1}. The background expectations before the fit (bottom) are given for comparison (see section 7 for a detailed description of how each background source is estimated). The uncertainties shown combine the statistical and systematic uncertainties. The 3-jet binned signal region uses the same event selection as the 3-jet single-bin signal region (see table 4); therefore it has the same event yields.

As mentioned in section 4, the soft-lepton channel has a slightly lower integrated luminosity than the hard-lepton channel. For consistency in all the following limit contour figures, the integrated luminosity is abbreviated to 20 fb^{-1}.

10.2.1 Limits on phenomenological models

The limits in the (m_0,$m_{1/2}$) mSUGRA/CMSSM plane obtained from the hard single-lepton signal regions are shown in figure 15. The observed limit is driven above the expected limit mainly by the shape fit to the $E_{\text{T}}^{\text{miss}}$ distribution in the 6-jet binned signal region (see figure 13) as no data event is found in the high-$E_{\text{T}}^{\text{miss}}$ bin. At large values of m_0, this analysis is able to exclude a gluino mass of up to 1.2 TeV. A 1.0 TeV limit on the gluino mass is obtained from the hard single-lepton channel in the bRPV model at high m_0, while the limit is at 1.13 TeV in the nGM model, as shown in figures 15 and 16, respectively. The observed exclusion limit obtained by the hard single-lepton channel for the NUHMG model is also shown in figure 16.

The limit obtained for the mUED scenario is shown in figure 17 in the ($1/R_{\text{c}}$,ΛR_{c}) plane. The soft dimuon channel complements the hard dilepton case, as it covers the low ΛR_{c} values. Because the signal regions in the two channels overlap, they cannot be combined in a straightforward manner. Instead, the limit, for each point in the plane, is obtained by using the better expected limit from either the soft dimuon or the hard dilepton channel. The limit obtained reaches up to a compactification radius of $1/R_{\text{c}} = 950$ GeV for a cut-off scale times radius (ΛR_{c}) of approximately 30.

JHEP04(2015)116

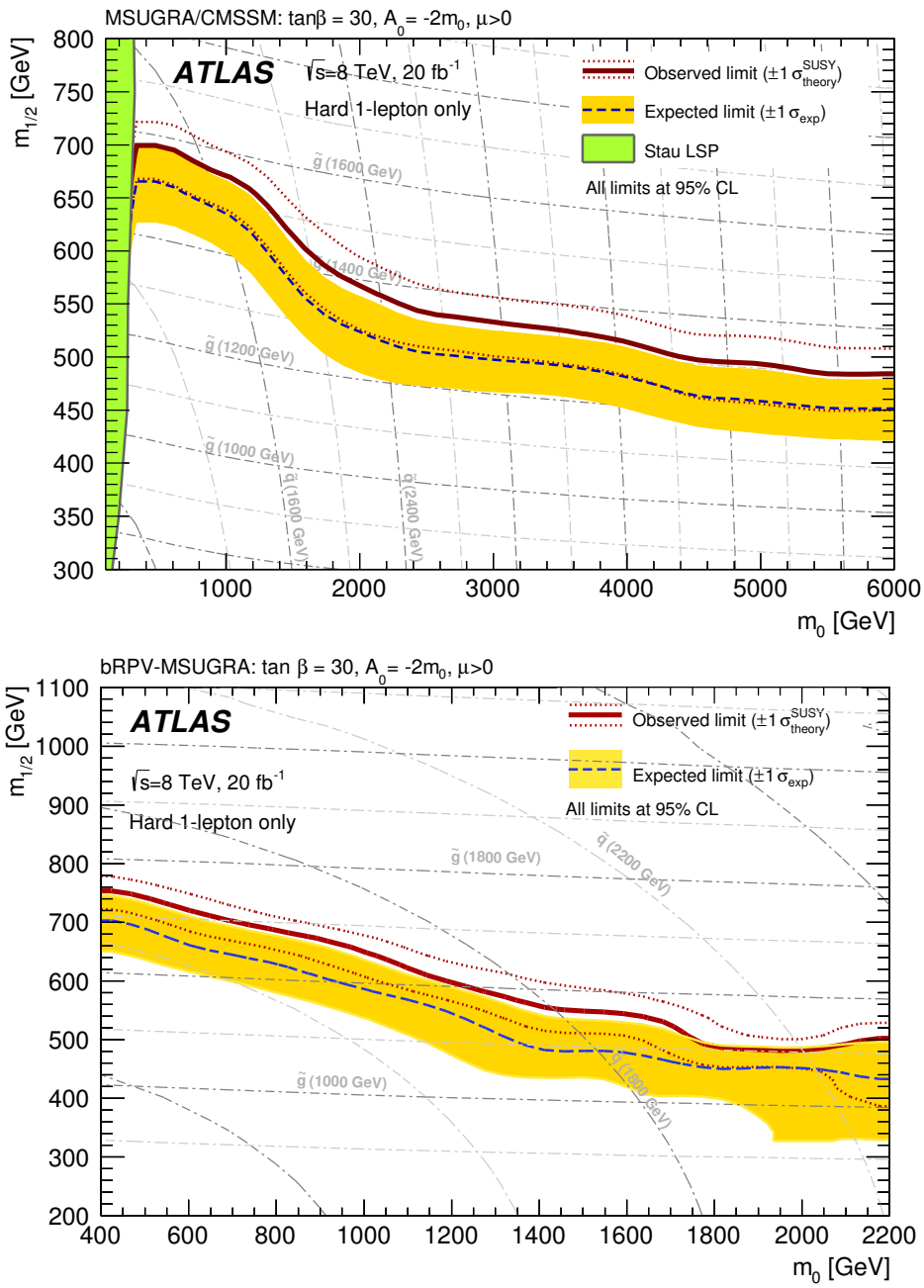

Figure 15. 95% CL exclusion limit from the hard single-lepton channel in the (m_0,$m_{1/2}$) plane for the mSUGRA/CMSSM model with $\tan\beta = 30$, $A_0 = -2m_0$ and $\mu > 0$ (top) and in the same plane for the bRPV model (bottom). The green area represents the region of the parameter space for which the stau is the LSP. The dark blue dashed line shows the expected limits at 95% CL, with the light (yellow) bands indicating the $\pm 1\sigma$ variation on the median expected limit due to the experimental and background-only theory uncertainties. The observed nominal limit is shown by a solid dark red line, with the dark red dotted lines indicating the $\pm 1\sigma$ variation on this limit due to the theoretical scale and PDF uncertainties on the signal cross section. Lines of constant squark and gluino masses are also shown.

JHEP04(2015)116

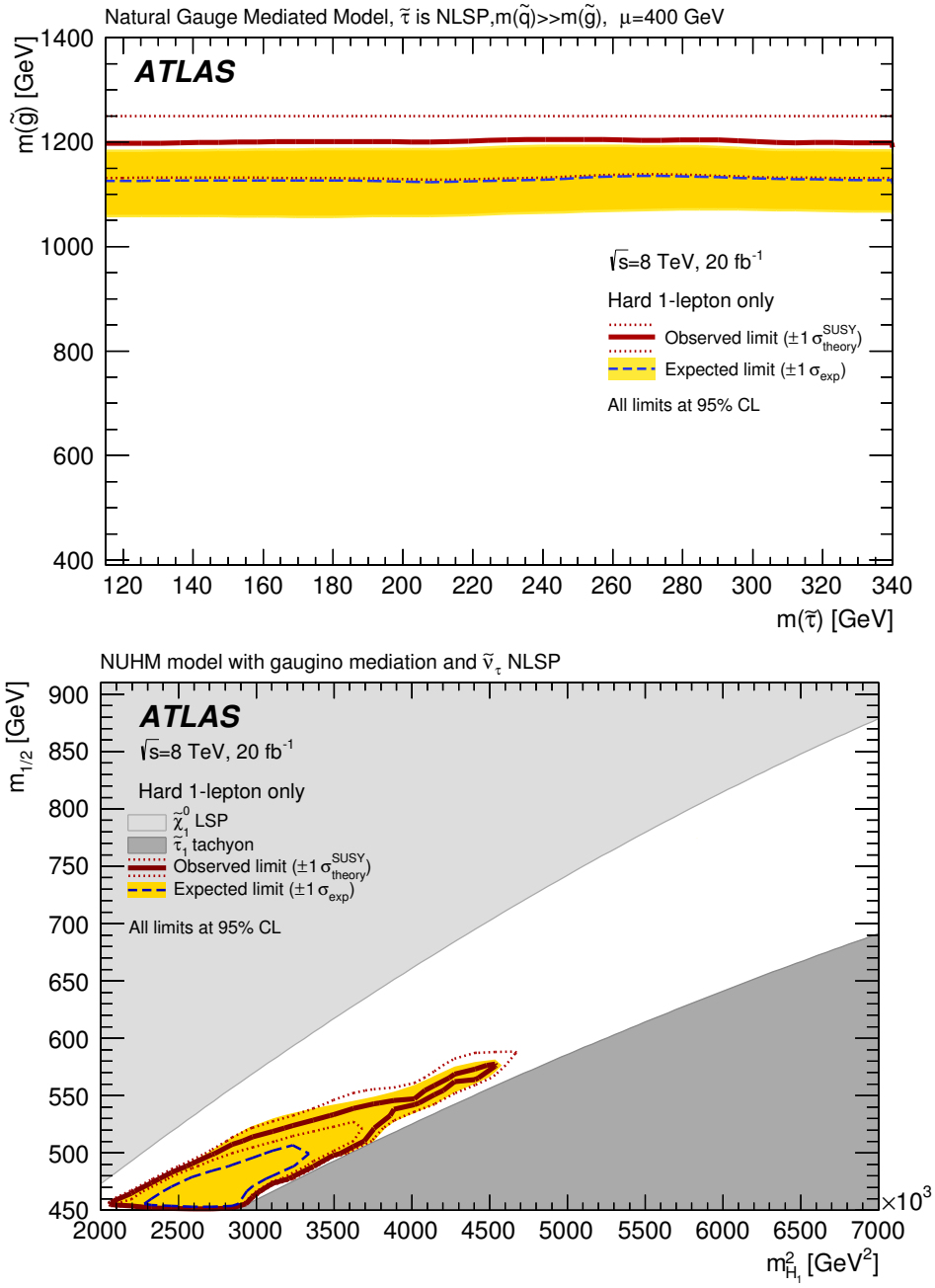

Figure 16. 95% CL exclusion limit from the hard single-lepton channel in the ($m_{\tilde{\tau}}$,$m_{\tilde{g}}$) plane for the nGM model (top) and in the ($m^2_{H_1}$,$m_{1/2}$) plane for the NUHMG model (bottom). The dark blue dashed line shows the expected limits at 95% CL, with the light (yellow) bands indicating the $\pm1\sigma$ variation on the median expected limit due to the experimental and background-only theory uncertainties. The observed nominal limit is shown by a solid dark red line, with the dark red dotted lines indicating the $\pm1\sigma$ variation on this limit due to the theoretical scale and PDF uncertainties on the signal cross section. In the NUHMG model, the shaded areas are excluded either because the LSP is the $\tilde{\chi}^0_1$ or because the $\tilde{\tau}_1$ is a tachyon.

JHEP04(2015)116

Signal region	$\langle\epsilon\sigma\rangle^{95}_{\text{obs}}$[fb]	S^{95}_{obs}	S^{95}_{exp}	CL_B	$p(s=0)$
Soft single-lepton channel					
3-jet inclusive	0.77	15.6	$17.3^{+6.9}_{-4.9}$	0.37	0.50
3-jet inclusive (electron)	0.55	11.1	$10.8^{+4.8}_{-3.0}$	0.52	0.48
3-jet inclusive (muon)	0.52	10.5	$12.4^{+5.2}_{-3.4}$	0.31	0.50
3-jet	0.35	7.0	$7.5^{+3.3}_{-2.2}$	0.44	0.50
3-jet (electron)	0.26	5.2	$5.7^{+2.6}_{-1.8}$	0.40	0.50
3-jet (muon)	0.29	5.9	$5.8^{+2.6}_{-1.8}$	0.52	0.48
5-jet	0.39	7.9	$10.4^{+4.4}_{-2.8}$	0.20	0.50
5-jet (electron)	0.38	7.7	$7.6^{+3.4}_{-2.2}$	0.52	0.48
5-jet (muon)	0.21	4.3	$7.1^{+3.2}_{-2.0}$	0.10	0.50
Soft dimuon channel	0.39	7.7	$7.8^{+3.5}_{-2.4}$	0.50	0.50
Single-bin hard single-lepton channel					
3-jet	0.40	8.2	$7.8^{+3.3}_{-2.2}$	0.59	0.41
3-jet (electron)	0.29	5.9	$6.2^{+2.1}_{-2.0}$	0.39	0.50
3-jet (muon)	0.35	7.0	$5.7^{+2.1}_{-1.5}$	0.72	0.27
5-jet	0.28	5.7	$7.2^{+3.1}_{-1.9}$	0.26	0.50
5-jet (electron)	0.29	6.0	$5.8^{+2.2}_{-1.2}$	0.55	0.50
5-jet (muon)	0.20	4.0	$5.4^{+1.6}_{-1.4}$	0.10	0.49
6-jet	0.22	4.5	$6.0^{+2.2}_{-1.6}$	0.10	0.50
6-jet (electron)	0.24	4.8	$5.3^{+1.6}_{-1.3}$	0.32	0.50
6-jet (muon)	0.16	3.2	$4.9^{+1.4}_{-1.3}$	0.08	0.50
Single-bin inclusive hard dilepton channel					
Low-multiplicity ee and $\mu\mu$ combined	0.44	11.6	$11.5^{+5.0}_{-3.4}$	0.50	0.49
Low-multiplicity $\mu\mu$	0.46	9.3	$8.4^{+3.9}_{-2.5}$	0.61	0.38
Low-multiplicity ee	0.35	7.2	$8.1^{+3.8}_{-2.4}$	0.37	0.50
Low-multiplicity $e\mu$	0.46	8.8	$12.4^{+5.4}_{-3.6}$	0.16	0.50
3-jet ee and $\mu\mu$ combined	0.29	5.8	$8.4^{+3.9}_{-2.6}$	0.15	0.50
3-jet ee	0.24	4.9	$6.3^{+3.2}_{-2.0}$	0.26	0.50
3-jet $\mu\mu$	0.22	4.4	$6.0^{+3.1}_{-1.9}$	0.19	0.50
3-jet $e\mu$	0.40	8.2	$8.8^{+4.0}_{-2.6}$	0.41	0.50

Table 16. From left to right: 95% confidence level (CL) upper limits on the visible cross section ($\langle\epsilon\sigma\rangle^{95}_{\text{obs}}$) and on the number of signal events (S^{95}_{obs}); S^{95}_{exp} shows the 95% CL upper limit on the number of signal events, given the expected number (and $\pm1\sigma$ excursions on the expectation) of background events; two-sided CL_B value, i.e. the confidence level observed for the background-only hypothesis, and the discovery p-value ($p(s=0)$). For an observed number of events lower than expected, the discovery p-value is truncated at 0.5. More details about the CL_S prescription can be found in ref. [125].

10.2.2 Limits on simplified models

The limits obtained from the hard single-lepton channel in the gluino-mediated top squark production models, favoured by naturalness arguments, are shown in figure 18. In the model where the mass gap between the $\tilde{t}_1$ and the LSP is fixed at 20 GeV, the observed exclusion reaches a gluino mass of 1.2 TeV. In this model, the hard single-lepton analysis is complementary to the 0-lepton analysis presented in ref. [32], in that the expected limit for the single-lepton analysis is able to cover higher top squark masses at intermediate gluino masses (e.g. 80 GeV higher at $m_{\tilde{g}} = 900$ GeV). In the model where the gluino exclusively

JHEP04(2015)116

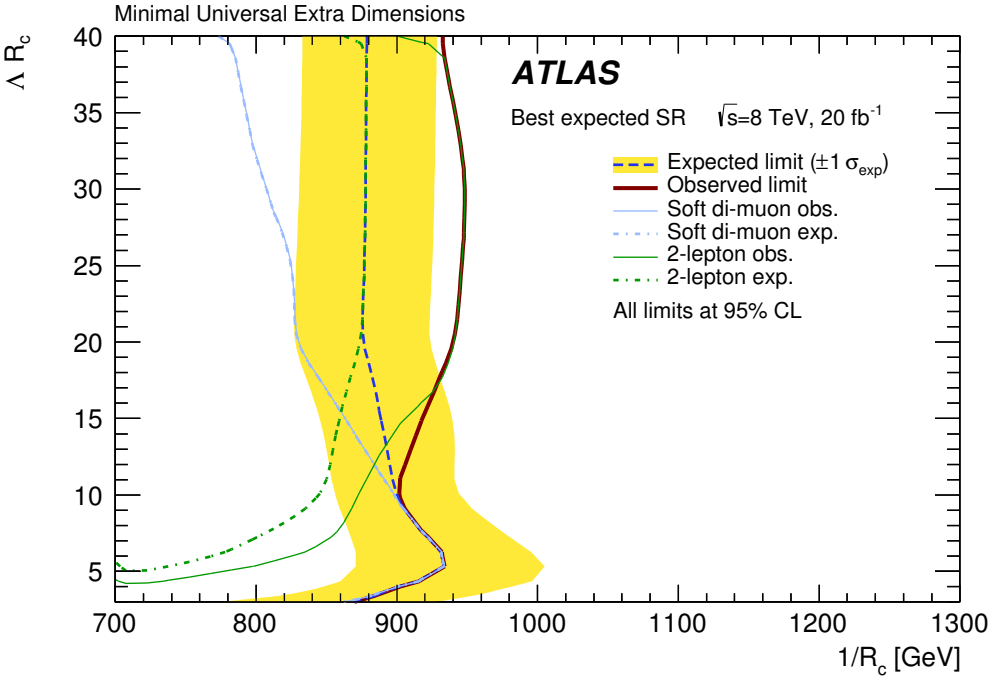

Figure 17. 95% CL exclusion limit from the combination of the soft dimuon and hard dilepton channels for the mUED model, presented in the $(1/R_c, \Lambda R_c)$ plane. The dark blue dashed line shows the expected limits at 95% CL, with the light (yellow) bands indicating the $\pm 1\sigma$ variation on the median expected limit due to the experimental and background-only theory uncertainties. The observed nominal limit is shown by a solid dark red line. The blue and green full (dashed) lines show the observed (expected) exclusion obtained by the soft dimuon and hard dilepton analyses, respectively. For each point in the plane, the limit is obtained by using the better expected limit from either the soft dimuon or the hard dilepton channel.

decays to a pair of top quarks and the lightest neutralino, the observed exclusion reaches a gluino mass of 1.28 TeV. As in the mSUGRA/CMSSM case, the observed limit is more stringent than the expected limit mainly because of the 6-jet binned signal region.

As the soft and hard single-lepton channels are orthogonal in their signal and control region definitions, a full statistical combination of all soft and hard single-lepton signal regions is possible; the limits obtained using this combination are shown in figures 19 for the gluino and the squark pair production simplified models. These limits are shown in the $(m_{\tilde{g}(\tilde{q})}, m_{\tilde{\chi}_1^0})$ mass plane for the case in which $x = (m_{\tilde{\chi}_1^\pm} - m_{\tilde{\chi}_1^0})/(m_{\tilde{g}(\tilde{q})} - m_{\tilde{\chi}_1^0}) = 1/2$. The soft single-lepton analysis is particularly powerful along the diagonal, where the masses of the gluino/squark and the lightest neutralino are almost degenerate. The combination improves the exclusion where the sensitivity of the soft and hard single-lepton signal regions are similar; for example, at $m_{\tilde{g}} \approx 800$ GeV, near the combined observed exclusion limit, the observed CL_S values for the individual channels are 0.27 and 0.19 for the soft and hard single-lepton signal regions, respectively, while the combination gives a CL_S value of 0.08. The combined limit on the gluino mass reaches up to 1.2 TeV. This result complements the statistically independent 0-lepton analysis, as the lepton channel offers a better sensitivity

JHEP04(2015)116

to more compressed scenarios at intermediate gluino masses while the 0-lepton analysis is able to reach slightly higher gluino masses. The squark limits are considerably weaker than those for the gluino due to the lower production cross section and only reach up to 750 GeV.[4] The very low squark masses are already excluded by previous analyses [22].

Limits are shown in figure 20 for the gluino and squark simplified models in which the LSP mass is set at 60 GeV and the value of x is varied, using again the hard single-lepton channel in combination with the soft single-lepton channel. In these models, a gluino mass up to 1.22 TeV and a squark mass up to 800 GeV are excluded. Again, the single-lepton and the 0-lepton channels cover different parameter space, the latter being able to exclude larger masses at low x (where it excludes a gluino mass up to 1.13 TeV), while the analysis presented here excludes higher squark masses at moderate to high x values.

For the two-step gluino/squark simplified models with sleptons, the limits are obtained using the hard dilepton signal regions either individually (for squark production) or in combination with the hard single-lepton signal regions (for gluino production). These limits are shown in figure 21. A gluino mass of up to 1.32 TeV and a squark mass up to 840 GeV can be excluded in these models. This result is complementary to the exclusion limit obtained in the 2-same-charge/3-lepton analysis described in ref. [30]. The analysis presented here is able to probe higher gluino/squark mass values (the expected limit is higher by approximately 100 GeV and 50 GeV for the gluino and squark cases, respectively), while the analysis presented in ref. [30] is able to cover higher neutralino masses at intermediate gluino/squark mass values (e.g. the expected limits are 160 GeV higher at $m_{\tilde{g}} = 1000$ GeV and 140 GeV higher at $m_{\tilde{q}} = 650$ GeV).

Using the hard single-lepton channel, a gluino mass up to 1.14 TeV can be excluded for the two-step simplified model without sleptons, as can be seen in figure 22. Also here, the hard single-lepton channel complements the exclusion limits obtained in the 2-same-charge/3-lepton analysis described in ref. [30] and the 0-lepton multijet analysis described in ref. [31]. In particular, this analysis reaches higher neutralino masses at high gluino mass values with respect to the 2-same-charge/3-lepton analysis (e.g. the expected limit is 80 GeV higher at $m_{\tilde{g}} = 1050$ GeV) and has an expected limit on the neutralino mass similar to that from the orthogonal multijet analysis for low-mass gluinos.

11 Conclusion

A search with the ATLAS detector at the LHC for SUSY in final states containing at least one isolated lepton (electron or muon), jets and large missing transverse momentum is presented. This analysis uses 20 fb^{-1} of proton-proton collision data collected at a centre-of-mass energy of 8 TeV. Several single-lepton and dilepton signal regions are used to cover a broad parameter space for a variety of models. The hard-lepton channel is complemented by a soft-lepton channel in order to increase the sensitivity to supersymmetric spectra with small mass splitting. Some signal regions are also subdivided in order to enhance the

[4] At high squark masses, the combined limit is not exactly the same as the hard single-lepton limit; this is due to the combination having slightly different CL_S values.

JHEP04(2015)116

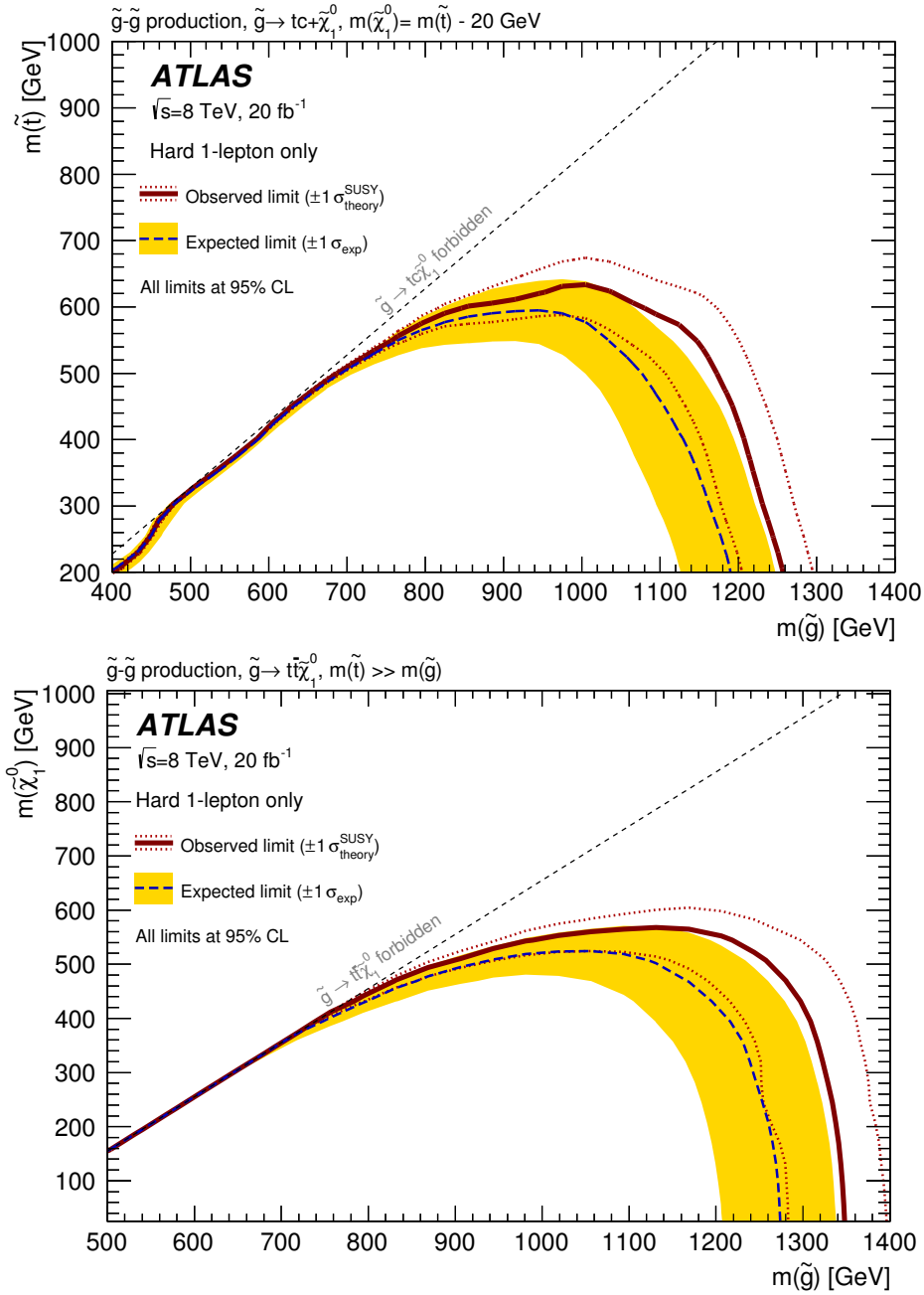

Figure 18. 95% CL exclusion limit from the hard single-lepton channel in the ($m_{\tilde{g}}$,$m_{\tilde{t}(\tilde{\chi}_1^0)}$) plane for the simplified model with gluino-mediated top squark production, where the top squark is assumed to decay exclusively via $\tilde{t} \to c\tilde{\chi}_1^0$ (top) or where the gluinos are assumed to decay exclusively through a virtual top squark, $\tilde{g} \to t\bar{t}\tilde{\chi}_1^0$ (bottom) . The dark blue dashed line shows the expected limits at 95% CL, with the light (yellow) bands indicating the $\pm 1\sigma$ variation on the median expected limit due to the experimental and background-only theory uncertainties. The observed nominal limit is shown by a solid dark red line, with the dark red dotted lines indicating the $\pm 1\sigma$ variation on this limit due to the theoretical scale and PDF uncertainties on the signal cross section.

JHEP04(2015)116

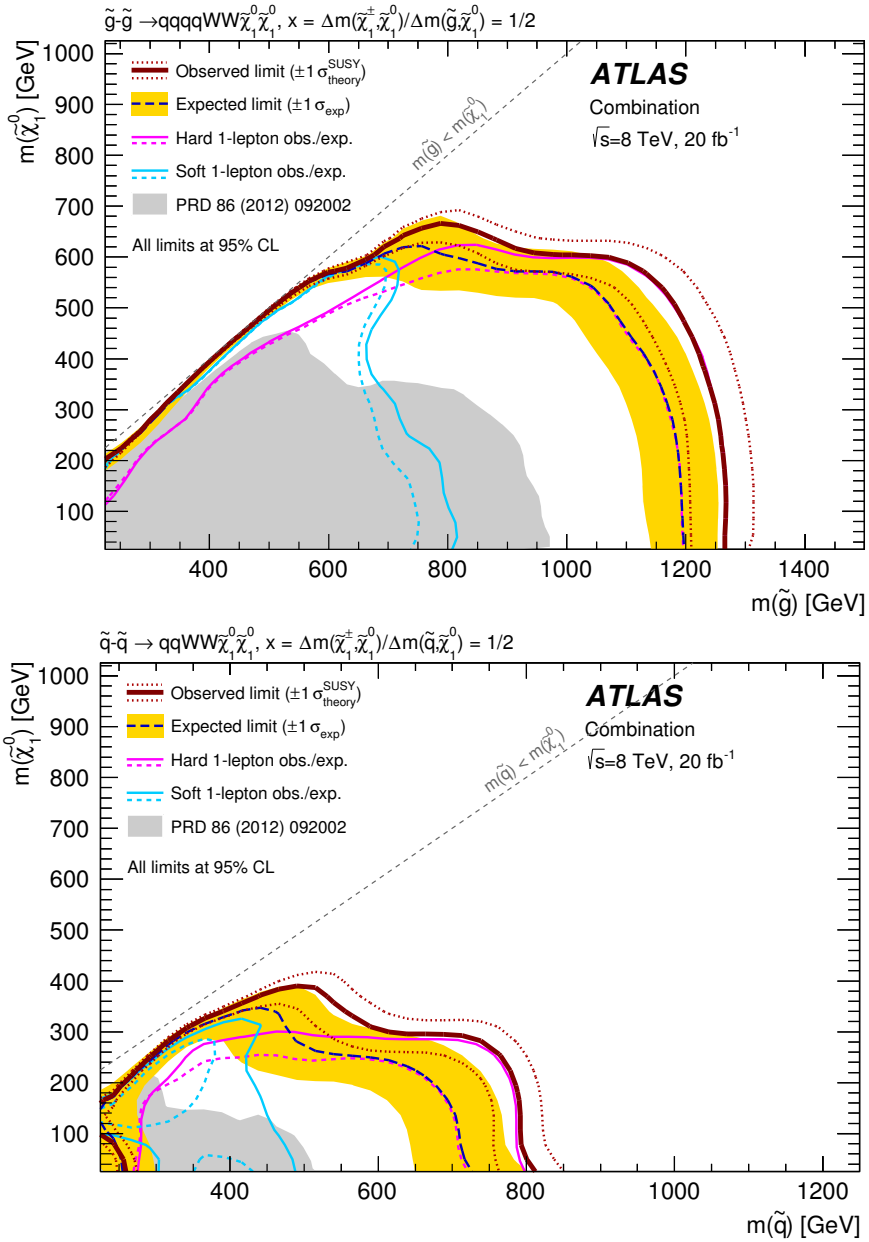

Figure 19. 95% CL exclusion limit for the gluino simplified model (top) and the first- and second-generation squark simplified model (bottom) from the combination of the soft and hard single-lepton analyses. The limits are presented in the $(m_{\tilde{g}(\tilde{q})}, m_{\tilde{\chi}_1^0})$ mass plane for the case in which the chargino mass is fixed at $x = (m_{\tilde{\chi}_1^\pm} - m_{\tilde{\chi}_1^0})/(m_{\tilde{g}(\tilde{q})} - m_{\tilde{\chi}_1^0}) = 1/2$. The dark blue dashed line shows the expected limits at 95% CL, with the light (yellow) bands indicating the $\pm 1\sigma$ variation on the median expected limit due to the experimental and background-only theory uncertainties. The observed nominal limit is shown by a solid dark red line, with the dark red dotted lines indicating the $\pm 1\sigma$ variation on this limit due to the theoretical scale and PDF uncertainties on the signal cross section. The observed limit set by the previous ATLAS analysis [22] using 7 TeV data is shown as a gray area. The light blue and purple full (dashed) lines show the observed (expected) exclusion obtained by the soft and hard single-lepton analyses, respectively.

JHEP04(2015)116

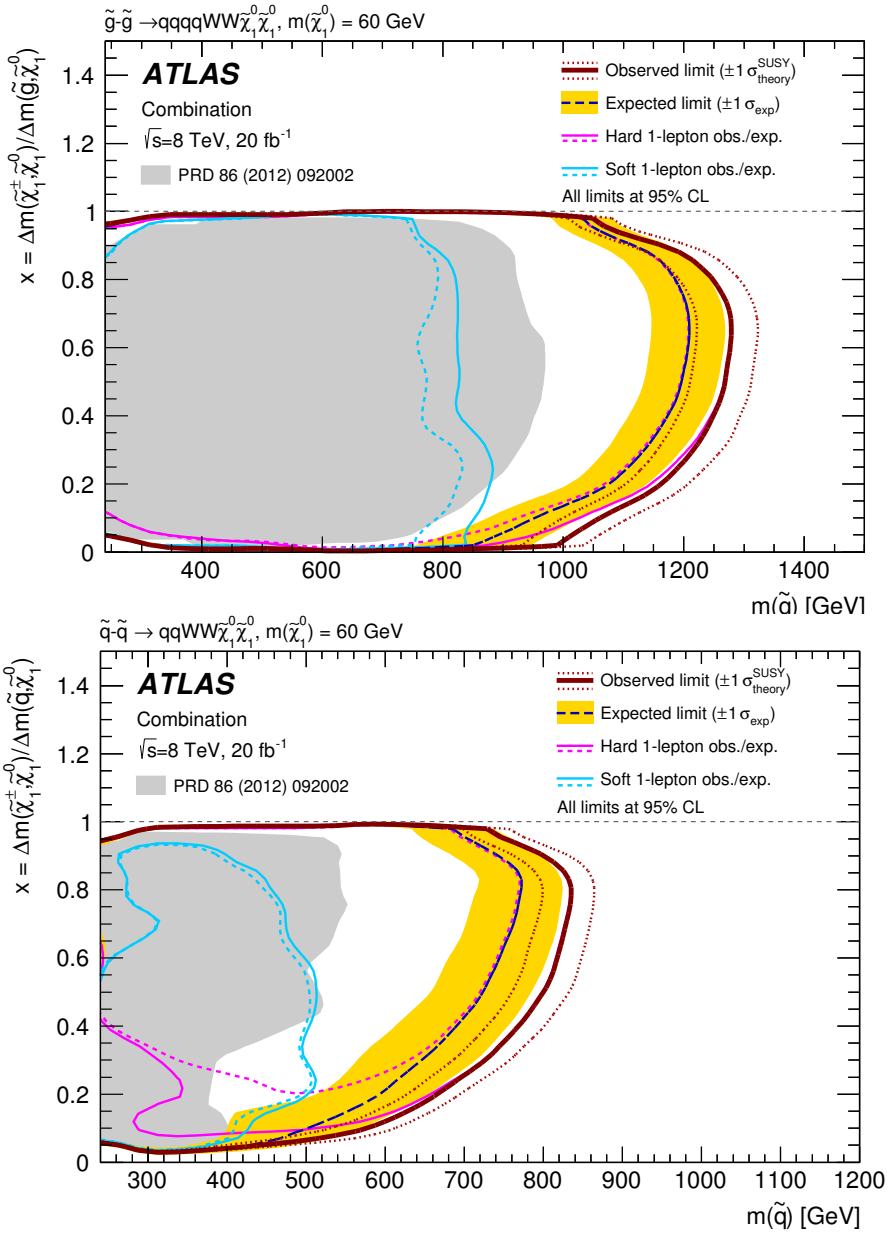

Figure 20. 95% CL exclusion limit for the gluino simplified model (top) and the first- and second-generation squark simplified model (bottom) from the combination of the soft and hard single-lepton analyses. The limits are presented in the $(m_{\tilde{g}(\tilde{q})},x)$ mass plane, where $x = (m_{\tilde{\chi}_1^\pm} - m_{\tilde{\chi}_1^0})/(m_{\tilde{g}(\tilde{q})} - m_{\tilde{\chi}_1^0})$, for the case in which the chargino mass is varied and the LSP mass is set at 60 GeV. The dark blue dashed line shows the expected limits at 95% CL, with the light (yellow) bands indicating the $\pm 1\sigma$ variation on the median expected limit due to the experimental and background-only theory uncertainties. The observed nominal limit is shown by a solid dark red line, with the dark red dotted lines indicating the $\pm 1\sigma$ variation on this limit due to the theoretical scale and PDF uncertainties on the signal cross section. The observed limit set by the previous ATLAS analysis [22] using 7 TeV data is shown as a gray area. The light blue and purple full (dashed) lines show the observed (expected) exclusion obtained by the soft and hard single-lepton analyses, respectively.

JHEP04(2015)116

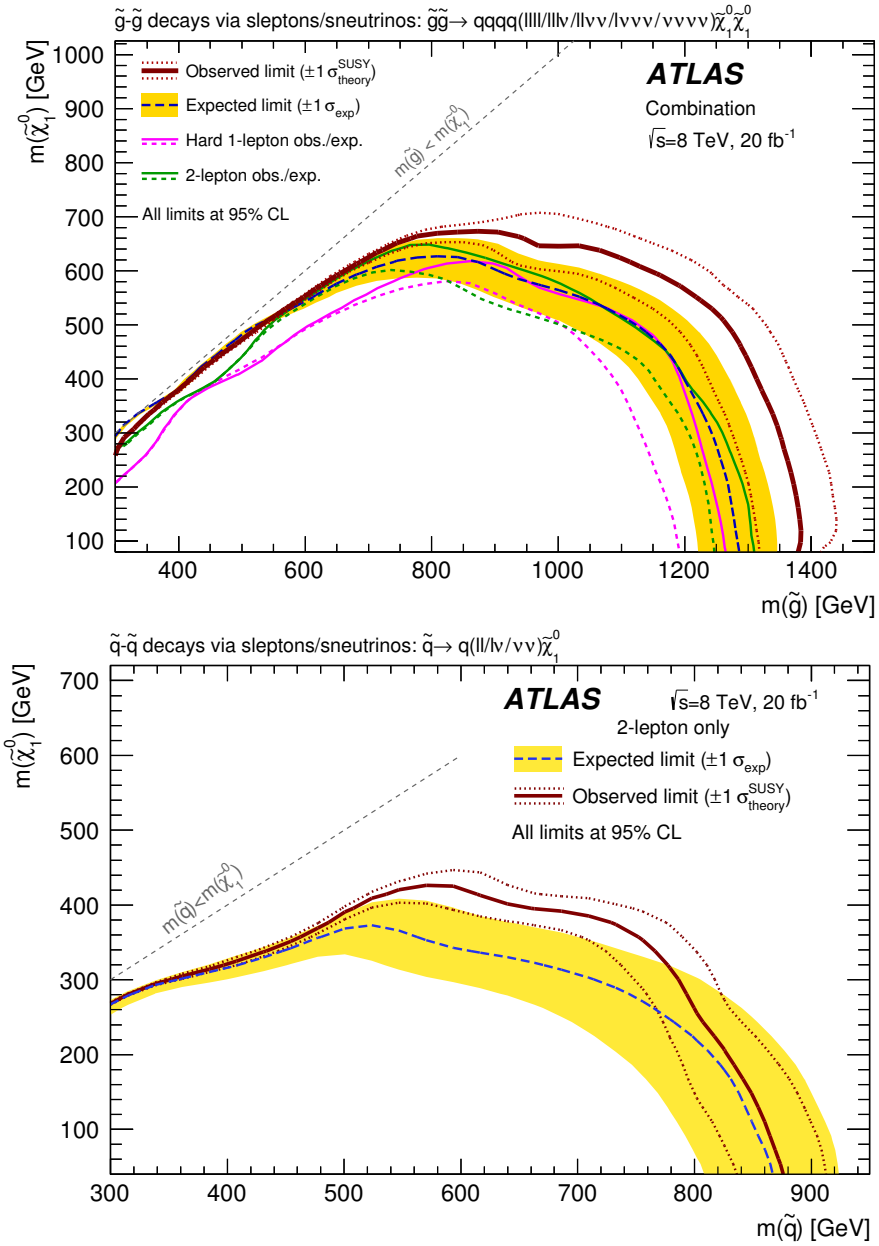

Figure 21. 95% CL exclusion limit for the two-step gluino simplified model with sleptons from the combination of the hard dilepton and single-lepton channels (top) and the two-step first- and second-generation squark simplified model with sleptons from the hard dilepton channel (bottom). The limits are presented in the $(m_{\tilde{g}(\tilde{q})}, m_{\tilde{\chi}_1^0})$ mass plane. The dark blue dashed line shows the expected limits at 95% CL, with the light (yellow) bands indicating the $\pm 1\sigma$ variation on the median expected limit due to the experimental and background-only theory uncertainties. The observed nominal limit is shown by a solid dark red line, with the dark red dotted lines indicating the $\pm 1\sigma$ variation on this limit due to the theoretical scale and PDF uncertainties on the signal cross section. The green and purple full (dashed) lines show the observed (expected) exclusion obtained by the hard dilepton and single-lepton analyses, respectively.

JHEP04(2015)116

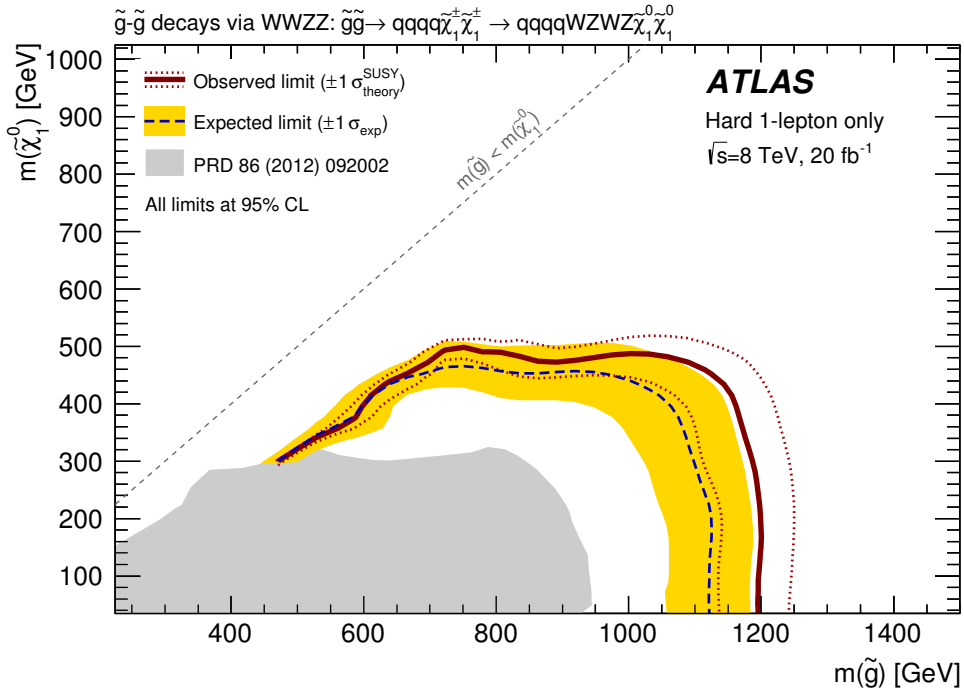

Figure 22. 95% CL exclusion limit from the hard single-lepton channel for the two-step gluino simplified model without sleptons presented in the ($m_{\tilde{g}}$,$m_{\tilde{\chi}_1^0}$) mass plane. The dark blue dashed line shows the expected limits at 95% CL, with the light (yellow) bands indicating the $\pm 1\sigma$ variation on the median expected limit due to the experimental and background-only theory uncertainties. The observed nominal limit is shown by a solid dark red line, with the dark red dotted lines indicating the $\pm 1\sigma$ variation on this limit due to the theoretical scale and PDF uncertainties on the signal cross section. The limit is not extrapolated to lower gluino/neutralino masses where no grid point was generated.

sensitivity to gluino or squark production, by requiring higher or lower jet multiplicity, or by placing requirements on the charge or flavour of the leptons in the dilepton channel.

Observations are in agreement with SM expectations in each signal region and limits are set on the visible cross section in models of new physics within the kinematic requirements of the searches. Exclusion limits are also placed on a large number of supersymmetric models, including a bRPV model, and on one model of mUED, for which a compactification radius of $1/R_c = 950$ GeV is excluded for a cut-off scale times radius (ΛR_c) of approximately 30. These limits are either new or extend the region of parameter space excluded by previous searches with the ATLAS detector. Depending on the model of supersymmetry considered, the limits are able to exclude gluino masses up to 1.32 TeV and squark masses up to 840 GeV.

Acknowledgments

We thank CERN for the very successful operation of the LHC, as well as the support staff from our institutions without whom ATLAS could not be operated efficiently.

JHEP04(2015)116

We acknowledge the support of ANPCyT, Argentina; YerPhI, Armenia; ARC, Australia; BMWFW and FWF, Austria; ANAS, Azerbaijan; SSTC, Belarus; CNPq and FAPESP, Brazil; NSERC, NRC and CFI, Canada; CERN; CONICYT, Chile; CAS, MOST and NSFC, China; COLCIENCIAS, Colombia; MSMT CR, MPO CR and VSC CR, Czech Republic; DNRF, DNSRC and Lundbeck Foundation, Denmark; EPLANET, ERC and NSRF, European Union; IN2P3-CNRS, CEA-DSM/IRFU, France; GNSF, Georgia; BMBF, DFG, HGF, MPG and AvH Foundation, Germany; GSRT and NSRF, Greece; RGC, Hong Kong SAR, China; ISF, MINERVA, GIF, I-CORE and Benoziyo Center, Israel; INFN, Italy; MEXT and JSPS, Japan; CNRST, Morocco; FOM and NWO, Netherlands; BRF and RCN, Norway; MNiSW and NCN, Poland; GRICES and FCT, Portugal; MNE/IFA, Romania; MES of Russia and NRC KI, Russian Federation; JINR; MSTD, Serbia; MSSR, Slovakia; ARRS and MIZŠ, Slovenia; DST/NRF, South Africa; MINECO, Spain; SRC and Wallenberg Foundation, Sweden; SER, SNSF and Cantons of Bern and Geneva, Switzerland; NSC, Taiwan; TAEK, Turkey; STFC, the Royal Society and Leverhulme Trust, United Kingdom; DOE and NSF, United States of America.

The crucial computing support from all WLCG partners is acknowledged gratefully, in particular from CERN and the ATLAS Tier-1 facilities at TRIUMF (Canada), NDGF (Denmark, Norway, Sweden), CC-IN2P3 (France), KIT/GridKA (Germany), INFN-CNAF (Italy), NL-T1 (Netherlands), PIC (Spain), ASGC (Taiwan), RAL (U.K.) and BNL (U.S.A.) and in the Tier-2 facilities worldwide.

Open Access. This article is distributed under the terms of the Creative Commons Attribution License (CC-BY 4.0), which permits any use, distribution and reproduction in any medium, provided the original author(s) and source are credited.

References

[1] H. Miyazawa, *Baryon number changing currents*, *Prog. Theor. Phys.* **36** (1966) 1266 [INSPIRE].

[2] P. Ramond, *Dual theory for free fermions*, *Phys. Rev.* **D 3** (1971) 2415 [INSPIRE].

[3] Y. Golfand and E.P. Likhtman, *Extension of the algebra of Poincaré group generators and violation of p invariance*, *JETP Lett.* **13** (1971) 323 [*Pisma Zh. Eksp. Teor. Fiz.* **13** (1971) 452] [INSPIRE].

[4] A. Neveu and J.H. Schwarz, *Factorizable dual model of pions*, *Nucl. Phys.* **B 31** (1971) 86 [INSPIRE].

[5] A. Neveu and J.H. Schwarz, *Quark model of dual pions*, *Phys. Rev.* **D 4** (1971) 1109 [INSPIRE].

[6] J.-L. Gervais and B. Sakita, *Field theory interpretation of supergauges in dual models*, *Nucl. Phys.* **B 34** (1971) 632 [INSPIRE].

[7] D.V. Volkov and V.P. Akulov, *Is the neutrino a Goldstone particle?*, *Phys. Lett.* **B 46** (1973) 109 [INSPIRE].

[8] J. Wess and B. Zumino, *A Lagrangian model invariant under supergauge transformations*, *Phys. Lett.* **B 49** (1974) 52 [INSPIRE].

JHEP04(2015)116

[9] J. Wess and B. Zumino, *Supergauge transformations in four-dimensions*, *Nucl. Phys.* **B 70** (1974) 39 [INSPIRE].

[10] E. Witten, *Dynamical breaking of supersymmetry*, *Nucl. Phys.* **B 188** (1981) 513 [INSPIRE].

[11] M. Dine, W. Fischler and M. Srednicki, *Supersymmetric technicolor*, *Nucl. Phys.* **B 189** (1981) 575 [INSPIRE].

[12] S. Dimopoulos and S. Raby, *Supercolor*, *Nucl. Phys.* **B 192** (1981) 353 [INSPIRE].

[13] N. Sakai, *Naturalness in supersymmetric guts*, *Z. Phys.* **C 11** (1981) 153 [INSPIRE].

[14] R.K. Kaul and P. Majumdar, *Cancellation of quadratically divergent mass corrections in globally supersymmetric spontaneously broken gauge theories*, *Nucl. Phys.* **B 199** (1982) 36 [INSPIRE].

[15] S. Dimopoulos and H. Georgi, *Softly broken supersymmetry and* SU(5), *Nucl. Phys.* **B 193** (1981) 150 [INSPIRE].

[16] P. Fayet, *Supersymmetry and weak, electromagnetic and strong interactions*, *Phys. Lett.* **B 64** (1976) 159 [INSPIRE].

[17] P. Fayet, *Spontaneously broken supersymmetric theories of weak, electromagnetic and strong interactions*, *Phys. Lett.* **B 69** (1977) 489 [INSPIRE].

[18] G.R. Farrar and P. Fayet, *Phenomenology of the production, decay and detection of new hadronic states associated with supersymmetry*, *Phys. Lett.* **B 76** (1978) 575 [INSPIRE].

[19] P. Fayet, *Relations between the masses of the superpartners of leptons and quarks, the Goldstino couplings and the neutral currents*, *Phys. Lett.* **B 84** (1979) 416 [INSPIRE].

[20] ATLAS collaboration, *The ATLAS experiment at the CERN Large Hadron Collider*, 2008 *JINST* **3** S08003 [INSPIRE].

[21] ATLAS collaboration, *Expected performance of the ATLAS experiment — detector, trigger and physics*, arXiv:0901.0512 [INSPIRE].

[22] ATLAS collaboration, *Further search for supersymmetry at* $\sqrt{s} = 7$ *TeV in final states with jets, missing transverse momentum and isolated leptons with the ATLAS detector*, *Phys. Rev.* **D 86** (2012) 092002 [arXiv:1208.4688] [INSPIRE].

[23] ATLAS collaboration, *Multi-channel search for squarks and gluinos in* $\sqrt{s} = 7$ *TeV pp collisions with the ATLAS detector*, *Eur. Phys. J.* **C 73** (2013) 2362 [arXiv:1212.6149] [INSPIRE].

[24] CMS collaboration, *Search for supersymmetry in pp collisions at* $\sqrt{s} = 7$ *TeV in events with a single lepton, jets and missing transverse momentum*, *Eur. Phys. J.* **C 73** (2013) 2404 [arXiv:1212.6428] [INSPIRE].

[25] ATLAS collaboration, *Performance of the ATLAS trigger system in* 2010, *Eur. Phys. J.* **C 72** (2012) 1849 [arXiv:1110.1530] [INSPIRE].

[26] J. Alwall, P. Schuster and N. Toro, *Simplified models for a first characterization of new physics at the LHC*, *Phys. Rev.* **D 79** (2009) 075020 [arXiv:0810.3921] [INSPIRE].

[27] LHC New Physics Working Group collaboration, D. Alves et al., *Simplified models for LHC new physics searches*, *J. Phys.* **G 39** (2012) 105005 [arXiv:1105.2838] [INSPIRE].

[28] T. Appelquist, H.-C. Cheng and B.A. Dobrescu, *Bounds on universal extra dimensions*, *Phys. Rev.* **D 64** (2001) 035002 [hep-ph/0012100] [INSPIRE].

JHEP04(2015)116

[29] H.-C. Cheng, K.T. Matchev and M. Schmaltz, *Bosonic supersymmetry? Getting fooled at the CERN LHC*, *Phys. Rev.* **D 66** (2002) 056006 [hep-ph/0205314] [INSPIRE].

[30] ATLAS collaboration, *Search for supersymmetry at $\sqrt{s} = 8$ TeV in final states with jets and two same-sign leptons or three leptons with the ATLAS detector*, *JHEP* **06** (2014) 035 [arXiv:1404.2500] [INSPIRE].

[31] ATLAS collaboration, *Search for new phenomena in final states with large jet multiplicities and missing transverse momentum at $\sqrt{s} = 8$ TeV proton-proton collisions using the ATLAS experiment*, *JHEP* **10** (2013) 130 [*Erratum ibid.* **01** (2014) 109] [arXiv:1308.1841] [INSPIRE].

[32] ATLAS collaboration, *Search for squarks and gluinos with the ATLAS detector in final states with jets and missing transverse momentum using $\sqrt{s} = 8$ TeV proton-proton collision data*, *JHEP* **09** (2014) 176 [arXiv:1405.7875] [INSPIRE].

[33] ATLAS collaboration, *Search for strong production of supersymmetric particles in final states with missing transverse momentum and at least three b-jets at $\sqrt{s} = 8$ TeV proton-proton collisions with the ATLAS detector*, *JHEP* **10** (2014) 024 [arXiv:1407.0600] [INSPIRE].

[34] ATLAS collaboration, *Search for supersymmetry in events with large missing transverse momentum, jets and at least one τ lepton in $20\,\mathrm{fb}^{-1}$ of $\sqrt{s} = 8$ TeV proton-proton collision data with the ATLAS detector*, *JHEP* **09** (2014) 103 [arXiv:1407.0603] [INSPIRE].

[35] A.H. Chamseddine, R.L. Arnowitt and P. Nath, *Locally supersymmetric grand unification*, *Phys. Rev. Lett.* **49** (1982) 970 [INSPIRE].

[36] R. Barbieri, S. Ferrara and C.A. Savoy, *Gauge models with spontaneously broken local supersymmetry*, *Phys. Lett.* **B 119** (1982) 343 [INSPIRE].

[37] L.E. Ibáñez, *Locally supersymmetric* SU(5) *grand unification*, *Phys. Lett.* **B 118** (1982) 73 [INSPIRE].

[38] L.J. Hall, J.D. Lykken and S. Weinberg, *Supergravity as the messenger of supersymmetry breaking*, *Phys. Rev.* **D 27** (1983) 2359 [INSPIRE].

[39] N. Ohta, *Grand unified theories based on local supersymmetry*, *Prog. Theor. Phys.* **70** (1983) 542 [INSPIRE].

[40] G.L. Kane, C.F. Kolda, L. Roszkowski and J.D. Wells, *Study of constrained minimal supersymmetry*, *Phys. Rev.* **D 49** (1994) 6173 [hep-ph/9312272] [INSPIRE].

[41] S. Roy and B. Mukhopadhyaya, *Some implications of a supersymmetric model with R-parity breaking bilinear interactions*, *Phys. Rev.* **D 55** (1997) 7020 [hep-ph/9612447] [INSPIRE].

[42] J. Barnard, B. Farmer, T. Gherghetta and M. White, *Natural gauge mediation with a bino NLSP at the LHC*, *Phys. Rev. Lett.* **109** (2012) 241801 [arXiv:1208.6062] [INSPIRE].

[43] L. Covi and S. Kraml, *Collider signatures of gravitino dark matter with a sneutrino NLSP*, *JHEP* **08** (2007) 015 [hep-ph/0703130] [INSPIRE].

[44] ATLAS collaboration, *Search for pair-produced third-generation squarks decaying via charm quarks or in compressed supersymmetric scenarios in pp collisions at $\sqrt{s} = 8$ TeV with the ATLAS detector*, *Phys. Rev.* **D 90** (2014) 052008 [arXiv:1407.0608] [INSPIRE].

JHEP04(2015)116

[45] D.F. Carvalho, M.E. Gomez and J.C. Romao, *Charged lepton flavor violation in supersymmetry with bilinear R-parity violation*, *Phys. Rev.* **D 65** (2002) 093013 [hep-ph/0202054] [INSPIRE].

[46] Y. Grossman and S. Rakshit, *Neutrino masses in R-parity violating supersymmetric models*, *Phys. Rev.* **D 69** (2004) 093002 [hep-ph/0311310] [INSPIRE].

[47] P. Meade, N. Seiberg and D. Shih, *General gauge mediation*, *Prog. Theor. Phys. Suppl.* **177** (2009) 143 [arXiv:0801.3278] [INSPIRE].

[48] M. Buican, P. Meade, N. Seiberg and D. Shih, *Exploring general gauge mediation*, *JHEP* **03** (2009) 016 [arXiv:0812.3668] [INSPIRE].

[49] A. Djouadi, M.M. Muhlleitner and M. Spira, *Decays of supersymmetric particles: the program SUSY-HIT (SUspect-SdecaY-HDECAY-InTerface)*, *Acta Phys. Polon.* **B 38** (2007) 635 [hep-ph/0609292] [INSPIRE].

[50] M. Muhlleitner, A. Djouadi and Y. Mambrini, *SDECAY: a fortran code for the decays of the supersymmetric particles in the MSSM*, *Comput. Phys. Commun.* **168** (2005) 46 [hep-ph/0311167] [INSPIRE].

[51] B.C. Allanach, *SOFTSUSY: a program for calculating supersymmetric spectra*, *Comput. Phys. Commun.* **143** (2002) 305 [hep-ph/0104145] [INSPIRE].

[52] J. Alwall, M. Herquet, F. Maltoni, O. Mattelaer and T. Stelzer, *MadGraph* 5*: going beyond*, *JHEP* **06** (2011) 128 [arXiv:1106.0522] [INSPIRE].

[53] T. Sjöstrand, S. Mrenna and P.Z. Skands, *PYTHIA* 6.4 *physics and manual*, *JHEP* **05** (2006) 026 [hep-ph/0603175] [INSPIRE].

[54] J. Alwall et al., *Comparative study of various algorithms for the merging of parton showers and matrix elements in hadronic collisions*, *Eur. Phys. J.* **C 53** (2008) 473 [arXiv:0706.2569] [INSPIRE].

[55] M. Bähr et al., *HERWIG++ physics and manual*, *Eur. Phys. J.* **C 58** (2008) 639 [arXiv:0803.0883] [INSPIRE].

[56] ATLAS collaboration, *New ATLAS event generator tunes to* 2010 *data*, ATL-PHYS-PUB-2011-008, CERN, Geneva Switzerland (2011).

[57] S. Gieseke, C. Rohr and A. Siodmok, *Colour reconnections in HERWIG++*, *Eur. Phys. J.* **C 72** (2012) 2225 [arXiv:1206.0041] [INSPIRE].

[58] J. Pumplin et al., *New generation of parton distributions with uncertainties from global QCD analysis*, *JHEP* **07** (2002) 012 [hep-ph/0201195] [INSPIRE].

[59] W. Beenakker, R. Hopker, M. Spira and P.M. Zerwas, *Squark and gluino production at hadron colliders*, *Nucl. Phys.* **B 492** (1997) 51 [hep-ph/9610490] [INSPIRE].

[60] A. Kulesza and L. Motyka, *Threshold resummation for squark-antisquark and gluino-pair production at the LHC*, *Phys. Rev. Lett.* **102** (2009) 111802 [arXiv:0807.2405] [INSPIRE].

[61] A. Kulesza and L. Motyka, *Soft gluon resummation for the production of gluino-gluino and squark-antisquark pairs at the LHC*, *Phys. Rev.* **D 80** (2009) 095004 [arXiv:0905.4749] [INSPIRE].

[62] W. Beenakker et al., *Soft-gluon resummation for squark and gluino hadroproduction*, *JHEP* **12** (2009) 041 [arXiv:0909.4418] [INSPIRE].

JHEP04(2015)116

[63] W. Beenakker et al., *Squark and gluino hadroproduction*, *Int. J. Mod. Phys.* **A 26** (2011) 2637 [arXiv:1105.1110] [INSPIRE].

[64] M. Krämer et al., *Supersymmetry production cross sections in pp collisions at* $\sqrt{s} = 7$ *TeV*, arXiv:1206.2892 [INSPIRE].

[65] T. Gleisberg et al., *Event generation with SHERPA* 1.1, *JHEP* **02** (2009) 007 [arXiv:0811.4622] [INSPIRE].

[66] S. Catani, L. Cieri, G. Ferrera, D. de Florian and M. Grazzini, *Vector boson production at hadron colliders: a fully exclusive QCD calculation at NNLO*, *Phys. Rev. Lett.* **103** (2009) 082001 [arXiv:0903.2120] [INSPIRE].

[67] S. Catani and M. Grazzini, *An NNLO subtraction formalism in hadron collisions and its application to Higgs boson production at the LHC*, *Phys. Rev. Lett.* **98** (2007) 222002 [hep-ph/0703012] [INSPIRE].

[68] H.-L. Lai et al., *New parton distributions for collider physics*, *Phys. Rev.* **D 82** (2010) 074024 [arXiv:1007.2241] [INSPIRE].

[69] P. Nason, *A new method for combining NLO QCD with shower Monte Carlo algorithms*, *JHEP* **11** (2004) 040 [hep-ph/0409146] [INSPIRE].

[70] S. Frixione, P. Nason and C. Oleari, *Matching NLO QCD computations with parton shower simulations: the POWHEG method*, *JHEP* **11** (2007) 070 [arXiv:0709.2092] [INSPIRE].

[71] S. Alioli, P. Nason, C. Oleari and E. Re, *A general framework for implementing NLO calculations in shower Monte Carlo programs: the POWHEG BOX*, *JHEP* **06** (2010) 043 [arXiv:1002.2581] [INSPIRE].

[72] M. Czakon, P. Fiedler and A. Mitov, *Total top-quark pair-production cross section at hadron colliders through* $O(\alpha_s^4)$, *Phys. Rev. Lett.* **110** (2013) 252004 [arXiv:1303.6254] [INSPIRE].

[73] M. Czakon and A. Mitov, *Top++: a program for the calculation of the top-pair cross-section at hadron colliders*, *Comput. Phys. Commun.* **185** (2014) 2930 [arXiv:1112.5675] [INSPIRE].

[74] B. Cooper et al., *Importance of a consistent choice of* α_s *in the matching of ALPGEN and PYTHIA*, *Eur. Phys. J.* **C 72** (2012) 2078 [arXiv:1109.5295] [INSPIRE].

[75] B.P. Kersevan and E. Richter-Was, *The Monte Carlo event generator AcerMC versions* 2.0 *to* 3.8 *with interfaces to PYTHIA* 6.4, *HERWIG* 6.5 *and ARIADNE* 4.1, *Comput. Phys. Commun.* **184** (2013) 919 [hep-ph/0405247] [INSPIRE].

[76] N. Kidonakis, *Next-to-next-to-leading-order collinear and soft gluon corrections for t-channel single top quark production*, *Phys. Rev.* **D 83** (2011) 091503 [arXiv:1103.2792] [INSPIRE].

[77] N. Kidonakis, *NNLL resummation for s-channel single top quark production*, *Phys. Rev.* **D 81** (2010) 054028 [arXiv:1001.5034] [INSPIRE].

[78] N. Kidonakis, *Two-loop soft anomalous dimensions for single top quark associated production with a* W^- *or* H^-, *Phys. Rev.* **D 82** (2010) 054018 [arXiv:1005.4451] [INSPIRE].

[79] J.M. Campbell and R.K. Ellis, $t\bar{t}W^{\pm}$ *production and decay at NLO*, *JHEP* **07** (2012) 052 [arXiv:1204.5678] [INSPIRE].

JHEP04(2015)116

[80] A. Lazopoulos, T. McElmurry, K. Melnikov and F. Petriello, *Next-to-leading order QCD corrections to $t\bar{t}Z$ production at the LHC*, Phys. Lett. **B 666** (2008) 62 [arXiv:0804.2220] [INSPIRE].

[81] J.M. Campbell and R.K. Ellis, *An update on vector boson pair production at hadron colliders*, Phys. Rev. **D 60** (1999) 113006 [hep-ph/9905386] [INSPIRE].

[82] J.M. Campbell, R.K. Ellis and C. Williams, *Vector boson pair production at the LHC*, JHEP **07** (2011) 018 [arXiv:1105.0020] [INSPIRE].

[83] P. Nason and G. Zanderighi, *W^+W^-, WZ and ZZ production in the POWHEG-BOX-V2*, Eur. Phys. J. **C 74** (2014) 2702 [arXiv:1311.1365] [INSPIRE].

[84] K. Melnikov and F. Petriello, *Electroweak gauge boson production at hadron colliders through $O(\alpha_s^2)$*, Phys. Rev. **D 74** (2006) 114017 [hep-ph/0609070] [INSPIRE].

[85] M.L. Mangano, M. Moretti, F. Piccinini, R. Pittau and A.D. Polosa, *ALPGEN, a generator for hard multiparton processes in hadronic collisions*, JHEP **07** (2003) 001 [hep-ph/0206293] [INSPIRE].

[86] G. Corcella et al., *HERWIG 6: an event generator for hadron emission reactions with interfering gluons (including supersymmetric processes)*, JHEP **01** (2001) 010 [hep-ph/0011363] [INSPIRE].

[87] J.M. Butterworth, J.R. Forshaw and M.H. Seymour, *Multiparton interactions in photoproduction at HERA*, Z. Phys. **C 72** (1996) 637 [hep-ph/9601371] [INSPIRE].

[88] T. Sjöstrand, S. Mrenna and P.Z. Skands, *A brief introduction to PYTHIA 8.1*, Comput. Phys. Commun. **178** (2008) 852 [arXiv:0710.3820] [INSPIRE].

[89] ATLAS collaboration, *The ATLAS simulation infrastructure*, Eur. Phys. J. **C 70** (2010) 823 [arXiv:1005.4568] [INSPIRE].

[90] GEANT4 collaboration, S. Agostinelli et al., *GEANT4: a simulation toolkit*, Nucl. Instrum. Meth. **A 506** (2003) 250 [INSPIRE].

[91] ATLAS collaboration, *The simulation principle and performance of the ATLAS fast calorimeter simulation FastCaloSim*, ATL-PHYS-PUB-2010-013, CERN, Geneva Switzerland (2010).

[92] A. Sherstnev and R.S. Thorne, *Parton distributions for LO generators*, Eur. Phys. J. **C 55** (2008) 553 [arXiv:0711.2473] [INSPIRE].

[93] ATLAS collaboration, *Further ATLAS tunes of PYTHIA 6 and PYTHIA 8*, ATL-PHYS-PUB-2011-014, CERN, Geneva Switzerland (2011).

[94] ATLAS collaboration, *Improved luminosity determination in pp collisions at $\sqrt{s} = 7$ TeV using the ATLAS detector at the LHC*, Eur. Phys. J. **C 73** (2013) 2518 [arXiv:1302.4393] [INSPIRE].

[95] ATLAS collaboration, *Performance of primary vertex reconstruction in proton-proton collisions at $\sqrt{s} = 7$ TeV in the ATLAS experiment*, ATLAS-CONF-2010-069, CERN, Geneva Switzerland (2010).

[96] M. Cacciari, G.P. Salam and G. Soyez, *The anti-k_t jet clustering algorithm*, JHEP **04** (2008) 063 [arXiv:0802.1189] [INSPIRE].

[97] M. Cacciari and G.P. Salam, *Dispelling the N^3 myth for the k_t jet-finder*, Phys. Lett. **B 641** (2006) 57 [hep-ph/0512210] [INSPIRE].

JHEP04(2015)116

[98] ATLAS collaboration, *Jet energy measurement with the ATLAS detector in proton-proton collisions at* $\sqrt{s} = 7$ *TeV*, *Eur. Phys. J.* **C 73** (2013) 2304 [arXiv:1112.6426] [INSPIRE].

[99] M. Cacciari, G.P. Salam and G. Soyez, *The catchment area of jets*, *JHEP* **04** (2008) 005 [arXiv:0802.1188] [INSPIRE].

[100] ATLAS collaboration, *Single hadron response measurement and calorimeter jet energy scale uncertainty with the ATLAS detector at the LHC*, *Eur. Phys. J.* **C 73** (2013) 2305 [arXiv:1203.1302] [INSPIRE].

[101] ATLAS collaboration, *Electron reconstruction and identification efficiency measurements with the ATLAS detector using the* 2011 *LHC proton-proton collision data*, *Eur. Phys. J.* **C 74** (2014) 2941 [arXiv:1404.2240] [INSPIRE].

[102] ATLAS collaboration, *Measurement of the muon reconstruction performance of the ATLAS detector using* 2011 *and* 2012 *LHC proton-proton collision data*, *Eur. Phys. J.* **C 74** (2014) 3130 [arXiv:1407.3935] [INSPIRE].

[103] ATLAS collaboration, *Search for supersymmetry in final states with jets, missing transverse momentum and one isolated lepton in* $\sqrt{s} = 7$ *TeV pp collisions using* $1\,\mathrm{fb}^{-1}$ *of ATLAS data*, *Phys. Rev.* **D 85** (2012) 012006 [*Erratum ibid.* **D 87** (2013) 099903] [arXiv:1109.6606] [INSPIRE].

[104] ATLAS collaboration, *Performance of missing transverse momentum reconstruction in proton-proton collisions at* 7 *TeV with ATLAS*, *Eur. Phys. J.* **C 72** (2012) 1844 [arXiv:1108.5602] [INSPIRE].

[105] ATLAS collaboration, *Pile-up subtraction and suppression for jets in ATLAS*, ATLAS-CONF-2013-083, CERN, Geneva Switzerland (2013).

[106] ATLAS collaboration, *Calibration of the performance of b-tagging for c and light-flavour jets in the* 2012 *ATLAS data*, ATLAS-CONF-2014-046, CERN, Geneva Switzerland (2014).

[107] ATLAS collaboration, *Measurement of the b-tag efficiency in a sample of jets containing muons with* $5\,\mathrm{fb}^{-1}$ *of data from the ATLAS detector*, ATLAS-CONF-2012-043, CERN, Geneva Switzerland (2012).

[108] ATLAS collaboration, *Characterisation and mitigation of beam-induced backgrounds observed in the ATLAS detector during the* 2011 *proton-proton run*, 2013 *JINST* **8** P07004 [arXiv:1303.0223] [INSPIRE].

[109] ATLAS collaboration, *Selection of jets produced in proton-proton collisions with the ATLAS detector using* 2011 *data*, ATLAS-CONF-2012-020, CERN, Geneva Switzerland (2012).

[110] C. Rogan, *Kinematical variables towards new dynamics at the LHC*, arXiv:1006.2727 [INSPIRE].

[111] ATLAS collaboration, *Measurement of the top quark-pair production cross section with ATLAS in pp collisions at* $\sqrt{s} = 7$ *TeV*, *Eur. Phys. J.* **C 71** (2011) 1577 [arXiv:1012.1792] [INSPIRE].

[112] ATLAS collaboration, *Jet energy resolution and selection efficiency relative to track jets from in-situ techniques with the ATLAS detector using proton-proton collisions at a center of mass energy* $\sqrt{s} = 7$ *TeV*, ATLAS-CONF-2010-054, CERN, Geneva Switzerland (2010).

[113] ATLAS collaboration, *Pile-up subtraction and suppression for jets in ATLAS*, ATLAS-CONF-2013-083, CERN, Geneva Switzerland (2013).

JHEP04(2015)116

[114] ATLAS collaboration, *Calibration of b-tagging using dileptonic top pair events in a combinatorial likelihood approach with the ATLAS experiment*, ATLAS-CONF-2014-004, CERN, Geneva Switzerland (2014).

[115] ATLAS collaboration, *Measurement of the mistag rate with* $5\,\mathrm{fb}^{-1}$ *of data collected by the ATLAS detector*, ATLAS-CONF-2012-040, CERN, Geneva Switzerland (2012).

[116] M. Botje et al., *The PDF4LHC working group interim recommendations*, arXiv:1101.0538 [INSPIRE].

[117] J. Alwall et al., *The automated computation of tree-level and next-to-leading order differential cross sections and their matching to parton shower simulations*, *JHEP* **07** (2014) 079 [arXiv:1405.0301] [INSPIRE].

[118] G. Cowan, K. Cranmer, E. Gross and O. Vitells, *Asymptotic formulae for likelihood-based tests of new physics*, *Eur. Phys. J.* **C 71** (2011) 1554 [*Erratum ibid.* **C 73** (2013) 2501] [arXiv:1007.1727] [INSPIRE].

[119] M. Baak et al., *HistFitter software framework for statistical data analysis*, arXiv:1410.1280 [INSPIRE].

[120] ATLAS collaboration, *Measurements of top quark pair relative differential cross-sections with ATLAS in pp collisions at* $\sqrt{s} = 7$ *TeV*, *Eur. Phys. J.* **C 73** (2013) 2261 [arXiv:1207.5644] [INSPIRE].

[121] ATLAS collaboration, *Measurements of normalized differential cross sections for* $t\bar{t}$ *production in pp collisions at* $\sqrt{s} = 7$ *TeV using the ATLAS detector*, *Phys. Rev.* **D 90** (2014) 072004 [arXiv:1407.0371] [INSPIRE].

[122] ATLAS collaboration, *Measurement of the production cross section of jets in association with a Z boson in pp collisions at* $\sqrt{s} = 7$ *TeV with the ATLAS detector*, *JHEP* **07** (2013) 032 [arXiv:1304.7098] [INSPIRE].

[123] ATLAS collaboration, *Measurements of the W production cross sections in association with jets with the ATLAS detector*, *Eur. Phys. J.* **C 75** (2015) 82 [arXiv:1409.8639] [INSPIRE].

[124] ATLAS collaboration, *A measurement of the ratio of the production cross sections for W and Z bosons in association with jets with the ATLAS detector*, *Eur. Phys. J.* **C 74** (2014) 3168 [arXiv:1408.6510] [INSPIRE].

[125] A.L. Read, *Presentation of search results: the* CL_s *technique*, *J. Phys.* **G 28** (2002) 2693 [INSPIRE].

JHEP04(2015)116

The ATLAS collaboration

G. Aad[85], B. Abbott[113], J. Abdallah[152], S. Abdel Khalek[117], O. Abdinov[11], R. Aben[107], B. Abi[114], M. Abolins[90], O.S. AbouZeid[159], H. Abramowicz[154], H. Abreu[153], R. Abreu[30], Y. Abulaiti[147a,147b], B.S. Acharya[165a,165b,a], L. Adamczyk[38a], D.L. Adams[25], J. Adelman[108], S. Adomeit[100], T. Adye[131], T. Agatonovic-Jovin[13a], J.A. Aguilar-Saavedra[126a,126f], M. Agustoni[17], S.P. Ahlen[22], F. Ahmadov[65,b], G. Aielli[134a,134b], H. Akerstedt[147a,147b], T.P.A. Åkesson[81], G. Akimoto[156], A.V. Akimov[96], G.L. Alberghi[20a,20b], J. Albert[170], S. Albrand[55], M.J. Alconada Verzini[71], M. Aleksa[30], I.N. Aleksandrov[65], C. Alexa[26a], G. Alexander[154], G. Alexandre[49], T. Alexopoulos[10], M. Alhroob[113], G. Alimonti[91a], L. Alio[85], J. Alison[31], B.M.M. Allbrooke[18], L.J. Allison[72], P.P. Allport[74], A. Aloisio[104a,104b], A. Alonso[36], F. Alonso[71], C. Alpigiani[76], A. Altheimer[35], B. Alvarez Gonzalez[90], M.G. Alviggi[104a,104b], K. Amako[66], Y. Amaral Coutinho[24a], C. Amelung[23], D. Amidei[89], S.P. Amor Dos Santos[126a,126c], A. Amorim[126a,126b], S. Amoroso[48], N. Amram[154], G. Amundsen[23], C. Anastopoulos[140], L.S. Ancu[49], N. Andari[30], T. Andeen[35], C.F. Anders[58b], G. Anders[30], K.J. Anderson[31], A. Andreazza[91a,91b], V. Andrei[58a], X.S. Anduaga[71], S. Angelidakis[9], I. Angelozzi[107], P. Anger[44], A. Angerami[35], F. Anghinolfi[30], A.V. Anisenkov[109,c], N. Anjos[12], A. Annovi[47], M. Antonelli[47], A. Antonov[98], J. Antos[145b], F. Anulli[133a], M. Aoki[66], L. Aperio Bella[18], G. Arabidze[90], Y. Arai[66], J.P. Araque[126a], A.T.H. Arce[45], F.A. Arduh[71], J-F. Arguin[95], S. Argyropoulos[42], M. Arik[19a], A.J. Armbruster[30], O. Arnaez[30], V. Arnal[82], H. Arnold[48], M. Arratia[28], O. Arslan[21], A. Artamonov[97], G. Artoni[23], S. Asai[156], N. Asbah[42], A. Ashkenazi[154], B. Åsman[147a,147b], L. Asquith[150], K. Assamagan[25], R. Astalos[145a], M. Atkinson[166], N.B. Atlay[142], B. Auerbach[6], K. Augsten[128], M. Aurousseau[146b], G. Avolio[30], B. Axen[15], G. Azuelos[95,d], Y. Azuma[156], M.A. Baak[30], A.E. Baas[58a], C. Bacci[135a,135b], H. Bachacou[137], K. Bachas[155], M. Backes[30], M. Backhaus[30], E. Badescu[26a], P. Bagiacchi[133a,133b], P. Bagnaia[133a,133b], Y. Bai[33a], T. Bain[35], J.T. Baines[131], O.K. Baker[177], P. Balek[129], F. Balli[84], E. Banas[39], Sw. Banerjee[174], A.A.E. Bannoura[176], H.S. Bansil[18], L. Barak[173], S.P. Baranov[96], E.L. Barberio[88], D. Barberis[50a,50b], M. Barbero[85], T. Barillari[101], M. Barisonzi[176], T. Barklow[144], N. Barlow[28], S.L. Barnes[84], B.M. Barnett[131], R.M. Barnett[15], Z. Barnovska[5], A. Baroncelli[135a], G. Barone[49], A.J. Barr[120], F. Barreiro[82], J. Barreiro Guimarães da Costa[57], R. Bartoldus[144], A.E. Barton[72], P. Bartos[145a], A. Bassalat[117], A. Basye[166], R.L. Bates[53], S.J. Batista[159], J.R. Batley[28], M. Battaglia[138], M. Battistin[30], F. Bauer[137], H.S. Bawa[144,e], J.B. Beacham[111], M.D. Beattie[72], T. Beau[80], P.H. Beauchemin[162], R. Beccherle[124a,124b], P. Bechtle[21], H.P. Beck[17,f], K. Becker[120], S. Becker[100], M. Beckingham[171], C. Becot[117], A.J. Beddall[19c], A. Beddall[19c], S. Bedikian[177], V.A. Bednyakov[65], C.P. Bee[149], L.J. Beemster[107], T.A. Beermann[176], M. Begel[25], K. Behr[120], C. Belanger-Champagne[87], P.J. Bell[49], W.H. Bell[49], G. Bella[154], L. Bellagamba[20a], A. Bellerive[29], M. Bellomo[86], K. Belotskiy[98], O. Beltramello[30], O. Benary[154], D. Benchekroun[136a], K. Bendtz[147a,147b], N. Benekos[166], Y. Benhammou[154], E. Benhar Noccioli[49], J.A. Benitez Garcia[160b], D.P. Benjamin[45], J.R. Bensinger[23], S. Bentvelsen[107], D. Berge[107], E. Bergeaas Kuutmann[167], N. Berger[5], F. Berghaus[170], J. Beringer[15], C. Bernard[22], N.R. Bernard[86], C. Bernius[110], F.U. Bernlochner[21], T. Berry[77], P. Berta[129], C. Bertella[83], G. Bertoli[147a,147b], F. Bertolucci[124a,124b], C. Bertsche[113], D. Bertsche[113], M.I. Besana[91a], G.J. Besjes[106], O. Bessidskaia Bylund[147a,147b], M. Bessner[42], N. Besson[137], C. Betancourt[48], S. Bethke[101], A.J. Bevan[76], W. Bhimji[46], R.M. Bianchi[125], L. Bianchini[23], M. Bianco[30], O. Biebel[100], S.P. Bieniek[78], K. Bierwagen[54], M. Biglietti[135a], J. Bilbao De Mendizabal[49], H. Bilokon[47], M. Bindi[54], S. Binet[117], A. Bingul[19c], C. Bini[133a,133b], C.W. Black[151], J.E. Black[144], K.M. Black[22], D. Blackburn[139], R.E. Blair[6], J.-B. Blanchard[137], T. Blazek[145a], I. Bloch[42], C. Blocker[23], W. Blum[83,*], U. Blumenschein[54], G.J. Bobbink[107], V.S. Bobrovnikov[109,c],

JHEP04(2015)116

S.S. Bocchetta[81], A. Bocci[45], C. Bock[100], C.R. Boddy[120], M. Boehler[48], T.T. Boek[176], J.A. Bogaerts[30], A.G. Bogdanchikov[109], A. Bogouch[92,*], C. Bohm[147a], V. Boisvert[77], T. Bold[38a], V. Boldea[26a], A.S. Boldyrev[99], M. Bomben[80], M. Bona[76], M. Boonekamp[137], A. Borisov[130], G. Borissov[72], S. Borroni[42], J. Bortfeldt[100], V. Bortolotto[60a], K. Bos[107], D. Boscherini[20a], M. Bosman[12], H. Boterenbrood[107], J. Boudreau[125], J. Bouffard[2], E.V. Bouhova-Thacker[72], D. Boumediene[34], C. Bourdarios[117], N. Bousson[114], S. Boutouil[136d], A. Boveia[31], J. Boyd[30], I.R. Boyko[65], I. Bozic[13a], J. Bracinik[18], A. Brandt[8], G. Brandt[15], O. Brandt[58a], U. Bratzler[157], B. Brau[86], J.E. Brau[116], H.M. Braun[176,*], S.F. Brazzale[165a,165c], B. Brelier[159], K. Brendlinger[122], A.J. Brennan[88], R. Brenner[167], S. Bressler[173], K. Bristow[146c], T.M. Bristow[46], D. Britton[53], F.M. Brochu[28], I. Brock[21], R. Brock[90], J. Bronner[101], G. Brooijmans[35], T. Brooks[77], W.K. Brooks[32b], J. Brosamer[15], E. Brost[116], J. Brown[55], P.A. Bruckman de Renstrom[39], D. Bruncko[145b], R. Bruneliere[48], S. Brunet[61], A. Bruni[20a], G. Bruni[20a], M. Bruschi[20a], L. Bryngemark[81], T. Buanes[14], Q. Buat[143], F. Bucci[49], P. Buchholz[142], A.G. Buckley[53], S.I. Buda[26a], I.A. Budagov[65], F. Buehrer[48], L. Bugge[119], M.K. Bugge[119], O. Bulekov[98], A.C. Bundock[74], H. Burckhart[30], S. Burdin[74], B. Burghgrave[108], S. Burke[131], I. Burmeister[43], E. Busato[34], D. Büscher[48], V. Büscher[83], P. Bussey[53], C.P. Buszello[167], B. Butler[57], J.M. Butler[22], A.I. Butt[3], C.M. Buttar[53], J.M. Butterworth[78], P. Butti[107], W. Buttinger[28], A. Buzatu[53], S. Cabrera Urbán[168], D. Caforio[20a,20b], O. Cakir[4a], P. Calafiura[15], A. Calandri[137], G. Calderini[80], P. Calfayan[100], L.P. Caloba[24a], D. Calvet[34], S. Calvet[34], R. Camacho Toro[49], S. Camarda[42], D. Cameron[119], L.M. Caminada[15], R. Caminal Armadans[12], S. Campana[30], M. Campanelli[78], A. Campoverde[149], V. Canale[104a,104b], A. Canepa[160a], M. Cano Bret[76], J. Cantero[82], R. Cantrill[126a], T. Cao[40], M.D.M. Capeans Garrido[30], I. Caprini[26a], M. Caprini[26a], M. Capua[37a,37b], R. Caputo[83], R. Cardarelli[134a], T. Carli[30], G. Carlino[104a], L. Carminati[91a,91b], S. Caron[106], E. Carquin[32a], G.D. Carrillo-Montoya[146c], J.R. Carter[28], J. Carvalho[126a,126c], D. Casadei[78], M.P. Casado[12], M. Casolino[12], E. Castaneda-Miranda[146b], A. Castelli[107], V. Castillo Gimenez[168], N.F. Castro[126a], P. Catastini[57], A. Catinaccio[30], J.R. Catmore[119], A. Cattai[30], G. Cattani[134a,134b], J. Caudron[83], V. Cavaliere[166], D. Cavalli[91a], M. Cavalli-Sforza[12], V. Cavasinni[124a,124b], F. Ceradini[135a,135b], B.C. Cerio[45], K. Cerny[129], A.S. Cerqueira[24b], A. Cerri[150], L. Cerrito[76], F. Cerutti[15], M. Cerv[30], A. Cervelli[17], S.A. Cetin[19b], A. Chafaq[136a], D. Chakraborty[108], I. Chalupkova[129], P. Chang[166], B. Chapleau[87], J.D. Chapman[28], D. Charfeddine[117], D.G. Charlton[18], C.C. Chau[159], C.A. Chavez Barajas[150], S. Cheatham[153], A. Chegwidden[90], S. Chekanov[6], S.V. Chekulaev[160a], G.A. Chelkov[65,g], M.A. Chelstowska[89], C. Chen[64], H. Chen[25], K. Chen[149], L. Chen[33d,h], S. Chen[33c], X. Chen[33f], Y. Chen[67], H.C. Cheng[89], Y. Cheng[31], A. Cheplakov[65], E. Cheremushkina[130], R. Cherkaoui El Moursli[136e], V. Chernyatin[25,*], E. Cheu[7], L. Chevalier[137], V. Chiarella[47], G. Chiefari[104a,104b], J.T. Childers[6], A. Chilingarov[72], G. Chiodini[73a], A.S. Chisholm[18], R.T. Chislett[78], A. Chitan[26a], M.V. Chizhov[65], S. Chouridou[9], B.K.B. Chow[100], D. Chromek-Burckhart[30], M.L. Chu[152], J. Chudoba[127], J.J. Chwastowski[39], L. Chytka[115], G. Ciapetti[133a,133b], A.K. Ciftci[4a], R. Ciftci[4a], D. Cinca[53], V. Cindro[75], A. Ciocio[15], Z.H. Citron[173], M. Citterio[91a], M. Ciubancan[26a], A. Clark[49], P.J. Clark[46], R.N. Clarke[15], W. Cleland[125], J.C. Clemens[85], C. Clement[147a,147b], Y. Coadou[85], M. Cobal[165a,165c], A. Coccaro[139], J. Cochran[64], L. Coffey[23], J.G. Cogan[144], B. Cole[35], S. Cole[108], A.P. Colijn[107], J. Collot[55], T. Colombo[58c], G. Compostella[101], P. Conde Muiño[126a,126b], E. Coniavitis[48], S.H. Connell[146b], I.A. Connelly[77], S.M. Consonni[91a,91b], V. Consorti[48], S. Constantinescu[26a], C. Conta[121a,121b], G. Conti[30], F. Conventi[104a,i], M. Cooke[15], B.D. Cooper[78], A.M. Cooper-Sarkar[120], N.J. Cooper-Smith[77], K. Copic[15], T. Cornelissen[176], M. Corradi[20a], F. Corriveau[87,j], A. Corso-Radu[164], A. Cortes-Gonzalez[12], G. Cortiana[101], G. Costa[91a], M.J. Costa[168], D. Costanzo[140], D. Côté[8], G. Cottin[28], G. Cowan[77], B.E. Cox[84], K. Cranmer[110], G. Cree[29], S. Crépé-Renaudin[55], F. Crescioli[80], W.A. Cribbs[147a,147b],

JHEP04(2015)116

M. Crispin Ortuzar[120], M. Cristinziani[21], V. Croft[106], G. Crosetti[37a,37b], T. Cuhadar Donszelmann[140], J. Cummings[177], M. Curatolo[47], C. Cuthbert[151], H. Czirr[142], P. Czodrowski[3], S. D'Auria[53], M. D'Onofrio[74], M.J. Da Cunha Sargedas De Sousa[126a,126b], C. Da Via[84], W. Dabrowski[38a], A. Dafinca[120], T. Dai[89], O. Dale[14], F. Dallaire[95], C. Dallapiccola[86], M. Dam[36], A.C. Daniells[18], M. Danninger[169], M. Dano Hoffmann[137], V. Dao[48], G. Darbo[50a], S. Darmora[8], J. Dassoulas[74], A. Dattagupta[61], W. Davey[21], C. David[170], T. Davidek[129], E. Davies[120,k], M. Davies[154], O. Davignon[80], A.R. Davison[78], P. Davison[78], Y. Davygora[58a], E. Dawe[143], I. Dawson[140], R.K. Daya-Ishmukhametova[86], K. De[8], R. de Asmundis[104a], S. De Castro[20a,20b], S. De Cecco[80], N. De Groot[106], P. de Jong[107], H. De la Torre[82], F. De Lorenzi[64], L. De Nooij[107], D. De Pedis[133a], A. De Salvo[133a], U. De Sanctis[150], A. De Santo[150], J.B. De Vivie De Regie[117], W.J. Dearnaley[72], R. Debbe[25], C. Debenedetti[138], B. Dechenaux[55], D.V. Dedovich[65], I. Deigaard[107], J. Del Peso[82], T. Del Prete[124a,124b], F. Deliot[137], C.M. Delitzsch[49], M. Deliyergiyev[75], A. Dell'Acqua[30], L. Dell'Asta[22], M. Dell'Orso[124a,124b], M. Della Pietra[104a,i], D. della Volpe[49], M. Delmastro[5], P.A. Delsart[55], C. Deluca[107], D.A. DeMarco[159], S. Demers[177], M. Demichev[65], A. Demilly[80], S.P. Denisov[130], D. Derendarz[39], J.E. Derkaoui[136d], F. Derue[80], P. Dervan[74], K. Desch[21], C. Deterre[42], P.O. Deviveiros[30], A. Dewhurst[131], S. Dhaliwal[107], A. Di Ciaccio[134a,134b], L. Di Ciaccio[5], A. Di Domenico[133a,133b], C. Di Donato[104a,104b], A. Di Girolamo[30], B. Di Girolamo[30], A. Di Mattia[153], B. Di Micco[135a,135b], R. Di Nardo[47], A. Di Simone[48], R. Di Sipio[20a,20b], D. Di Valentino[29], F.A. Dias[46], M.A. Diaz[32a], E.B. Diehl[89], J. Dietrich[16], T.A. Dietzsch[58a], S. Diglio[85], A. Dimitrievska[13a], J. Dingfelder[21], P. Dita[26a], S. Dita[26a], F. Dittus[30], F. Djama[85], T. Djobava[51b], J.I. Djuvsland[58a], M.A.B. do Vale[24c], D. Dobos[30], C. Doglioni[49], T. Doherty[53], T. Dohmae[156], J. Dolejsi[129], Z. Dolezal[129], B.A. Dolgoshein[98,*], M. Donadelli[24d], S. Donati[124a,124b], P. Dondero[121a,121b], J. Donini[34], J. Dopke[131], A. Doria[104a], M.T. Dova[71], A.T. Doyle[53], M. Dris[10], J. Dubbert[89], S. Dube[15], E. Dubreuil[34], E. Duchovni[173], G. Duckeck[100], O.A. Ducu[26a], D. Duda[176], A. Dudarev[30], L. Duflot[117], L. Duguid[77], M. Dührssen[30], M. Dunford[58a], H. Duran Yildiz[4a], M. Düren[52], A. Durglishvili[51b], D. Duschinger[44], M. Dwuznik[38a], M. Dyndal[38a], W. Edson[2], N.C. Edwards[46], W. Ehrenfeld[21], T. Eifert[30], G. Eigen[14], K. Einsweiler[15], T. Ekelof[167], M. El Kacimi[136c], M. Ellert[167], S. Elles[5], F. Ellinghaus[83], A.A. Elliot[170], N. Ellis[30], J. Elmsheuser[100], M. Elsing[30], D. Emeliyanov[131], Y. Enari[156], O.C. Endner[83], M. Endo[118], R. Engelmann[149], J. Erdmann[43], A. Ereditato[17], D. Eriksson[147a], G. Ernis[176], J. Ernst[2], M. Ernst[25], J. Ernwein[137], S. Errede[166], E. Ertel[83], M. Escalier[117], H. Esch[43], C. Escobar[125], B. Esposito[47], A.I. Etienvre[137], E. Etzion[154], H. Evans[61], A. Ezhilov[123], L. Fabbri[20a,20b], G. Facini[31], R.M. Fakhrutdinov[130], S. Falciano[133a], R.J. Falla[78], J. Faltova[129], Y. Fang[33a], M. Fanti[91a,91b], A. Farbin[8], A. Farilla[135a], T. Farooque[12], S. Farrell[15], S.M. Farrington[171], P. Farthouat[30], F. Fassi[136e], P. Fassnacht[30], D. Fassouliotis[9], A. Favareto[50a,50b], L. Fayard[117], P. Federic[145a], O.L. Fedin[123,l], W. Fedorko[169], S. Feigl[30], L. Feligioni[85], C. Feng[33d], E.J. Feng[6], H. Feng[89], A.B. Fenyuk[130], P. Fernandez Martinez[168], S. Fernandez Perez[30], S. Ferrag[53], J. Ferrando[53], A. Ferrari[167], P. Ferrari[107], R. Ferrari[121a], D.E. Ferreira de Lima[53], A. Ferrer[168], D. Ferrere[49], C. Ferretti[89], A. Ferretto Parodi[50a,50b], M. Fiascaris[31], F. Fiedler[83], A. Filipčič[75], M. Filipuzzi[42], F. Filthaut[106], M. Fincke-Keeler[170], K.D. Finelli[151], M.C.N. Fiolhais[126a,126c], L. Fiorini[168], A. Firan[40], A. Fischer[2], J. Fischer[176], W.C. Fisher[90], E.A. Fitzgerald[23], M. Flechl[48], I. Fleck[142], P. Fleischmann[89], S. Fleischmann[176], G.T. Fletcher[140], G. Fletcher[76], T. Flick[176], A. Floderus[81], L.R. Flores Castillo[60a], M.J. Flowerdew[101], A. Formica[137], A. Forti[84], D. Fournier[117], H. Fox[72], S. Fracchia[12], P. Francavilla[80], M. Franchini[20a,20b], S. Franchino[30], D. Francis[30], L. Franconi[119], M. Franklin[57], M. Fraternali[121a,121b], S.T. French[28], C. Friedrich[42], F. Friedrich[44], D. Froidevaux[30], J.A. Frost[120], C. Fukunaga[157], E. Fullana Torregrosa[83], B.G. Fulsom[144], J. Fuster[168],

JHEP04(2015)116

C. Gabaldon[55], O. Gabizon[176], A. Gabrielli[20a,20b], A. Gabrielli[133a,133b], S. Gadatsch[107], S. Gadomski[49], G. Gagliardi[50a,50b], P. Gagnon[61], C. Galea[106], B. Galhardo[126a,126c], E.J. Gallas[120], B.J. Gallop[131], P. Gallus[128], G. Galster[36], K.K. Gan[111], J. Gao[33b], Y.S. Gao[144,e], F.M. Garay Walls[46], F. Garberson[177], C. García[168], J.E. García Navarro[168], M. Garcia-Sciveres[15], R.W. Gardner[31], N. Garelli[144], V. Garonne[30], C. Gatti[47], G. Gaudio[121a], B. Gaur[142], L. Gauthier[95], P. Gauzzi[133a,133b], I.L. Gavrilenko[96], C. Gay[169], G. Gaycken[21], E.N. Gazis[10], P. Ge[33d], Z. Gecse[169], C.N.P. Gee[131], D.A.A. Geerts[107], Ch. Geich-Gimbel[21], K. Gellerstedt[147a,147b], C. Gemme[50a], A. Gemmell[53], M.H. Genest[55], S. Gentile[133a,133b], M. George[54], S. George[77], D. Gerbaudo[164], A. Gershon[154], H. Ghazlane[136b], N. Ghodbane[34], B. Giacobbe[20a], S. Giagu[133a,133b], V. Giangiobbe[12], P. Giannetti[124a,124b], F. Gianotti[30], B. Gibbard[25], S.M. Gibson[77], M. Gilchriese[15], T.P.S. Gillam[28], D. Gillberg[30], G. Gilles[34], D.M. Gingrich[3,d], N. Giokaris[9], M.P. Giordani[165a,165c], R. Giordano[104a,104b], F.M. Giorgi[20a], F.M. Giorgi[16], P.F. Giraud[137], D. Giugni[91a], C. Giuliani[48], M. Giulini[58b], B.K. Gjelsten[119], S. Gkaitatzis[155], I. Gkialas[155], E.L. Gkougkousis[117], L.K. Gladilin[99], C. Glasman[82], J. Glatzer[30], P.C.F. Glaysher[46], A. Glazov[42], G.L. Glonti[62], M. Goblirsch-Kolb[101], J.R. Goddard[76], J. Godlewski[30], S. Goldfarb[89], T. Golling[49], D. Golubkov[130], A. Gomes[126a,126b,126d], R. Gonçalo[126a], J. Goncalves Pinto Firmino Da Costa[137], L. Gonella[21], S. González de la Hoz[168], G. Gonzalez Parra[12], S. Gonzalez-Sevilla[49], L. Goossens[30], P.A. Gorbounov[97], H.A. Gordon[25], I. Gorelov[105], B. Gorini[30], E. Gorini[73a,73b], A. Gorišek[75], E. Gornicki[39], A.T. Goshaw[45], C. Gössling[43], M.I. Gostkin[65], M. Gouighri[136a], D. Goujdami[136c], M.P. Goulette[49], A.G. Goussiou[139], C. Goy[5], H.M.X. Grabas[138], L. Graber[54], I. Grabowska-Bold[38a], P. Grafström[20a,20b], K-J. Grahn[42], J. Gramling[49], E. Gramstad[119], S. Grancagnolo[16], V. Grassi[149], V. Gratchev[123], H.M. Gray[30], E. Graziani[135a], O.G. Grebenyuk[123], Z.D. Greenwood[79,m], K. Gregersen[78], I.M. Gregor[42], P. Grenier[144], J. Griffiths[8], A.A. Grillo[138], K. Grimm[72], S. Grinstein[12,n], Ph. Gris[34], Y.V. Grishkevich[99], J.-F. Grivaz[117], J.P. Grohs[44], A. Grohsjean[42], E. Gross[173], J. Grosse-Knetter[54], G.C. Grossi[134a,134b], Z.J. Grout[150], L. Guan[33b], J. Guenther[128], F. Guescini[49], D. Guest[177], O. Gueta[154], C. Guicheney[34], E. Guido[50a,50b], T. Guillemin[117], S. Guindon[2], U. Gul[53], C. Gumpert[44], J. Guo[35], S. Gupta[120], P. Gutierrez[113], N.G. Gutierrez Ortiz[53], C. Gutschow[78], N. Guttman[154], C. Guyot[137], C. Gwenlan[120], C.B. Gwilliam[74], A. Haas[110], C. Haber[15], H.K. Hadavand[8], N. Haddad[136e], P. Haefner[21], S. Hageböck[21], Z. Hajduk[39], H. Hakobyan[178], M. Haleem[42], J. Haley[114], D. Hall[120], G. Halladjian[90], G.D. Hallewell[85], K. Hamacher[176], P. Hamal[115], K. Hamano[170], M. Hamer[54], A. Hamilton[146a], S. Hamilton[162], G.N. Hamity[146c], P.G. Hamnett[42], L. Han[33b], K. Hanagaki[118], K. Hanawa[156], M. Hance[15], P. Hanke[58a], R. Hanna[137], J.B. Hansen[36], J.D. Hansen[36], P.H. Hansen[36], K. Hara[161], A.S. Hard[174], T. Harenberg[176], F. Hariri[117], S. Harkusha[92], R.D. Harrington[46], P.F. Harrison[171], F. Hartjes[107], M. Hasegawa[67], S. Hasegawa[103], Y. Hasegawa[141], A. Hasib[113], S. Hassani[137], S. Haug[17], M. Hauschild[30], R. Hauser[90], M. Havranek[127], C.M. Hawkes[18], R.J. Hawkings[30], A.D. Hawkins[81], T. Hayashi[161], D. Hayden[90], C.P. Hays[120], J.M. Hays[76], H.S. Hayward[74], S.J. Haywood[131], S.J. Head[18], T. Heck[83], V. Hedberg[81], L. Heelan[8], S. Heim[122], T. Heim[176], B. Heinemann[15], L. Heinrich[110], J. Hejbal[127], L. Helary[22], M. Heller[30], S. Hellman[147a,147b], D. Hellmich[21], C. Helsens[30], J. Henderson[120], R.C.W. Henderson[72], Y. Heng[174], C. Hengler[42], A. Henrichs[177], A.M. Henriques Correia[30], S. Henrot-Versille[117], G.H. Herbert[16], Y. Hernández Jiménez[168], R. Herrberg-Schubert[16], G. Herten[48], R. Hertenberger[100], L. Hervas[30], G.G. Hesketh[78], N.P. Hessey[107], R. Hickling[76], E. Higón-Rodriguez[168], E. Hill[170], J.C. Hill[28], K.H. Hiller[42], S.J. Hillier[18], I. Hinchliffe[15], E. Hines[122], R.R. Hinman[15], M. Hirose[158], D. Hirschbuehl[176], J. Hobbs[149], N. Hod[107], M.C. Hodgkinson[140], P. Hodgson[140], A. Hoecker[30], M.R. Hoeferkamp[105], F. Hoenig[100], D. Hoffmann[85], M. Hohlfeld[83], T.R. Holmes[15], T.M. Hong[122], L. Hooft van Huysduynen[110],

JHEP04(2015)116

W.H. Hopkins[116], Y. Horii[103], A.J. Horton[143], J-Y. Hostachy[55], S. Hou[152], A. Hoummada[136a], J. Howard[120], J. Howarth[42], M. Hrabovsky[115], I. Hristova[16], J. Hrivnac[117], T. Hryn'ova[5], A. Hrynevich[93], C. Hsu[146c], P.J. Hsu[152,o], S.-C. Hsu[139], D. Hu[35], X. Hu[89], Y. Huang[42], Z. Hubacek[30], F. Hubaut[85], F. Huegging[21], T.B. Huffman[120], E.W. Hughes[35], G. Hughes[72], M. Huhtinen[30], T.A. Hülsing[83], M. Hurwitz[15], N. Huseynov[65,b], J. Huston[90], J. Huth[57], G. Iacobucci[49], G. Iakovidis[10], I. Ibragimov[142], L. Iconomidou-Fayard[117], E. Ideal[177], Z. Idrissi[136e], P. Iengo[104a], O. Igonkina[107], T. Iizawa[172], Y. Ikegami[66], K. Ikematsu[142], M. Ikeno[66], Y. Ilchenko[31,p], D. Iliadis[155], N. Ilic[159], Y. Inamaru[67], T. Ince[101], P. Ioannou[9], M. Iodice[135a], K. Iordanidou[9], V. Ippolito[57], A. Irles Quiles[168], C. Isaksson[167], M. Ishino[68], M. Ishitsuka[158], R. Ishmukhametov[111], C. Issever[120], S. Istin[19a], J.M. Iturbe Ponce[84], R. Iuppa[134a,134b], J. Ivarsson[81], W. Iwanski[39], H. Iwasaki[66], J.M. Izen[41], V. Izzo[104a], B. Jackson[122], M. Jackson[74], P. Jackson[1], M.R. Jaekel[30], V. Jain[2], K. Jakobs[48], S. Jakobsen[30], T. Jakoubek[127], J. Jakubek[128], D.O. Jamin[152], D.K. Jana[79], E. Jansen[78], J. Janssen[21], M. Janus[171], G. Jarlskog[81], N. Javadov[65,b], T. Javůrek[48], L. Jeanty[15], J. Jejelava[51a,q], G.-Y. Jeng[151], D. Jennens[88], P. Jenni[48,r], J. Jentzsch[43], C. Jeske[171], S. Jézéquel[5], H. Ji[174], J. Jia[149], Y. Jiang[33b], M. Jimenez Belenguer[42], J. Jimenez Pena[168], S. Jin[33a], A. Jinaru[26a], O. Jinnouchi[158], M.D. Joergensen[36], P. Johansson[140], K.A. Johns[7], K. Jon-And[147a,147b], G. Jones[171], R.W.L. Jones[72], T.J. Jones[74], J. Jongmanns[58a], P.M. Jorge[126a,126b], K.D. Joshi[84], J. Jovicevic[148], X. Ju[174], C.A. Jung[43], P. Jussel[62], A. Juste Rozas[12,n], M. Kaci[168], A. Kaczmarska[39], M. Kado[117], H. Kagan[111], M. Kagan[144], E. Kajomovitz[45], C.W. Kalderon[120], S. Kama[40], A. Kamenshchikov[130], N. Kanaya[156], M. Kaneda[30], S. Kaneti[28], V.A. Kantserov[98], J. Kanzaki[66], B. Kaplan[110], A. Kapliy[31], D. Kar[53], K. Karakostas[10], A. Karamaoun[3], N. Karastathis[10], M.J. Kareem[54], M. Karnevskiy[83], S.N. Karpov[65], Z.M. Karpova[65], K. Karthik[110], V. Kartvelishvili[72], A.N. Karyukhin[130], L. Kashif[174], G. Kasieczka[58b], R.D. Kass[111], A. Kastanas[14], Y. Kataoka[156], A. Katre[49], J. Katzy[42], V. Kaushik[7], K. Kawagoe[70], T. Kawamoto[156], G. Kawamura[54], S. Kazama[156], V.F. Kazanin[109], M.Y. Kazarinov[65], R. Keeler[170], R. Kehoe[40], M. Keil[54], J.S. Keller[42], J.J. Kempster[77], H. Keoshkerian[5], O. Kepka[127], B.P. Kerševan[75], S. Kersten[176], K. Kessoku[156], R.A. Keyes[87], F. Khalil-zada[11], H. Khandanyan[147a,147b], A. Khanov[114], A. Kharlamov[109], A. Khodinov[98], A. Khomich[58a], T.J. Khoo[28], G. Khoriauli[21], V. Khovanskiy[97], E. Khramov[65], J. Khubua[51b], H.Y. Kim[8], H. Kim[147a,147b], S.H. Kim[161], N. Kimura[155], O. Kind[16], B.T. King[74], M. King[168], R.S.B. King[120], S.B. King[169], J. Kirk[131], A.E. Kiryunin[101], T. Kishimoto[67], D. Kisielewska[38a], F. Kiss[48], K. Kiuchi[161], E. Kladiva[145b], M. Klein[74], U. Klein[74], K. Kleinknecht[83], P. Klimek[147a,147b], A. Klimentov[25], R. Klingenberg[43], J.A. Klinger[84], T. Klioutchnikova[30], P.F. Klok[106], E.-E. Kluge[58a], P. Kluit[107], S. Kluth[101], E. Kneringer[62], E.B.F.G. Knoops[85], A. Knue[53], D. Kobayashi[158], T. Kobayashi[156], M. Kobel[44], M. Kocian[144], P. Kodys[129], T. Koffas[29], E. Koffeman[107], L.A. Kogan[120], S. Kohlmann[176], Z. Kohout[128], T. Kohriki[66], T. Koi[144], H. Kolanoski[16], I. Koletsou[5], J. Koll[90], A.A. Komar[96,*], Y. Komori[156], T. Kondo[66], N. Kondrashova[42], K. Köneke[48], A.C. König[106], S. König[83], T. Kono[66,s], R. Konoplich[110,t], N. Konstantinidis[78], R. Kopeliansky[153], S. Koperny[38a], L. Köpke[83], A.K. Kopp[48], K. Korcyl[39], K. Kordas[155], A. Korn[78], A.A. Korol[109,c], I. Korolkov[12], E.V. Korolkova[140], V.A. Korotkov[130], O. Kortner[101], S. Kortner[101], V.V. Kostyukhin[21], V.M. Kotov[65], A. Kotwal[45], A. Kourkoumeli-Charalampidi[155], C. Kourkoumelis[9], V. Kouskoura[25], A. Koutsman[160a], R. Kowalewski[170], T.Z. Kowalski[38a], W. Kozanecki[137], A.S. Kozhin[130], V.A. Kramarenko[99], G. Kramberger[75], D. Krasnopevtsev[98], M.W. Krasny[80], A. Krasznahorkay[30], J.K. Kraus[21], A. Kravchenko[25], S. Kreiss[110], M. Kretz[58c], J. Kretzschmar[74], K. Kreutzfeldt[52], P. Krieger[159], K. Krizka[31], K. Kroeninger[43], H. Kroha[101], J. Kroll[122], J. Kroseberg[21], J. Krstic[13a], U. Kruchonak[65], H. Krüger[21], N. Krumnack[64], Z.V. Krumshteyn[65], A. Kruse[174], M.C. Kruse[45],

JHEP04(2015)116

M. Kruskal[22], T. Kubota[88], H. Kucuk[78], S. Kuday[4c], S. Kuehn[48], A. Kugel[58c], F. Kuger[175], A. Kuhl[138], T. Kuhl[42], V. Kukhtin[65], Y. Kulchitsky[92], S. Kuleshov[32b], M. Kuna[133a,133b], T. Kunigo[68], A. Kupco[127], H. Kurashige[67], Y.A. Kurochkin[92], R. Kurumida[67], V. Kus[127], E.S. Kuwertz[148], M. Kuze[158], J. Kvita[115], D. Kyriazopoulos[140], A. La Rosa[49], L. La Rotonda[37a,37b], C. Lacasta[168], F. Lacava[133a,133b], J. Lacey[29], H. Lacker[16], D. Lacour[80], V.R. Lacuesta[168], E. Ladygin[65], R. Lafaye[5], B. Laforge[80], T. Lagouri[177], S. Lai[48], H. Laier[58a], L. Lambourne[78], S. Lammers[61], C.L. Lampen[7], W. Lampl[7], E. Lançon[137], U. Landgraf[48], M.P.J. Landon[76], V.S. Lang[58a], A.J. Lankford[164], F. Lanni[25], K. Lantzsch[30], S. Laplace[80], C. Lapoire[21], J.F. Laporte[137], T. Lari[91a], F. Lasagni Manghi[20a,20b], M. Lassnig[30], P. Laurelli[47], W. Lavrijsen[15], A.T. Law[138], P. Laycock[74], O. Le Dortz[80], E. Le Guirriec[85], E. Le Menedeu[12], T. LeCompte[6], F. Ledroit-Guillon[55], C.A. Lee[146b], H. Lee[107], S.C. Lee[152], L. Lee[1], G. Lefebvre[80], M. Lefebvre[170], F. Legger[100], C. Leggett[15], A. Lehan[74], G. Lehmann Miotto[30], X. Lei[7], W.A. Leight[29], A. Leisos[155], A.G. Leister[177], M.A.L. Leite[24d], R. Leitner[129], D. Lellouch[173], B. Lemmer[54], K.J.C. Leney[78], T. Lenz[21], G. Lenzen[176], B. Lenzi[30], R. Leone[7], S. Leone[124a,124b], C. Leonidopoulos[46], S. Leontsinis[10], C. Leroy[95], C.G. Lester[28], C.M. Lester[122], M. Levchenko[123], J. Levêque[5], D. Levin[89], L.J. Levinson[173], M. Levy[18], A. Lewis[120], A.M. Leyko[21], M. Leyton[41], B. Li[33b,u], B. Li[85], H. Li[149], H.L. Li[31], L. Li[45], L. Li[33e], S. Li[45], Y. Li[33c,v], Z. Liang[138], H. Liao[34], B. Liberti[134a], P. Lichard[30], K. Lie[166], J. Liebal[21], W. Liebig[14], C. Limbach[21], A. Limosani[151], S.C. Lin[152,w], T.H. Lin[83], F. Linde[107], B.E. Lindquist[149], J.T. Linnemann[90], E. Lipeles[122], A. Lipniacka[14], M. Lisovyi[42], T.M. Liss[166], D. Lissauer[25], A. Lister[169], A.M. Litke[138], B. Liu[152], D. Liu[152], J. Liu[85], J.B. Liu[33b], K. Liu[33b,x], L. Liu[89], M. Liu[45], M. Liu[33b], Y. Liu[33b], M. Livan[121a,121b], A. Lleres[55], J. Llorente Merino[82], S.L. Lloyd[76], F. Lo Sterzo[152], E. Lobodzinska[42], P. Loch[7], W.S. Lockman[138], F.K. Loebinger[84], A.E. Loevschall-Jensen[36], A. Loginov[177], T. Lohse[16], K. Lohwasser[42], M. Lokajicek[127], B.A. Long[22], J.D. Long[89], R.E. Long[72], K.A. Looper[111], L. Lopes[126a], D. Lopez Mateos[57], B. Lopez Paredes[140], I. Lopez Paz[12], J. Lorenz[100], N. Lorenzo Martinez[61], M. Losada[163], P. Loscutoff[15], X. Lou[33a], A. Lounis[117], J. Love[6], P.A. Love[72], A.J. Lowe[144,e], F. Lu[33a], N. Lu[89], H.J. Lubatti[139], C. Luci[133a,133b], A. Lucotte[55], F. Luehring[61], W. Lukas[62], L. Luminari[133a], O. Lundberg[147a,147b], B. Lund-Jensen[148], M. Lungwitz[83], D. Lynn[25], R. Lysak[127], E. Lytken[81], H. Ma[25], L.L. Ma[33d], G. Maccarrone[47], A. Macchiolo[101], J. Machado Miguens[126a,126b], D. Macina[30], D. Madaffari[85], R. Madar[48], H.J. Maddocks[72], W.F. Mader[44], A. Madsen[167], M. Maeno[8], T. Maeno[25], A. Maevskiy[99], E. Magradze[54], K. Mahboubi[48], J. Mahlstedt[107], S. Mahmoud[74], C. Maiani[137], C. Maidantchik[24a], A.A. Maier[101], A. Maio[126a,126b,126d], S. Majewski[116], Y. Makida[66], N. Makovec[117], P. Mal[137,y], B. Malaescu[80], Pa. Malecki[39], V.P. Maleev[123], F. Malek[55], U. Mallik[63], D. Malon[6], C. Malone[144], S. Maltezos[10], V.M. Malyshev[109], S. Malyukov[30], J. Mamuzic[13b], B. Mandelli[30], L. Mandelli[91a], I. Mandić[75], R. Mandrysch[63], J. Maneira[126a,126b], A. Manfredini[101], L. Manhaes de Andrade Filho[24b], J. Manjarres Ramos[160b], A. Mann[100], P.M. Manning[138], A. Manousakis-Katsikakis[9], B. Mansoulie[137], R. Mantifel[87], M. Mantoani[54], L. Mapelli[30], L. March[146c], J.F. Marchand[29], G. Marchiori[80], M. Marcisovsky[127], C.P. Marino[170], M. Marjanovic[13a], F. Marroquim[24a], S.P. Marsden[84], Z. Marshall[15], L.F. Marti[17], S. Marti-Garcia[168], B. Martin[30], B. Martin[90], T.A. Martin[171], V.J. Martin[46], B. Martin dit Latour[14], H. Martinez[137], M. Martinez[12,n], S. Martin-Haugh[131], A.C. Martyniuk[78], M. Marx[139], F. Marzano[133a], A. Marzin[30], L. Masetti[83], T. Mashimo[156], R. Mashinistov[96], J. Masik[84], A.L. Maslennikov[109,c], I. Massa[20a,20b], L. Massa[20a,20b], N. Massol[5], P. Mastrandrea[149], A. Mastroberardino[37a,37b], T. Masubuchi[156], P. Mättig[176], J. Mattmann[83], J. Maurer[26a], S.J. Maxfield[74], D.A. Maximov[109,c], R. Mazini[152], S.M. Mazza[91a,91b], L. Mazzaferro[134a,134b], G. Mc Goldrick[159], S.P. Mc Kee[89], A. McCarn[89], R.L. McCarthy[149], T.G. McCarthy[29], N.A. McCubbin[131], K.W. McFarlane[56,*], J.A. Mcfayden[78], G. Mchedlidze[54],

JHEP04(2015)116

S.J. McMahon[131], R.A. McPherson[170,j], J. Mechnich[107], M. Medinnis[42], S. Meehan[31], S. Mehlhase[100], A. Mehta[74], K. Meier[58a], C. Meineck[100], B. Meirose[41], C. Melachrinos[31], B.R. Mellado Garcia[146c], F. Meloni[17], A. Mengarelli[20a,20b], S. Menke[101], E. Meoni[162], K.M. Mercurio[57], S. Mergelmeyer[21], N. Meric[137], P. Mermod[49], L. Merola[104a,104b], C. Meroni[91a], F.S. Merritt[31], H. Merritt[111], A. Messina[30,z], J. Metcalfe[25], A.S. Mete[164], C. Meyer[83], C. Meyer[122], J-P. Meyer[137], J. Meyer[30], R.P. Middleton[131], S. Migas[74], S. Miglioranzi[165a,165c], L. Mijović[21], G. Mikenberg[173], M. Mikestikova[127], M. Mikuž[75], A. Milic[30], D.W. Miller[31], C. Mills[46], A. Milov[173], D.A. Milstead[147a,147b], A.A. Minaenko[130], Y. Minami[156], I.A. Minashvili[65], A.I. Mincer[110], B. Mindur[38a], M. Mineev[65], Y. Ming[174], L.M. Mir[12], G. Mirabelli[133a], T. Mitani[172], J. Mitrevski[100], V.A. Mitsou[168], A. Miucci[49], P.S. Miyagawa[140], J.U. Mjörnmark[81], T. Moa[147a,147b], K. Mochizuki[85], S. Mohapatra[35], W. Mohr[48], S. Molander[147a,147b], R. Moles-Valls[168], K. Mönig[42], C. Monini[55], J. Monk[36], E. Monnier[85], J. Montejo Berlingen[12], F. Monticelli[71], S. Monzani[133a,133b], R.W. Moore[3], N. Morange[63], D. Moreno[163], M. Moreno Llácer[54], P. Morettini[50a], M. Morgenstern[44], M. Morii[57], V. Morisbak[119], S. Moritz[83], A.K. Morley[148], G. Mornacchi[30], J.D. Morris[76], A. Morton[42], L. Morvaj[103], H.G. Moser[101], M. Mosidze[51b], J. Moss[111], K. Motohashi[158], R. Mount[144], E. Mountricha[25], S.V. Mouraviev[96,*], E.J.W. Moyse[86], S. Muanza[85], R.D. Mudd[18], F. Mueller[58a], J. Mueller[125], K. Mueller[21], T. Mueller[28], D. Muenstermann[49], P. Mullen[53], Y. Munwes[154], J.A. Murillo Quijada[18], W.J. Murray[171,131], H. Musheghyan[54], E. Musto[153], A.G. Myagkov[130,aa], M. Myska[128], O. Nackenhorst[54], J. Nadal[54], K. Nagai[120], R. Nagai[158], Y. Nagai[85], K. Nagano[66], A. Nagarkar[111], Y. Nagasaka[59], K. Nagata[161], M. Nagel[101], A.M. Nairz[30], Y. Nakahama[30], K. Nakamura[66], T. Nakamura[156], I. Nakano[112], H. Namasivayam[41], G. Nanava[21], R.F. Naranjo Garcia[42], R. Narayan[58b], T. Nattermann[21], T. Naumann[42], G. Navarro[163], R. Nayyar[7], H.A. Neal[89], P.Yu. Nechaeva[96], T.J. Neep[84], P.D. Nef[144], A. Negri[121a,121b], G. Negri[30], M. Negrini[20a], S. Nektarijevic[49], C. Nellist[117], A. Nelson[164], T.K. Nelson[144], S. Nemecek[127], P. Nemethy[110], A.A. Nepomuceno[24a], M. Nessi[30,ab], M.S. Neubauer[166], M. Neumann[176], R.M. Neves[110], P. Nevski[25], P.R. Newman[18], D.H. Nguyen[6], R.B. Nickerson[120], R. Nicolaidou[137], B. Nicquevert[30], J. Nielsen[138], N. Nikiforou[35], A. Nikiforov[16], V. Nikolaenko[130,aa], I. Nikolic-Audit[80], K. Nikolics[49], K. Nikolopoulos[18], P. Nilsson[25], Y. Ninomiya[156], A. Nisati[133a], R. Nisius[101], T. Nobe[158], M. Nomachi[118], I. Nomidis[29], S. Norberg[113], M. Nordberg[30], O. Novgorodova[44], S. Nowak[101], M. Nozaki[66], L. Nozka[115], K. Ntekas[10], G. Nunes Hanninger[88], T. Nunnemann[100], E. Nurse[78], F. Nuti[88], B.J. O'Brien[46], F. O'grady[7], D.C. O'Neil[143], V. O'Shea[53], F.G. Oakham[29,d], H. Oberlack[101], T. Obermann[21], J. Ocariz[80], A. Ochi[67], I. Ochoa[78], S. Oda[70], S. Odaka[66], H. Ogren[61], A. Oh[84], S.H. Oh[45], C.C. Ohm[15], H. Ohman[167], H. Oide[30], W. Okamura[118], H. Okawa[161], Y. Okumura[31], T. Okuyama[156], A. Olariu[26a], A.G. Olchevski[65], S.A. Olivares Pino[46], D. Oliveira Damazio[25], E. Oliver Garcia[168], A. Olszewski[39], J. Olszowska[39], A. Onofre[126a,126e], P.U.E. Onyisi[31,p], C.J. Oram[160a], M.J. Oreglia[31], Y. Oren[154], D. Orestano[135a,135b], N. Orlando[73a,73b], C. Oropeza Barrera[53], R.S. Orr[159], B. Osculati[50a,50b], R. Ospanov[122], G. Otero y Garzon[27], H. Otono[70], M. Ouchrif[136d], E.A. Ouellette[170], F. Ould-Saada[119], A. Ouraou[137], K.P. Oussoren[107], Q. Ouyang[33a], A. Ovcharova[15], M. Owen[84], V.E. Ozcan[19a], N. Ozturk[8], K. Pachal[120], A. Pacheco Pages[12], C. Padilla Aranda[12], M. Pagáčová[48], S. Pagan Griso[15], E. Paganis[140], C. Pahl[101], F. Paige[25], P. Pais[86], K. Pajchel[119], G. Palacino[160b], S. Palestini[30], M. Palka[38b], D. Pallin[34], A. Palma[126a,126b], J.D. Palmer[18], Y.B. Pan[174], E. Panagiotopoulou[10], J.G. Panduro Vazquez[77], P. Pani[107], N. Panikashvili[89], S. Panitkin[25], D. Pantea[26a], L. Paolozzi[134a,134b], Th.D. Papadopoulou[10], K. Papageorgiou[155], A. Paramonov[6], D. Paredes Hernandez[155], M.A. Parker[28], F. Parodi[50a,50b], J.A. Parsons[35], U. Parzefall[48], E. Pasqualucci[133a], S. Passaggio[50a], A. Passeri[135a], F. Pastore[135a,135b,*], Fr. Pastore[77],

JHEP04(2015)116

G. Pásztor[29], S. Pataraia[176], N.D. Patel[151], J.R. Pater[84], S. Patricelli[104a,104b], T. Pauly[30], J. Pearce[170], L.E. Pedersen[36], M. Pedersen[119], S. Pedraza Lopez[168], R. Pedro[126a,126b], S.V. Peleganchuk[109], D. Pelikan[167], H. Peng[33b], B. Penning[31], J. Penwell[61], D.V. Perepelitsa[25], E. Perez Codina[160a], M.T. Pérez García-Estañ[168], L. Perini[91a,91b], H. Pernegger[30], S. Perrella[104a,104b], R. Peschke[42], V.D. Peshekhonov[65], K. Peters[30], R.F.Y. Peters[84], B.A. Petersen[30], T.C. Petersen[36], E. Petit[42], A. Petridis[147a,147b], C. Petridou[155], E. Petrolo[133a], F. Petrucci[135a,135b], N.E. Pettersson[158], R. Pezoa[32b], P.W. Phillips[131], G. Piacquadio[144], E. Pianori[171], A. Picazio[49], E. Piccaro[76], M. Piccinini[20a,20b], M.A. Pickering[120], R. Piegaia[27], D.T. Pignotti[111], J.E. Pilcher[31], A.D. Pilkington[78], J. Pina[126a,126b,126d], M. Pinamonti[165a,165c,ac], A. Pinder[120], J.L. Pinfold[3], A. Pingel[36], B. Pinto[126a], S. Pires[80], M. Pitt[173], C. Pizio[91a,91b], L. Plazak[145a], M.-A. Pleier[25], V. Pleskot[129], E. Plotnikova[65], P. Plucinski[147a,147b], D. Pluth[64], S. Poddar[58a], F. Podlyski[34], R. Poettgen[83], L. Poggioli[117], D. Pohl[21], M. Pohl[49], G. Polesello[121a], A. Policicchio[37a,37b], R. Polifka[159], A. Polini[20a], C.S. Pollard[53], V. Polychronakos[25], K. Pommès[30], L. Pontecorvo[133a], B.G. Pope[90], G.A. Popeneciu[26b], D.S. Popovic[13a], A. Poppleton[30], S. Pospisil[128], K. Potamianos[15], I.N. Potrap[65], C.J. Potter[150], C.T. Potter[116], G. Poulard[30], J. Poveda[30], V. Pozdnyakov[65], P. Pralavorio[85], A. Pranko[15], S. Prasad[30], S. Prell[64], D. Price[84], J. Price[74], L.E. Price[6], D. Prieur[125], M. Primavera[73a], S. Prince[87], M. Proissl[46], K. Prokofiev[60c], F. Prokoshin[32b], E. Protopapadaki[137], S. Protopopescu[25], J. Proudfoot[6], M. Przybycien[38a], H. Przysiezniak[5], E. Ptacek[116], D. Puddu[135a,135b], E. Pueschel[86], D. Puldon[149], M. Purohit[25,ad], P. Puzo[117], J. Qian[89], G. Qin[53], Y. Qin[84], A. Quadt[54], D.R. Quarrie[15], W.B. Quayle[165a,165b], M. Queitsch-Maitland[84], D. Quilty[53], A. Qureshi[160b], V. Radeka[25], V. Radescu[42], S.K. Radhakrishnan[149], P. Radloff[116], P. Rados[88], F. Ragusa[91a,91b], G. Rahal[179], S. Rajagopalan[25], M. Rammensee[30], C. Rangel-Smith[167], K. Rao[164], F. Rauscher[100], S. Rave[83], T.C. Rave[48], T. Ravenscroft[53], M. Raymond[30], A.L. Read[119], N.P. Readioff[74], D.M. Rebuzzi[121a,121b], A. Redelbach[175], G. Redlinger[25], R. Reece[138], K. Reeves[41], L. Rehnisch[16], H. Reisin[27], M. Relich[164], C. Rembser[30], H. Ren[33a], Z.L. Ren[152], A. Renaud[117], M. Rescigno[133a], S. Resconi[91a], O.L. Rezanova[109,c], P. Reznicek[129], R. Rezvani[95], R. Richter[101], E. Richter-Was[38b], M. Ridel[80], P. Rieck[16], J. Rieger[54], M. Rijssenbeek[149], A. Rimoldi[121a,121b], L. Rinaldi[20a], E. Ritsch[62], I. Riu[12], F. Rizatdinova[114], E. Rizvi[76], S.H. Robertson[87,j], A. Robichaud-Veronneau[87], D. Robinson[28], J.E.M. Robinson[84], A. Robson[53], C. Roda[124a,124b], L. Rodrigues[30], S. Roe[30], O. Røhne[119], S. Rolli[162], A. Romaniouk[98], M. Romano[20a,20b], E. Romero Adam[168], N. Rompotis[139], M. Ronzani[48], L. Roos[80], E. Ros[168], S. Rosati[133a], K. Rosbach[49], M. Rose[77], P. Rose[138], P.L. Rosendahl[14], O. Rosenthal[142], V. Rossetti[147a,147b], E. Rossi[104a,104b], L.P. Rossi[50a], R. Rosten[139], M. Rotaru[26a], I. Roth[173], J. Rothberg[139], D. Rousseau[117], C.R. Royon[137], A. Rozanov[85], Y. Rozen[153], X. Ruan[146c], F. Rubbo[12], I. Rubinskiy[42], V.I. Rud[99], C. Rudolph[44], M.S. Rudolph[159], F. Rühr[48], A. Ruiz-Martinez[30], Z. Rurikova[48], N.A. Rusakovich[65], A. Ruschke[100], H.L. Russell[139], J.P. Rutherfoord[7], N. Ruthmann[48], Y.F. Ryabov[123], M. Rybar[129], G. Rybkin[117], N.C. Ryder[120], A.F. Saavedra[151], G. Sabato[107], S. Sacerdoti[27], A. Saddique[3], H.F-W. Sadrozinski[138], R. Sadykov[65], F. Safai Tehrani[133a], H. Sakamoto[156], Y. Sakurai[172], G. Salamanna[135a,135b], A. Salamon[134a], M. Saleem[113], D. Salek[107], P.H. Sales De Bruin[139], D. Salihagic[101], A. Salnikov[144], J. Salt[168], D. Salvatore[37a,37b], F. Salvatore[150], A. Salvucci[106], A. Salzburger[30], D. Sampsonidis[155], A. Sanchez[104a,104b], J. Sánchez[168], V. Sanchez Martinez[168], H. Sandaker[14], R.L. Sandbach[76], H.G. Sander[83], M.P. Sanders[100], M. Sandhoff[176], T. Sandoval[28], C. Sandoval[163], R. Sandstroem[101], D.P.C. Sankey[131], A. Sansoni[47], C. Santoni[34], R. Santonico[134a,134b], H. Santos[126a], I. Santoyo Castillo[150], K. Sapp[125], A. Sapronov[65], J.G. Saraiva[126a,126d], B. Sarrazin[21], G. Sartisohn[176], O. Sasaki[66], Y. Sasaki[156], K. Sato[161], G. Sauvage[5,*], E. Sauvan[5], G. Savage[77], P. Savard[159,d], C. Sawyer[120], L. Sawyer[79,m], D.H. Saxon[53], J. Saxon[31], C. Sbarra[20a],

JHEP04(2015)116

A. Sbrizzi[20a,20b], T. Scanlon[78], D.A. Scannicchio[164], M. Scarcella[151], V. Scarfone[37a,37b], J. Schaarschmidt[173], P. Schacht[101], D. Schaefer[30], R. Schaefer[42], S. Schaepe[21], S. Schaetzel[58b], U. Schäfer[83], A.C. Schaffer[117], D. Schaile[100], R.D. Schamberger[149], V. Scharf[58a], V.A. Schegelsky[123], D. Scheirich[129], M. Schernau[164], C. Schiavi[50a,50b], J. Schieck[100], C. Schillo[48], M. Schioppa[37a,37b], S. Schlenker[30], E. Schmidt[48], K. Schmieden[30], C. Schmitt[83], S. Schmitt[58b], B. Schneider[17], Y.J. Schnellbach[74], U. Schnoor[44], L. Schoeffel[137], A. Schoening[58b], B.D. Schoenrock[90], A.L.S. Schorlemmer[54], M. Schott[83], D. Schouten[160a], J. Schovancova[25], S. Schramm[159], M. Schreyer[175], C. Schroeder[83], N. Schuh[83], M.J. Schultens[21], H.-C. Schultz-Coulon[58a], H. Schulz[16], M. Schumacher[48], B.A. Schumm[138], Ph. Schune[137], C. Schwanenberger[84], A. Schwartzman[144], T.A. Schwarz[89], Ph. Schwegler[101], Ph. Schwemling[137], R. Schwienhorst[90], J. Schwindling[137], T. Schwindt[21], M. Schwoerer[5], F.G. Sciacca[17], E. Scifo[117], G. Sciolla[23], F. Scuri[124a,124b], F. Scutti[21], J. Searcy[89], G. Sedov[42], E. Sedykh[123], P. Seema[21], S.C. Seidel[105], A. Seiden[138], F. Seifert[128], J.M. Seixas[24a], G. Sekhniaidze[104a], S.J. Sekula[40], K.E. Selbach[46], D.M. Seliverstov[123,*], G. Sellers[74], N. Semprini-Cesari[20a,20b], C. Serfon[30], L. Serin[117], L. Serkin[54], T. Serre[85], R. Seuster[160a], H. Severini[113], T. Sfiligoj[75], F. Sforza[101], A. Sfyrla[30], E. Shabalina[54], M. Shamim[116], L.Y. Shan[33a], R. Shang[166], J.T. Shank[22], M. Shapiro[15], P.B. Shatalov[97], K. Shaw[165a,165b], A. Shcherbakova[147a,147b], C.Y. Shehu[150], P. Sherwood[78], L. Shi[152,ae], S. Shimizu[67], C.O. Shimmin[164], M. Shimojima[102], M. Shiyakova[65], A. Shmeleva[96], D. Shoaleh Saadi[95], M.J. Shochet[31], S. Shojaii[91a,91b], D. Short[120], S. Shrestha[111], E. Shulga[98], M.A. Shupe[7], S. Shushkevich[42], P. Sicho[127], O. Sidiropoulou[155], D. Sidorov[114], A. Sidoti[133a], F. Siegert[44], Dj. Sijacki[13a], J. Silva[126a,126d], Y. Silver[154], D. Silverstein[144], S.B. Silverstein[147a], V. Simak[128], O. Simard[5], Lj. Simic[13a], S. Simion[117], E. Simioni[83], B. Simmons[78], D. Simon[34], R. Simoniello[91a,91b], P. Sinervo[159], N.B. Sinev[116], G. Siragusa[175], A. Sircar[79], A.N. Sisakyan[65,*], S.Yu. Sivoklokov[99], J. Sjölin[147a,147b], T.B. Sjursen[14], H.P. Skottowe[57], P. Skubic[113], M. Slater[18], T. Slavicek[128], M. Slawinska[107], K. Sliwa[162], V. Smakhtin[173], B.H. Smart[46], L. Smestad[14], S.Yu. Smirnov[98], Y. Smirnov[98], L.N. Smirnova[99,af], O. Smirnova[81], K.M. Smith[53], M. Smith[35], M. Smizanska[72], K. Smolek[128], A.A. Snesarev[96], G. Snidero[76], S. Snyder[25], R. Sobie[170,j], F. Socher[44], A. Soffer[154], D.A. Soh[152,ae], C.A. Solans[30], M. Solar[128], J. Solc[128], E.Yu. Soldatov[98], U. Soldevila[168], A.A. Solodkov[130], A. Soloshenko[65], O.V. Solovyanov[130], V. Solovyev[123], P. Sommer[48], H.Y. Song[33b], N. Soni[1], A. Sood[15], A. Sopczak[128], B. Sopko[128], V. Sopko[128], V. Sorin[12], D. Sosa[58b], M. Sosebee[8], R. Soualah[165a,165c], P. Soueid[95], A.M. Soukharev[109,c], D. South[42], S. Spagnolo[73a,73b], F. Spanò[77], W.R. Spearman[57], F. Spettel[101], R. Spighi[20a], G. Spigo[30], L.A. Spiller[88], M. Spousta[129], T. Spreitzer[159], R.D. St. Denis[53,*], S. Staerz[44], J. Stahlman[122], R. Stamen[58a], S. Stamm[16], E. Stanecka[39], C. Stanescu[135a], M. Stanescu-Bellu[42], M.M. Stanitzki[42], S. Stapnes[119], E.A. Starchenko[130], J. Stark[55], P. Staroba[127], P. Starovoitov[42], R. Staszewski[39], P. Stavina[145a,*], P. Steinberg[25], B. Stelzer[143], H.J. Stelzer[30], O. Stelzer-Chilton[160a], H. Stenzel[52], S. Stern[101], G.A. Stewart[53], J.A. Stillings[21], M.C. Stockton[87], M. Stoebe[87], G. Stoicea[26a], P. Stolte[54], S. Stonjek[101], A.R. Stradling[8], A. Straessner[44], M.E. Stramaglia[17], J. Strandberg[148], S. Strandberg[147a,147b], A. Strandlie[119], E. Strauss[144], M. Strauss[113], P. Strizenec[145b], R. Ströhmer[175], D.M. Strom[116], R. Stroynowski[40], A. Strubig[106], S.A. Stucci[17], B. Stugu[14], N.A. Styles[42], D. Su[144], J. Su[125], R. Subramaniam[79], A. Succurro[12], Y. Sugaya[118], C. Suhr[108], M. Suk[128], V.V. Sulin[96], S. Sultansoy[4d], T. Sumida[68], S. Sun[57], X. Sun[33a], J.E. Sundermann[48], K. Suruliz[150], G. Susinno[37a,37b], M.R. Sutton[150], Y. Suzuki[66], M. Svatos[127], S. Swedish[169], M. Swiatlowski[144], I. Sykora[145a], T. Sykora[129], D. Ta[90], C. Taccini[135a,135b], K. Tackmann[42], J. Taenzer[159], A. Taffard[164], R. Tafirout[160a], N. Taiblum[154], H. Takai[25], R. Takashima[69], H. Takeda[67], T. Takeshita[141], Y. Takubo[66], M. Talby[85], A.A. Talyshev[109,c], J.Y.C. Tam[175], K.G. Tan[88], J. Tanaka[156], R. Tanaka[117], S. Tanaka[132], S. Tanaka[66], A.J. Tanasijczuk[143], B.B. Tannenwald[111],

JHEP04(2015)116

N. Tannoury[21], S. Tapprogge[83], S. Tarem[153], F. Tarrade[29], G.F. Tartarelli[91a], P. Tas[129], M. Tasevsky[127], T. Tashiro[68], E. Tassi[37a,37b], A. Tavares Delgado[126a,126b], Y. Tayalati[136d], F.E. Taylor[94], G.N. Taylor[88], W. Taylor[160b], F.A. Teischinger[30], M. Teixeira Dias Castanheira[76], P. Teixeira-Dias[77], K.K. Temming[48], H. Ten Kate[30], P.K. Teng[152], J.J. Teoh[118], F. Tepel[176], S. Terada[66], K. Terashi[156], J. Terron[82], S. Terzo[101], M. Testa[47], R.J. Teuscher[159,j], J. Therhaag[21], T. Theveneaux-Pelzer[34], J.P. Thomas[18], J. Thomas-Wilsker[77], E.N. Thompson[35], P.D. Thompson[18], R.J. Thompson[84], A.S. Thompson[53], L.A. Thomsen[36], E. Thomson[122], M. Thomson[28], W.M. Thong[88], R.P. Thun[89,*], F. Tian[35], M.J. Tibbetts[15], V.O. Tikhomirov[96,ag], Yu.A. Tikhonov[109,c], S. Timoshenko[98], E. Tiouchichine[85], P. Tipton[177], S. Tisserant[85], T. Todorov[5,*], S. Todorova-Nova[129], J. Tojo[70], S. Tokár[145a], K. Tokushuku[66], K. Tollefson[90], E. Tolley[57], L. Tomlinson[84], M. Tomoto[103], L. Tompkins[31], K. Toms[105], N.D. Topilin[65], E. Torrence[116], H. Torres[143], E. Torró Pastor[168], J. Toth[85,ah], F. Touchard[85], D.R. Tovey[140], H.L. Tran[117], T. Trefzger[175], L. Tremblet[30], A. Tricoli[30], I.M. Trigger[160a], S. Trincaz-Duvoid[80], M.F. Tripiana[12], W. Trischuk[159], B. Trocmé[55], C. Troncon[91a], M. Trottier-McDonald[15], M. Trovatelli[135a,135b], P. True[90], M. Trzebinski[39], A. Trzupek[39], C. Tsarouchas[30], J.C-L. Tseng[120], P.V. Tsiareshka[92], D. Tsionou[137], G. Tsipolitis[10], N. Tsirintanis[9], S. Tsiskaridze[12], V. Tsiskaridze[48], E.G. Tskhadadze[51a], I.I. Tsukerman[97], V. Tsulaia[15], S. Tsuno[66], D. Tsybychev[149], A. Tudorache[26a], V. Tudorache[26a], A.N. Tuna[122], S.A. Tupputi[20a,20b], S. Turchikhin[99,af], D. Turecek[128], I. Turk Cakir[4c], R. Turra[91a,91b], A.J. Turvey[40], P.M. Tuts[35], A. Tykhonov[49], M. Tylmad[147a,147b], M. Tyndel[131], I. Ueda[156], R. Ueno[29], M. Ughetto[85], M. Ugland[14], M. Uhlenbrock[21], F. Ukegawa[161], G. Unal[30], A. Undrus[25], G. Unel[164], F.C. Ungaro[48], Y. Unno[66], C. Unverdorben[100], J. Urban[145b], D. Urbaniec[35], P. Urquijo[88], P. Urrejola[83], G. Usai[8], A. Usanova[62], L. Vacavant[85], V. Vacek[128], B. Vachon[87], N. Valencic[107], S. Valentinetti[20a,20b], A. Valero[168], L. Valery[34], S. Valkar[129], E. Valladolid Gallego[168], S. Vallecorsa[49], J.A. Valls Ferrer[168], W. Van Den Wollenberg[107], P.C. Van Der Deijl[107], R. van der Geer[107], H. van der Graaf[107], R. Van Der Leeuw[107], D. van der Ster[30], N. van Eldik[30], P. van Gemmeren[6], J. Van Nieuwkoop[143], I. van Vulpen[107], M.C. van Woerden[30], M. Vanadia[133a,133b], W. Vandelli[30], R. Vanguri[122], A. Vaniachine[6], P. Vankov[42], F. Vannucci[80], G. Vardanyan[178], R. Vari[133a], E.W. Varnes[7], T. Varol[86], D. Varouchas[80], A. Vartapetian[8], K.E. Varvell[151], F. Vazeille[34], T. Vazquez Schroeder[54], J. Veatch[7], F. Veloso[126a,126c], T. Velz[21], S. Veneziano[133a], A. Ventura[73a,73b], D. Ventura[86], M. Venturi[170], N. Venturi[159], A. Venturini[23], V. Vercesi[121a], M. Verducci[133a,133b], W. Verkerke[107], J.C. Vermeulen[107], A. Vest[44], M.C. Vetterli[143,d], O. Viazlo[81], I. Vichou[166], T. Vickey[146c,ai], O.E. Vickey Boeriu[146c], G.H.A. Viehhauser[120], S. Viel[169], R. Vigne[30], M. Villa[20a,20b], M. Villaplana Perez[91a,91b], E. Vilucchi[47], M.G. Vincter[29], V.B. Vinogradov[65], J. Virzi[15], I. Vivarelli[150], F. Vives Vaque[3], S. Vlachos[10], D. Vladoiu[100], M. Vlasak[128], A. Vogel[21], M. Vogel[32a], P. Vokac[128], G. Volpi[124a,124b], M. Volpi[88], H. von der Schmitt[101], H. von Radziewski[48], E. von Toerne[21], V. Vorobel[129], K. Vorobev[98], M. Vos[168], R. Voss[30], J.H. Vossebeld[74], N. Vranjes[137], M. Vranjes Milosavljevic[13a], V. Vrba[127], M. Vreeswijk[107], T. Vu Anh[48], R. Vuillermet[30], I. Vukotic[31], Z. Vykydal[128], P. Wagner[21], W. Wagner[176], H. Wahlberg[71], S. Wahrmund[44], J. Wakabayashi[103], J. Walder[72], R. Walker[100], W. Walkowiak[142], R. Wall[177], P. Waller[74], B. Walsh[177], C. Wang[33c], C. Wang[45], F. Wang[174], H. Wang[15], H. Wang[40], J. Wang[42], J. Wang[33a], K. Wang[87], R. Wang[105], S.M. Wang[152], T. Wang[21], X. Wang[177], C. Wanotayaroj[116], A. Warburton[87], C.P. Ward[28], D.R. Wardrope[78], M. Warsinsky[48], A. Washbrook[46], C. Wasicki[42], P.M. Watkins[18], A.T. Watson[18], I.J. Watson[151], M.F. Watson[18], G. Watts[139], S. Watts[84], B.M. Waugh[78], S. Webb[84], M.S. Weber[17], S.W. Weber[175], J.S. Webster[31], A.R. Weidberg[120], B. Weinert[61], J. Weingarten[54], C. Weiser[48], H. Weits[107], P.S. Wells[30], T. Wenaus[25], D. Wendland[16], Z. Weng[152,ae], T. Wengler[30], S. Wenig[30], N. Wermes[21], M. Werner[48], P. Werner[30], M. Wessels[58a],

JHEP04(2015)116

J. Wetter[162], K. Whalen[29], A. White[8], M.J. White[1], R. White[32b], S. White[124a,124b], D. Whiteson[164], D. Wicke[176], F.J. Wickens[131], W. Wiedenmann[174], M. Wielers[131], P. Wienemann[21], C. Wiglesworth[36], L.A.M. Wiik-Fuchs[21], P.A. Wijeratne[78], A. Wildauer[101], M.A. Wildt[42,aj], H.G. Wilkens[30], H.H. Williams[122], S. Williams[28], C. Willis[90], S. Willocq[86], A. Wilson[89], J.A. Wilson[18], I. Wingerter-Seez[5], F. Winklmeier[116], B.T. Winter[21], M. Wittgen[144], J. Wittkowski[100], S.J. Wollstadt[83], M.W. Wolter[39], H. Wolters[126a,126c], B.K. Wosiek[39], J. Wotschack[30], M.J. Woudstra[84], K.W. Wozniak[39], M. Wright[53], M. Wu[55], S.L. Wu[174], X. Wu[49], Y. Wu[89], T.R. Wyatt[84], B.M. Wynne[46], S. Xella[36], M. Xiao[137], D. Xu[33a], L. Xu[33b,ak], B. Yabsley[151], S. Yacoob[146b,al], R. Yakabe[67], M. Yamada[66], H. Yamaguchi[156], Y. Yamaguchi[118], A. Yamamoto[66], S. Yamamoto[156], T. Yamamura[156], T. Yamanaka[156], K. Yamauchi[103], Y. Yamazaki[67], Z. Yan[22], H. Yang[33e], H. Yang[174], Y. Yang[111], S. Yanush[93], L. Yao[33a], W-M. Yao[15], Y. Yasu[66], E. Yatsenko[42], K.H. Yau Wong[21], J. Ye[40], S. Ye[25], I. Yeletskikh[65], A.L. Yen[57], E. Yildirim[42], K. Yorita[172], R. Yoshida[6], K. Yoshihara[156], C. Young[144], C.J.S. Young[30], S. Youssef[22], D.R. Yu[15], J. Yu[8], J.M. Yu[89], J. Yu[114], L. Yuan[67], A. Yurkewicz[108], I. Yusuff[28,am], B. Zabinski[39], R. Zaidan[63], A.M. Zaitsev[130,aa], A. Zaman[149], S. Zambito[23], L. Zanello[133a,133b], D. Zanzi[88], C. Zeitnitz[176], M. Zeman[128], A. Zemla[38a], K. Zengel[23], O. Zenin[130], T. Ženiš[145a], D. Zerwas[117], G. Zevi della Porta[57], D. Zhang[89], F. Zhang[174], H. Zhang[90], J. Zhang[6], L. Zhang[152], R. Zhang[33b], X. Zhang[33d], Z. Zhang[117], X. Zhao[40], Y. Zhao[33d], Z. Zhao[33b], A. Zhemchugov[65], J. Zhong[120], B. Zhou[89], C. Zhou[45], L. Zhou[35], L. Zhou[40], N. Zhou[164], C.G. Zhu[33d], H. Zhu[33a], J. Zhu[89], Y. Zhu[33b], X. Zhuang[33a], K. Zhukov[96], A. Zibell[175], D. Zieminska[61], N.I. Zimine[65], C. Zimmermann[83], R. Zimmermann[21], S. Zimmermann[21], S. Zimmermann[48], Z. Zinonos[54], M. Ziolkowski[142], G. Zobernig[174], A. Zoccoli[20a,20b], M. zur Nedden[16], G. Zurzolo[104a,104b] and L. Zwalinski[30].

[1] *Department of Physics, University of Adelaide, Adelaide, Australia*
[2] *Physics Department, SUNY Albany, Albany NY, United States of America*
[3] *Department of Physics, University of Alberta, Edmonton AB, Canada*
[4] [(a)] *Department of Physics, Ankara University, Ankara;* [(c)] *Istanbul Aydin University, Istanbul;* [(d)] *Division of Physics, TOBB University of Economics and Technology, Ankara, Turkey*
[5] *LAPP, CNRS/IN2P3 and Université de Savoie, Annecy-le-Vieux, France*
[6] *High Energy Physics Division, Argonne National Laboratory, Argonne IL, United States of America*
[7] *Department of Physics, University of Arizona, Tucson AZ, United States of America*
[8] *Department of Physics, The University of Texas at Arlington, Arlington TX, United States of America*
[9] *Physics Department, University of Athens, Athens, Greece*
[10] *Physics Department, National Technical University of Athens, Zografou, Greece*
[11] *Institute of Physics, Azerbaijan Academy of Sciences, Baku, Azerbaijan*
[12] *Institut de Física d'Altes Energies and Departament de Física de la Universitat Autònoma de Barcelona, Barcelona, Spain*
[13] [(a)] *Institute of Physics, University of Belgrade, Belgrade;* [(b)] *Vinca Institute of Nuclear Sciences, University of Belgrade, Belgrade, Serbia*
[14] *Department for Physics and Technology, University of Bergen, Bergen, Norway*
[15] *Physics Division, Lawrence Berkeley National Laboratory and University of California, Berkeley CA, United States of America*
[16] *Department of Physics, Humboldt University, Berlin, Germany*
[17] *Albert Einstein Center for Fundamental Physics and Laboratory for High Energy Physics, University of Bern, Bern, Switzerland*
[18] *School of Physics and Astronomy, University of Birmingham, Birmingham, United Kingdom*
[19] [(a)] *Department of Physics, Bogazici University, Istanbul;* [(b)] *Department of Physics, Dogus University, Istanbul;* [(c)] *Department of Physics Engineering, Gaziantep University, Gaziantep,*

JHEP04(2015)116

Turkey
[20] [(a)] *INFN Sezione di Bologna;* [(b)] *Dipartimento di Fisica e Astronomia, Università di Bologna, Bologna, Italy*
[21] *Physikalisches Institut, University of Bonn, Bonn, Germany*
[22] *Department of Physics, Boston University, Boston MA, United States of America*
[23] *Department of Physics, Brandeis University, Waltham MA, United States of America*
[24] [(a)] *Universidade Federal do Rio De Janeiro COPPE/EE/IF, Rio de Janeiro;* [(b)] *Electrical Circuits Department, Federal University of Juiz de Fora (UFJF), Juiz de Fora;* [(c)] *Federal University of Sao Joao del Rei (UFSJ), Sao Joao del Rei;* [(d)] *Instituto de Fisica, Universidade de Sao Paulo, Sao Paulo, Brazil*
[25] *Physics Department, Brookhaven National Laboratory, Upton NY, United States of America*
[26] [(a)] *National Institute of Physics and Nuclear Engineering, Bucharest;* [(b)] *National Institute for Research and Development of Isotopic and Molecular Technologies, Physics Department, Cluj Napoca;* [(c)] *University Politehnica Bucharest, Bucharest;* [(d)] *West University in Timisoara, Timisoara, Romania*
[27] *Departamento de Física, Universidad de Buenos Aires, Buenos Aires, Argentina*
[28] *Cavendish Laboratory, University of Cambridge, Cambridge, United Kingdom*
[29] *Department of Physics, Carleton University, Ottawa ON, Canada*
[30] *CERN, Geneva, Switzerland*
[31] *Enrico Fermi Institute, University of Chicago, Chicago IL, United States of America*
[32] [(a)] *Departamento de Física, Pontificia Universidad Católica de Chile, Santiago;* [(b)] *Departamento de Física, Universidad Técnica Federico Santa María, Valparaíso, Chile*
[33] [(a)] *Institute of High Energy Physics, Chinese Academy of Sciences, Beijing;* [(b)] *Department of Modern Physics, University of Science and Technology of China, Anhui;* [(c)] *Department of Physics, Nanjing University, Jiangsu;* [(d)] *School of Physics, Shandong University, Shandong;* [(e)] *Physics Department, Shanghai Jiao Tong University, Shanghai;* [(f)] *Physics Department, Tsinghua University, Beijing 100084, China*
[34] *Laboratoire de Physique Corpusculaire, Clermont Université and Université Blaise Pascal and CNRS/IN2P3, Clermont-Ferrand, France*
[35] *Nevis Laboratory, Columbia University, Irvington NY, United States of America*
[36] *Niels Bohr Institute, University of Copenhagen, Kobenhavn, Denmark*
[37] [(a)] *INFN Gruppo Collegato di Cosenza, Laboratori Nazionali di Frascati;* [(b)] *Dipartimento di Fisica, Università della Calabria, Rende, Italy*
[38] [(a)] *AGH University of Science and Technology, Faculty of Physics and Applied Computer Science, Krakow;* [(b)] *Marian Smoluchowski Institute of Physics, Jagiellonian University, Krakow, Poland*
[39] *The Henryk Niewodniczanski Institute of Nuclear Physics, Polish Academy of Sciences, Krakow, Poland*
[40] *Physics Department, Southern Methodist University, Dallas TX, United States of America*
[41] *Physics Department, University of Texas at Dallas, Richardson TX, United States of America*
[42] *DESY, Hamburg and Zeuthen, Germany*
[43] *Institut für Experimentelle Physik IV, Technische Universität Dortmund, Dortmund, Germany*
[44] *Institut für Kern- und Teilchenphysik, Technische Universität Dresden, Dresden, Germany*
[45] *Department of Physics, Duke University, Durham NC, United States of America*
[46] *SUPA - School of Physics and Astronomy, University of Edinburgh, Edinburgh, United Kingdom*
[47] *INFN Laboratori Nazionali di Frascati, Frascati, Italy*
[48] *Fakultät für Mathematik und Physik, Albert-Ludwigs-Universität, Freiburg, Germany*
[49] *Section de Physique, Université de Genève, Geneva, Switzerland*
[50] [(a)] *INFN Sezione di Genova;* [(b)] *Dipartimento di Fisica, Università di Genova, Genova, Italy*
[51] [(a)] *E. Andronikashvili Institute of Physics, Iv. Javakhishvili Tbilisi State University, Tbilisi;* [(b)] *High Energy Physics Institute, Tbilisi State University, Tbilisi, Georgia*
[52] *II Physikalisches Institut, Justus-Liebig-Universität Giessen, Giessen, Germany*
[53] *SUPA - School of Physics and Astronomy, University of Glasgow, Glasgow, United Kingdom*

JHEP04(2015)116

[54] *II Physikalisches Institut, Georg-August-Universität, Göttingen, Germany*
[55] *Laboratoire de Physique Subatomique et de Cosmologie, Université Grenoble-Alpes, CNRS/IN2P3, Grenoble, France*
[56] *Department of Physics, Hampton University, Hampton VA, United States of America*
[57] *Laboratory for Particle Physics and Cosmology, Harvard University, Cambridge MA, United States of America*
[58] [(a)] *Kirchhoff-Institut für Physik, Ruprecht-Karls-Universität Heidelberg, Heidelberg;* [(b)] *Physikalisches Institut, Ruprecht-Karls-Universität Heidelberg, Heidelberg;* [(c)] *ZITI Institut für technische Informatik, Ruprecht-Karls-Universität Heidelberg, Mannheim, Germany*
[59] *Faculty of Applied Information Science, Hiroshima Institute of Technology, Hiroshima, Japan*
[60] [(a)] *Department of Physics, The Chinese University of Hong Kong, Shatin, N.T., Hong Kong;* [(b)] *Department of Physics, The University of Hong Kong, Hong Kong;* [(c)] *Department of Physics, The Hong Kong University of Science and Technology, Clear Water Bay, Kowloon, Hong Kong, China*
[61] *Department of Physics, Indiana University, Bloomington IN, United States of America*
[62] *Institut für Astro- und Teilchenphysik, Leopold-Franzens-Universität, Innsbruck, Austria*
[63] *University of Iowa, Iowa City IA, United States of America*
[64] *Department of Physics and Astronomy, Iowa State University, Ames IA, United States of America*
[65] *Joint Institute for Nuclear Research, JINR Dubna, Dubna, Russia*
[66] *KEK, High Energy Accelerator Research Organization, Tsukuba, Japan*
[67] *Graduate School of Science, Kobe University, Kobe, Japan*
[68] *Faculty of Science, Kyoto University, Kyoto, Japan*
[69] *Kyoto University of Education, Kyoto, Japan*
[70] *Department of Physics, Kyushu University, Fukuoka, Japan*
[71] *Instituto de Física La Plata, Universidad Nacional de La Plata and CONICET, La Plata, Argentina*
[72] *Physics Department, Lancaster University, Lancaster, United Kingdom*
[73] [(a)] *INFN Sezione di Lecce;* [(b)] *Dipartimento di Matematica e Fisica, Università del Salento, Lecce, Italy*
[74] *Oliver Lodge Laboratory, University of Liverpool, Liverpool, United Kingdom*
[75] *Department of Physics, Jožef Stefan Institute and University of Ljubljana, Ljubljana, Slovenia*
[76] *School of Physics and Astronomy, Queen Mary University of London, London, United Kingdom*
[77] *Department of Physics, Royal Holloway University of London, Surrey, United Kingdom*
[78] *Department of Physics and Astronomy, University College London, London, United Kingdom*
[79] *Louisiana Tech University, Ruston LA, United States of America*
[80] *Laboratoire de Physique Nucléaire et de Hautes Energies, UPMC and Université Paris-Diderot and CNRS/IN2P3, Paris, France*
[81] *Fysiska institutionen, Lunds universitet, Lund, Sweden*
[82] *Departamento de Fisica Teorica C-15, Universidad Autonoma de Madrid, Madrid, Spain*
[83] *Institut für Physik, Universität Mainz, Mainz, Germany*
[84] *School of Physics and Astronomy, University of Manchester, Manchester, United Kingdom*
[85] *CPPM, Aix-Marseille Université and CNRS/IN2P3, Marseille, France*
[86] *Department of Physics, University of Massachusetts, Amherst MA, United States of America*
[87] *Department of Physics, McGill University, Montreal QC, Canada*
[88] *School of Physics, University of Melbourne, Victoria, Australia*
[89] *Department of Physics, The University of Michigan, Ann Arbor MI, United States of America*
[90] *Department of Physics and Astronomy, Michigan State University, East Lansing MI, United States of America*
[91] [(a)] *INFN Sezione di Milano;* [(b)] *Dipartimento di Fisica, Università di Milano, Milano, Italy*
[92] *B.I. Stepanov Institute of Physics, National Academy of Sciences of Belarus, Minsk, Republic of Belarus*
[93] *National Scientific and Educational Centre for Particle and High Energy Physics, Minsk, Republic of Belarus*
[94] *Department of Physics, Massachusetts Institute of Technology, Cambridge MA, United States of*

JHEP04(2015)116

America
[95] Group of Particle Physics, University of Montreal, Montreal QC, Canada
[96] P.N. Lebedev Institute of Physics, Academy of Sciences, Moscow, Russia
[97] Institute for Theoretical and Experimental Physics (ITEP), Moscow, Russia
[98] National Research Nuclear University MEPhI, Moscow, Russia
[99] D.V. Skobeltsyn Institute of Nuclear Physics, M.V. Lomonosov Moscow State University, Moscow, Russia
[100] Fakultät für Physik, Ludwig-Maximilians-Universität München, München, Germany
[101] Max-Planck-Institut für Physik (Werner-Heisenberg-Institut), München, Germany
[102] Nagasaki Institute of Applied Science, Nagasaki, Japan
[103] Graduate School of Science and Kobayashi-Maskawa Institute, Nagoya University, Nagoya, Japan
[104] [(a)] INFN Sezione di Napoli; [(b)] Dipartimento di Fisica, Università di Napoli, Napoli, Italy
[105] Department of Physics and Astronomy, University of New Mexico, Albuquerque NM, United States of America
[106] Institute for Mathematics, Astrophysics and Particle Physics, Radboud University Nijmegen/Nikhef, Nijmegen, Netherlands
[107] Nikhef National Institute for Subatomic Physics and University of Amsterdam, Amsterdam, Netherlands
[108] Department of Physics, Northern Illinois University, DeKalb IL, United States of America
[109] Budker Institute of Nuclear Physics, SB RAS, Novosibirsk, Russia
[110] Department of Physics, New York University, New York NY, United States of America
[111] Ohio State University, Columbus OH, United States of America
[112] Faculty of Science, Okayama University, Okayama, Japan
[113] Homer L. Dodge Department of Physics and Astronomy, University of Oklahoma, Norman OK, United States of America
[114] Department of Physics, Oklahoma State University, Stillwater OK, United States of America
[115] Palacký University, RCPTM, Olomouc, Czech Republic
[116] Center for High Energy Physics, University of Oregon, Eugene OR, United States of America
[117] LAL, Université Paris-Sud and CNRS/IN2P3, Orsay, France
[118] Graduate School of Science, Osaka University, Osaka, Japan
[119] Department of Physics, University of Oslo, Oslo, Norway
[120] Department of Physics, Oxford University, Oxford, United Kingdom
[121] [(a)] INFN Sezione di Pavia; [(b)] Dipartimento di Fisica, Università di Pavia, Pavia, Italy
[122] Department of Physics, University of Pennsylvania, Philadelphia PA, United States of America
[123] Petersburg Nuclear Physics Institute, Gatchina, Russia
[124] [(a)] INFN Sezione di Pisa; [(b)] Dipartimento di Fisica E. Fermi, Università di Pisa, Pisa, Italy
[125] Department of Physics and Astronomy, University of Pittsburgh, Pittsburgh PA, United States of America
[126] [(a)] Laboratorio de Instrumentacao e Fisica Experimental de Particulas - LIP, Lisboa; [(b)] Faculdade de Ciências, Universidade de Lisboa, Lisboa; [(c)] Department of Physics, University of Coimbra, Coimbra; [(d)] Centro de Física Nuclear da Universidade de Lisboa, Lisboa; [(e)] Departamento de Fisica, Universidade do Minho, Braga; [(f)] Departamento de Fisica Teorica y del Cosmos and CAFPE, Universidad de Granada, Granada (Spain); [(g)] Dep Fisica and CEFITEC of Faculdade de Ciencias e Tecnologia, Universidade Nova de Lisboa, Caparica, Portugal
[127] Institute of Physics, Academy of Sciences of the Czech Republic, Praha, Czech Republic
[128] Czech Technical University in Prague, Praha, Czech Republic
[129] Faculty of Mathematics and Physics, Charles University in Prague, Praha, Czech Republic
[130] State Research Center Institute for High Energy Physics, Protvino, Russia
[131] Particle Physics Department, Rutherford Appleton Laboratory, Didcot, United Kingdom
[132] Ritsumeikan University, Kusatsu, Shiga, Japan
[133] [(a)] INFN Sezione di Roma; [(b)] Dipartimento di Fisica, Sapienza Università di Roma, Roma, Italy
[134] [(a)] INFN Sezione di Roma Tor Vergata; [(b)] Dipartimento di Fisica, Università di Roma Tor

JHEP04(2015)116

Vergata, Roma, Italy
[135] [(a)] INFN Sezione di Roma Tre; [(b)] Dipartimento di Matematica e Fisica, Università Roma Tre, Roma, Italy
[136] [(a)] Faculté des Sciences Ain Chock, Réseau Universitaire de Physique des Hautes Energies - Université Hassan II, Casablanca; [(b)] Centre National de l'Energie des Sciences Techniques Nucleaires, Rabat; [(c)] Faculté des Sciences Semlalia, Université Cadi Ayyad, LPHEA-Marrakech; [(d)] Faculté des Sciences, Université Mohamed Premier and LPTPM, Oujda; [(e)] Faculté des sciences, Université Mohammed V-Agdal, Rabat, Morocco
[137] DSM/IRFU (Institut de Recherches sur les Lois Fondamentales de l'Univers), CEA Saclay (Commissariat à l'Energie Atomique et aux Energies Alternatives), Gif-sur-Yvette, France
[138] Santa Cruz Institute for Particle Physics, University of California Santa Cruz, Santa Cruz CA, United States of America
[139] Department of Physics, University of Washington, Seattle WA, United States of America
[140] Department of Physics and Astronomy, University of Sheffield, Sheffield, United Kingdom
[141] Department of Physics, Shinshu University, Nagano, Japan
[142] Fachbereich Physik, Universität Siegen, Siegen, Germany
[143] Department of Physics, Simon Fraser University, Burnaby BC, Canada
[144] SLAC National Accelerator Laboratory, Stanford CA, United States of America
[145] [(a)] Faculty of Mathematics, Physics & Informatics, Comenius University, Bratislava; [(b)] Department of Subnuclear Physics, Institute of Experimental Physics of the Slovak Academy of Sciences, Kosice, Slovak Republic
[146] [(a)] Department of Physics, University of Cape Town, Cape Town; [(b)] Department of Physics, University of Johannesburg, Johannesburg; [(c)] School of Physics, University of the Witwatersrand, Johannesburg, South Africa
[147] [(a)] Department of Physics, Stockholm University; [(b)] The Oskar Klein Centre, Stockholm, Sweden
[148] Physics Department, Royal Institute of Technology, Stockholm, Sweden
[149] Departments of Physics & Astronomy and Chemistry, Stony Brook University, Stony Brook NY, United States of America
[150] Department of Physics and Astronomy, University of Sussex, Brighton, United Kingdom
[151] School of Physics, University of Sydney, Sydney, Australia
[152] Institute of Physics, Academia Sinica, Taipei, Taiwan
[153] Department of Physics, Technion: Israel Institute of Technology, Haifa, Israel
[154] Raymond and Beverly Sackler School of Physics and Astronomy, Tel Aviv University, Tel Aviv, Israel
[155] Department of Physics, Aristotle University of Thessaloniki, Thessaloniki, Greece
[156] International Center for Elementary Particle Physics and Department of Physics, The University of Tokyo, Tokyo, Japan
[157] Graduate School of Science and Technology, Tokyo Metropolitan University, Tokyo, Japan
[158] Department of Physics, Tokyo Institute of Technology, Tokyo, Japan
[159] Department of Physics, University of Toronto, Toronto ON, Canada
[160] [(a)] TRIUMF, Vancouver BC; [(b)] Department of Physics and Astronomy, York University, Toronto ON, Canada
[161] Faculty of Pure and Applied Sciences, University of Tsukuba, Tsukuba, Japan
[162] Department of Physics and Astronomy, Tufts University, Medford MA, United States of America
[163] Centro de Investigaciones, Universidad Antonio Narino, Bogota, Colombia
[164] Department of Physics and Astronomy, University of California Irvine, Irvine CA, United States of America
[165] [(a)] INFN Gruppo Collegato di Udine, Sezione di Trieste, Udine; [(b)] ICTP, Trieste; [(c)] Dipartimento di Chimica, Fisica e Ambiente, Università di Udine, Udine, Italy
[166] Department of Physics, University of Illinois, Urbana IL, United States of America
[167] Department of Physics and Astronomy, University of Uppsala, Uppsala, Sweden
[168] Instituto de Física Corpuscular (IFIC) and Departamento de Física Atómica, Molecular y Nuclear

JHEP04(2015)116

and Departamento de Ingeniería Electrónica and Instituto de Microelectrónica de Barcelona (IMB-CNM), University of Valencia and CSIC, Valencia, Spain
[169] Department of Physics, University of British Columbia, Vancouver BC, Canada
[170] Department of Physics and Astronomy, University of Victoria, Victoria BC, Canada
[171] Department of Physics, University of Warwick, Coventry, United Kingdom
[172] Waseda University, Tokyo, Japan
[173] Department of Particle Physics, The Weizmann Institute of Science, Rehovot, Israel
[174] Department of Physics, University of Wisconsin, Madison WI, United States of America
[175] Fakultät für Physik und Astronomie, Julius-Maximilians-Universität, Würzburg, Germany
[176] Fachbereich C Physik, Bergische Universität Wuppertal, Wuppertal, Germany
[177] Department of Physics, Yale University, New Haven CT, United States of America
[178] Yerevan Physics Institute, Yerevan, Armenia
[179] Centre de Calcul de l'Institut National de Physique Nucléaire et de Physique des Particules (IN2P3), Villeurbanne, France
[a] Also at Department of Physics, King's College London, London, United Kingdom
[b] Also at Institute of Physics, Azerbaijan Academy of Sciences, Baku, Azerbaijan
[c] Also at Novosibirsk State University, Novosibirsk, Russia
[d] Also at TRIUMF, Vancouver BC, Canada
[e] Also at Department of Physics, California State University, Fresno CA, United States of America
[f] Also at Department of Physics, University of Fribourg, Fribourg, Switzerland
[g] Also at Tomsk State University, Tomsk, Russia
[h] Also at CPPM, Aix-Marseille Université and CNRS/IN2P3, Marseille, France
[i] Also at Università di Napoli Parthenope, Napoli, Italy
[j] Also at Institute of Particle Physics (IPP), Canada
[k] Also at Particle Physics Department, Rutherford Appleton Laboratory, Didcot, United Kingdom
[l] Also at Department of Physics, St. Petersburg State Polytechnical University, St. Petersburg, Russia
[m] Also at Louisiana Tech University, Ruston LA, United States of America
[n] Also at Institucio Catalana de Recerca i Estudis Avancats, ICREA, Barcelona, Spain
[o] Also at Department of Physics, National Tsing Hua University, Taiwan
[p] Also at Department of Physics, The University of Texas at Austin, Austin TX, United States of America
[q] Also at Institute of Theoretical Physics, Ilia State University, Tbilisi, Georgia
[r] Also at CERN, Geneva, Switzerland
[s] Also at Ochadai Academic Production, Ochanomizu University, Tokyo, Japan
[t] Also at Manhattan College, New York NY, United States of America
[u] Also at Institute of Physics, Academia Sinica, Taipei, Taiwan
[v] Also at LAL, Université Paris-Sud and CNRS/IN2P3, Orsay, France
[w] Also at Academia Sinica Grid Computing, Institute of Physics, Academia Sinica, Taipei, Taiwan
[x] Also at Laboratoire de Physique Nucléaire et de Hautes Energies, UPMC and Université Paris-Diderot and CNRS/IN2P3, Paris, France
[y] Also at School of Physical Sciences, National Institute of Science Education and Research, Bhubaneswar, India
[z] Also at Dipartimento di Fisica, Sapienza Università di Roma, Roma, Italy
[aa] Also at Moscow Institute of Physics and Technology State University, Dolgoprudny, Russia
[ab] Also at Section de Physique, Université de Genève, Geneva, Switzerland
[ac] Also at International School for Advanced Studies (SISSA), Trieste, Italy
[ad] Also at Department of Physics and Astronomy, University of South Carolina, Columbia SC, United States of America
[ae] Also at School of Physics and Engineering, Sun Yat-sen University, Guangzhou, China
[af] Also at Faculty of Physics, M.V.Lomonosov Moscow State University, Moscow, Russia
[ag] Also at National Research Nuclear University MEPhI, Moscow, Russia

JHEP04(2015)116

[ah] *Also at Institute for Particle and Nuclear Physics, Wigner Research Centre for Physics, Budapest, Hungary*
[ai] *Also at Department of Physics, Oxford University, Oxford, United Kingdom*
[aj] *Also at Institut für Experimentalphysik, Universität Hamburg, Hamburg, Germany*
[ak] *Also at Department of Physics, The University of Michigan, Ann Arbor MI, United States of America*
[al] *Also at Discipline of Physics, University of KwaZulu-Natal, Durban, South Africa*
[am] *Also at University of Malaya, Department of Physics, Kuala Lumpur, Malaysia*
[*] *Deceased*

JHEP04(2015)116